

VIBRATION CONTROL BY USING SHAPE MEMORY ALLOY
IN COMPOSITES AND SANDWICH STRUCTURES

By

CHIN HAI LEE

A DISSERTATION PRESENTED TO THE GRADUATE SCHOOL
OF THE UNIVERSITY OF FLORIDA IN PARTIAL FULFILLMENT
OF THE REQUIREMENTS FOR THE DEGREE OF
DOCTOR OF PHILOSOPHY

UNIVERSITY OF FLORIDA

1993

ACKNOWLEDGMENTS

The author wishes to express his gratitude to his committee chairman, Professor Chang-Tsan Sun, for his encouragement and guidance. The author could not have completed this work without the assistance of Dr. C. T. Sun, who was particularly helpful in procuring partial facilities for the experiments.

The author would also like to express his appreciation to every member of the committee and the composite group. Each one of them has helped him to learn the technique of testing, fabricating, and tooling of composites.

Most of all, the author would like to thank his sponsor, CSIST, for granting him this opportunity to study at the University of Florida. The author could not have accomplished his goal without their generous financial support.

TABLE OF CONTENTS

ACKNOWLEDGMENTS	ii
ABSTRACT	vi
CHAPTERS	
1. INTRODUCTION	1
1.1 Backgrounds of the Project	1
1.2 Special Features of SMA	4
1.3 Outline of This Study	9
1.3.1 Thermal Response of SMA Hybrid Composites	9
1.3.2 The Fabrication of SMA Hybrid Specimens	10
1.3.3 Stress-Strain in SMA Hybrid Laminate	10
1.3.4 Dynamic Test of SMA Hybrid Laminates	11
1.3.5 The Dynamic Model of SMA Sandwich Structure	11
2. SMA HYBRID COMPOSITE PLATE	12
2.1 Application of SMA Hybrid Laminates	12
2.2 ASET Set-Up Concept	12
2.3 Thermal Response of SMA Hybrid Beam	13
3. THE SPECIMEN FABRICATION AND TESTING PLAN	20
3.1 Specimen Fabrication of SMA Hybrid Beam	20
3.1.1 Selection of Fabrication Tool	21
3.1.1.1 Properties of Nitinol	21
3.1.2 Tool Design and Fabrication Procedure	23
3.1.3 First Batch Specimen Fabrication	24
3.1.4 Second Batch Specimen	26
3.2 Specimen Testing Plan	26
3.3 Facilities for Specimen Fabrication, Testing	28
4. EXPERIMENT, ANALYSIS OF SPECIMEN TRANSIENT THERMAL RESPONSE	33
4.1 Analysis of Transient Thermal Response	33
4.2 Experiment of Transient Thermal Response	34

5.	CONSTITUTIVE EQUATIONS OF SMA HYBRID COMPOSITE LAMINATE	43
5.1	Stress/Strain in SMA Hybrid Composites	43
5.1.1	Thermal Strain of Laminate	44
5.1.2	SMA Hybrid Laminate Strain	46
5.2	Internal Stresses of SMA Hybrid Beam	51
5.2.1	Stresses Distribution at Interface	51
5.2.2	Micromechanics and Internal Stresses	64
5.3	Dynamic Model of SMA Hybrid Laminate	66
5.3.1	General Dynamic Model	67
5.3.2	Dynamic Model--Orthotropic Laminate (APT)	68
5.3.3	Dynamic Model--Orthotropic Laminate (ASET)	68
6.	EXPERIMENTS OF SMA HYBRID LAMINATES MODAL RESPONSE	70
6.1	Experiment Facilities	70
6.2	First Batch of Specimen Test	72
6.3	Calculated 1st Mode Natural Frequency	76
6.4	Second Batch Specimen Test	78
7.	VIBRATION CONTROL OF SANDWICH BEAMS	88
7.1	Vibration Suppression in Structures	90
7.1.1	Passive Vibration Control	90
7.1.2	Active Vibration Control	92
7.2	Equation of Motion of Sandwich Panel	93
7.2.1	Derivation of Equation of Motion	94
7.2.2	Simply-Supported Sandwich Beam	106
7.2.3	Cantilever Sandwich Beam (Static)	106
7.3	Vibration Analysis of Sandwich Beam	107
7.3.1	Solution of Simply-Supported Beam	111
7.3.1.1	Case Study of Linear Vibration	115
7.3.2	Damped System under Harmonic Excitation	118
7.3.3	Analysis of Nonlinear Vibration	123
7.3.3.1	Free Vibration of Short Beam	123
7.3.3.2	Free Vibration of Long Beam	125
7.3.3.3	Dynamic Response of SMA Sandwich Beam	134
8.	CONCLUSION AND FUTURE WORK	140
8.1	Conclusion of Current Study	140
8.2	Future Study of SMA Hybrid Structures	143

APPENDICES

A	THE EQUATION OF MOTION OF SANDWICH PANEL	145
---	--	-----

B	CANTILEVER SANDWICH BEAM	155
	REFERENCES	160
	BIOGRAPHICAL SKETCH	165

Abstract of Dissertation Presented to the Graduate School
of the University of Florida in Partial Fulfillment of the
Requirements for the Degree of Doctor of Philosophy

VIBRATION CONTROL BY USING SHAPE MEMORY ALLOY
IN COMPOSITES AND SANDWICH STRUCTURES

By

Chin Hai Lee

August 1993

Chairman: Dr. Chang-Tsan Sun
Major Department: Aerospace Engineering, Mechanics and
Engineering Science

The main objective of this study was to explore a new technique to improve the dynamic response and vibration characteristics of composite plates or beams by using shape memory alloy (SMA). Detailed descriptions of the making, testing, and modeling of SMA hybrid structures are reported in this paper.

The unique properties of SMA and its applications are described at the beginning. Analyses were made to determine the transient thermal response of SMA laminates activated by electric current. A finite element analysis to verify the activation of beam specimens is presented in the paper and shows good agreement with the test. A complete tooling, fabricating, and wire-straining device of the specimens is also developed.

An analytical tool was developed to calculate such properties of SMA hybrid laminates as the A, B, D matrices of in-plane, coupling, and bending stiffness.

A theoretical method of predicting the internal stress distribution of SMA hybrid laminates was also formulated under a fully activated condition of SMA wires. The classical lamination theory (CLT), combined with this method, gives a feasible approach to estimate stress-strain relations in the SMA hybrid laminates.

The dynamic responses of SMA hybrid laminated beams (thin laminates) were tested experimentally. The results showed evidence of natural frequency shifting for beams with clamped-clamped boundary condition. The failure rate of the experiment was high due to the particular boundary condition, and other boundary conditions were not investigated.

Finally, a dynamic model based on large deformation theory was derived for the SMA hybrid composite sandwich beam. This model can predict the natural frequencies at first order nonlinearity and the dynamic response under harmonic excitations. Analytical results showed good improvements in the beam vibration suppression under hinged-simply supported boundary condition. Parametric studies revealed that the in-plane forces induced by embedded SMA wires in composites were the major contributor in beam vibration control under the said boundary condition.

CHAPTER 1 INTRODUCTION

1.1 Backgrounds of The Project

There have been many problems in dealing with vibration control in every engineering field. The relevant techniques in solving vibration problems fall into two major groups; passive vibration control and active vibration control. Passive vibration control has been widely used in structure components of spacecraft, aircraft, ships, ground vehicles, rotating machines, buildings, bridges, and so on. Simply, passive vibration control uses tuned masses, viscous dampers, dashpots, or visco-elastic tapes fixed on the structure's components to alter the damping level and the system response. Active vibration control, on the other hand, uses sensors to measure the structure's response and generate signals to the feed-back control block to activate actuators [1]. Materials having both sensors and actuators in closed loop control are called adaptive materials. The active vibration control systems possess both sensors and actuators which, fastened on structure components, constitute what is called an adaptive structure.

New kinds of materials, called smart materials, have come to play a more important role in the last decade. Smart

materials [1] have unique abilities to change their physical properties and geometries (i.e., stiffness, damping, viscosity, shape, etc.) in response to certain stimuli. At this time, optical fibers, piezoelectric polymers, piezoceramics, electro-strictors, electro-rheological fluids, shape memory alloy (SMA), and magnetostrictors are examples of some smart materials most often studied. It is said that adaptive materials and structures are a subset of smart materials and structures [1].

Smart structures [1] have embedded or bonded intrinsic sensors which recognize and measure the intensity of the stimuli. These stimuli may be stresses, strains, temperatures, electrical voltages, magnetic fields, chemical compounds, or radiation. Smart structures have embedded or bonded intrinsic actuators that can respond to stimuli. Smart structures have certain mechanisms for controlling the responses to the stimuli according to a predetermined relationship and are capable of selecting the best response if more than one option is available.

In the last decade, adaptive structures have shown great potential for modal control of large space structures or for use in certain mechanical devices. Smart materials are employed to reach full adaptive control of the dynamic responses of structures, such as space cranes, robot arms, and similar mechanisms. Smart materials have not only reduced the weight of traditional adaptive actuators but

have stimulated the evolution of a new concept of dynamic property tuning in smart structures.

The shape memory alloy, used in the past decade on robot arms [2], has proven to be an effective actuator because of its simple construction and smooth mobility. The utilization of SMA enables the designer to reduce the complexity of mechanical elements. In addition, the facts that it has long fatigue life and corrosion-resistant capability have made the material more useful to engineering applications. To activate the SMA requires heat, a common form of energy. Heat can be generated by electric current through SMA wires in the same way as electric current through electric resistors generates heat. Through thermal activation, the SMA hybrid structures can change its stiffness and material strength as well as the structure's natural frequencies.

A large structure has many spars, rods, and beams. For instance, the structure may be a truss or a drawbridge. The modal response of a drawbridge would change if only one property (e.g., stiffness, strength) of one element of the structure changed. A light structure possessing many members may not be strong or stiff enough to withstand changing external loads, or a stiff structure is strong but too heavy. By replacing a few of the components with SMA hybrid beams, one could achieve the purpose of improving the dynamic responses of the structure. Therefore, because of

weight saving, it could be more efficient to use the SMA material for dynamic control.

1.2 Special Features of SMA

There are two types of solid state transformation of materials. One is diffusional transformation, where migrating atoms randomly form a new phase with a different chemical composition from the original matrix. This progression of transformation is dependent upon both time and temperature. The other transformation is displacive transformation, which does not require either atomic migration or change in the chemical nature of the matrix to alter its solid state. Instead, its crystal structure is merely rearranged into a more stable one. This displacive progression of transformation is only dependent upon temperature [2].

An example of displacive transformation is the austenite \leftrightarrow martensite phase transformation of SMA. The 2-D diagram, Figure 1.1 schematically shows the progression of transformation from one phase to the other. The volume fraction of martensite increases as temperature decreases at the parent, or austenite phase. In the austenite phase, each atomic layer is packed together in a rectangular shape, and each fine layer tilts to achieve the twinned martensite phase. This phenomenon is called Bain strain [2].

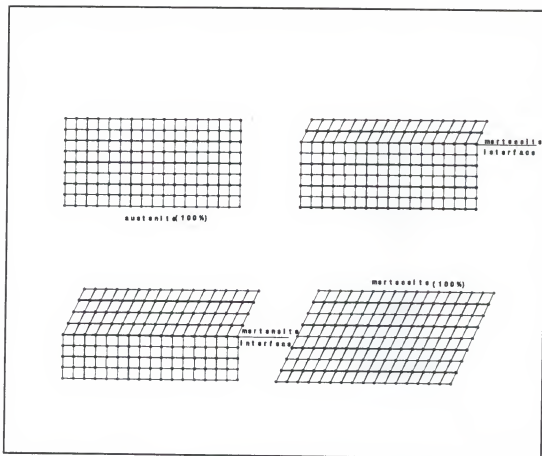


Figure 1.1. Displacive transformation of austenite to martensite [2]

Nickel-titanium (Ni-Ti) alloy (Nitinol) is a kind of polycrystal SMA. The metal crystal structure has grain boundaries in both phases [3]. It is stiffer than most of the SMA products currently available. This particular material is applicable in the fields of actuators, electrical connectors, and fasteners. It also has superior characteristics in corrosion-resistance.

In general, this Nitinol-type of shape memory alloy will undergo an accommodation step. The change in lattice shape is not merely caused by Bain strain because the other

layers of austenite may not always change to the slant typical of martensite, shown in Figure 1.1, but may accommodate themselves to a more relaxed shape, dubbed twinning. Figure 1.2 shows the general shape of martensite after cooling, and the shape-changing process is reversible. This phenomenon is called lattice invariant shear [2].

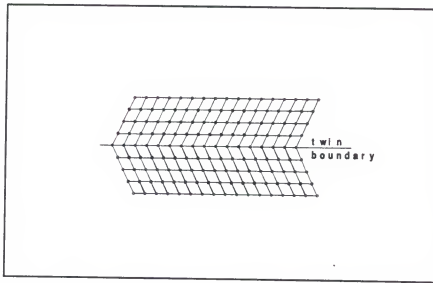


Figure 1.2. Twinning of shape memory alloy

The twinning process plays a key role in the shape memory effect. We can see from Figure 1.2 that the boundary at each fine plate (four thin plates above and four thin plates below the midplane [2]) slants at a different angle, but still has all the atomic bonds intact without slippage. The energy state of this condition is very low, and it becomes very mobile.

An optical micrograph by Duerig et al. [2] of surface relief due to the formation of martensite in a Cu-Zn shape memory alloy shows the twinning stage [2] and better depicts the true twinning shape in contrast to the 2-D lattice diagram shown previously in Figure 1.2. This phenomenon, true in fine plates of molecular structures, is also true in thicker plate sizes up to the entire crystal structure.

Twinning in ordered alloys is not always impossible, as Cu-Al-Ni martensite shows both $\{121\}_{r1}$ and $\{101\}_{r1}$ twinning [3]. Cu-14Al-3Ni is a type of single crystal SMA, where the stress-assisted transformation (stress induced martensitic transformation) produces a typical example of memory effect. At $T < M_f$ (where T is the temperature at which stress is applied, M_f is martensite final temperature), the true activation temperature of 130°C is higher than that of non-stress induced martensitic transformation. Yet, at $M_s < T < A_f$ (where M_s is the martensite starting temperature and A_f is the austenite final temperature), the true activation temperature becomes lower (approximately 100°C). Therefore, the twinning can be easily changed into deformed martensite alloy by applying stresses or by heating up to austenite alloy as shown in Figure 1.3. For example, a twinned martensite SMA wire, like Cu-Zn single crystal material,

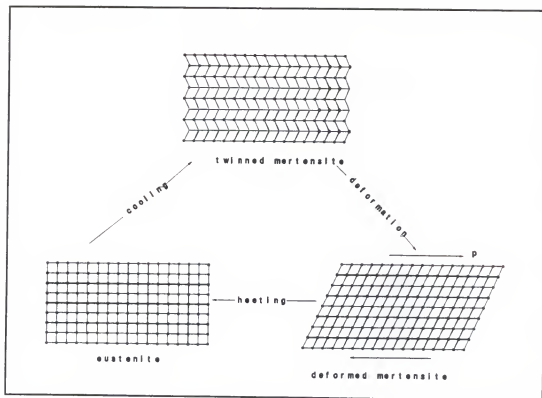


Figure 1.3. Shape memory process shown microscopically

deforms plastically (pseudoelastic deformation) under a tension load above M_s (martensite-starting temperature). The deformed crystal length tends to shrink when heat is applied, as if the heat energy is absorbed by the crystal to pack itself more tightly to achieve a higher energy state (austenite state). This phenomenon is the memory effect found in most of the SMA materials. In addition, the single crystal SMA usually has a better memory effect than that of a polycrystal SMA [2].

This phenomenon clearly explains why Nitinol wire, which deforms plastically above M_s (approximately 70°F) at

a constant load "P," must shrink back to austenite phase when heat is applied. It also indicates that properties of the wire will have changed at the activation temperature.

1.3 Outline of This Study

The research [1] reports that SMA wires can be embedded in various kinds of composite materials, resulting in vibration suppression, to change structure stiffness to avoid resonance [1,4], for acoustic vibration control [5], and for working as a geometry variation device.

The objective of the study is to seek an effective way to suppress vibration by using SMA as an actuator in a composite structure. Five major areas of studying SMA hybrid composites are described in this paper. These are: [Thermal response of SMA hybrid composites; The fabrication of SMA hybrid specimens; Stress-strain in SMA hybrid laminate; Dynamic test of SMA hybrid laminates; The dynamic model of SMA sandwich structure].

1.3.1 Thermal Response of SMA Hybrid Composites

Analytical means were introduced [6] by employing the Finite Difference Method to analyze the transient thermal response of a SMA-graphite/epoxy beam. The beam temperature is the only key related to the activation/deactivation of the hybrid structure. The author uses the thermal analysis

module in ANSYS¹, based on the modeling method described by Hawkins et al. [6], to investigate the temperature in the beam cross section. The specimens, made of SMA-fiber glass/epoxy, were also tested to compare with the analytical thermal response. Results are reported in Chapters 2 and 4.

1.3.2 The Fabrication of SMA Hybrid Specimens

The SMA wire embedding concept is described by Rogers and Barker [4]. Based on this concept, the author developed a different wire-straining and fabricating method for the SMA hybrid laminate. Details is presented in Chapter 3.

1.3.3 Stress-Strain in SMA Hybrid Laminate

Because the hybrid laminate performs differently from that of the general composite laminate, the hybrid lamina properties must be calculated in a different fashion [7]. The compound effect of the composite thermal stress, the boundary stress, and the special recovery stress [2] of SMA wires produce the laminate in-plane force [7] when the activation occurs. As a result, the combined effects of both in-plane force and internal stress at the SMA/composite interface present a complicated stress-strain problem. The author made a first attempt to estimate the internal stress distribution by using the principles of solid mechanics as Detailed in Chapter 5.

¹: ANSYS is a finite element package for structural, and thermal analysis

1.3.4 Dynamic Test of SMA Hybrid Laminates

The test work by Rogers and Barker [4] and Saunders et al. [5] showed the phenomenon of natural frequency shifting at the activation temperature. The author uses the same concept, with different SMA-composite laminate, to verify the natural frequency change. The modal test results are listed in Chapter 6.

1.3.5 The Dynamic Model of SMA Sandwich Structure

There are several studies of SMA hybrid laminated beams and plates, but none of them has involved the employment of SMA in a sandwich structure. The author used the nonlinear approach, based on the proven theory, to find the governing equations of the SMA composite sandwich panel. The complete derivations and the analytical results are discussed in Chapter 7.

CHAPTER 2 SMA HYBRID COMPOSITE PLATE

2.1 Application of SMA Hybrid Laminates

Vibration suppression can be achieved by using the SMA active strain energy tuning (ASET) method [1,4], where the SMA wires are plastically elongated [2] prior to being embedded in a composite structure. This gives the structure the ability to create large distributed loads in the composite material upon heating. The wires are generally placed in the structure in such a way that no bending deflection will occur during the activation (heating) process. Instead, the structure is placed in a residual state of strain. The resulting stored energy changes the modal response of a structure in a way similar to that of a guitar string [4]. The result is, the natural frequencies of the hybrid laminate increase at the activation temperature. This is a direct use of shape memory effect as described in Figure 1.3 of Chapter 1.

2.2 ASET Set-Up Concept

The author used a specimen [0/90/SMA/0/90]_s SMA-GF/EP hybrid composite laminate beam (GF/EP: glass fiber

unidirectional prepreg). The embedded SMA was heated up to accomplish the transformation from the martensitic phase to the austenite phase. During this procedure, the Young's modulus changes by a factor of three. The heating process is accomplished by running an electric current through the wire. This procedure is shown schematically in Figure 2.1.

The consolidation process of composite laminate in fabrication [4] can affect the mechanical behavior of the SMA actuators, because the wires are constrained from moving during the cure cycle by clamping each wire to the curing plate. A clamped-clamped hybrid composite beam (Figure 2.2), has a constant current power supply controlled manually to bring the temperature of the beam (activation) to the desired austenite finish temperature.

An electromagnetic displacement transducer is used to sense the dynamic response of a composite beam. It can convert analog data to digital data and transmit it to a data acquisition system for modal testing [4,5].

2.3 Thermal Response of SMA Hybrid Beam

The author chose Nitinol wire as the SMA wire for use in the hybrid composites. The SMA metal content is 55% nickel and 45% titanium. The SMA density is 6.45 g/cm^3 . The Melting point of SMA is 1240°C - 1310°C . The SMA Young's modulus E_a for the austenite (parent phase) is $11.0\text{E}06 \text{ psi}$.

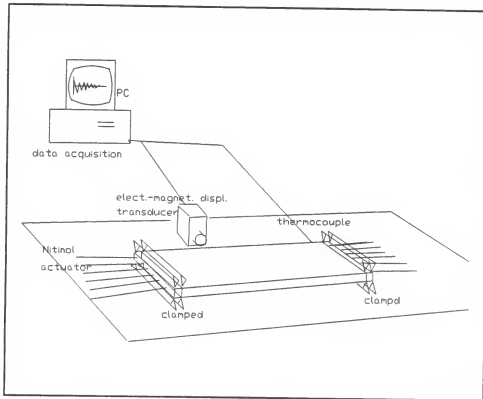


Figure 2.1. Active Strain Energy Tuning test set

The SMA Young's modulus E_m for martensite (twined material phase) is $3.5E06$ psi. The SMA Wire diameter is 0.01". Data source is from the manufacturer, Precision Wire Corporation [8].

The SMA wires are heated to activate and cooled to deactivate. The speed of adaptability is governed solely by the thermal activation and deactivation times for the SMA hybrid composite beam. Hawkins et al. [6] reported that an impulse electric power supply can effectively activate a hybrid beam in a short time. The energy supply can then be cut back to sustain the activation temperature.

Because of the strong relations between the activation time and the dynamic response, a thermal analysis of the hybrid composite is necessary [6]. Furthermore, a series of tests on real specimens is imperative to verify the transient thermal response inside the hybrid composite beam.

The theoretical approach to transient thermal response [6] is shown in Figure 2.2. Equation (2.1) describes heat conduction in the hybrid laminate, with heat source q (generated by electric resistance heating) of a SMA wire. The q (volumetric heat) is the energy that functions as an active force for the SMA actuator.

$$\frac{\partial}{\partial x} (k_x \frac{\partial T}{\partial x}) + \frac{\partial}{\partial y} (k_y \frac{\partial T}{\partial y}) + q = \rho c_p \frac{\partial T}{\partial t} \quad (2.1)$$

Equation (2.2), where

$I(t)$ = current (amp);

R_e = electric resistance (ohm), $R_e = \rho_e * L / l^2$;

ρ_e = electric resistivity;

V_w = volume of $\frac{1}{4}$ wire (m^3) = $l^2 L$;

l^2 = $\frac{1}{4}$ SMA cross sectional area;

L = SMA unit length (set to 1");

$$q = \frac{I^2(t) R_e}{V_w} = \frac{I^2(t) \rho_e}{l^4}, \quad (\text{the actuator}) \quad (2.2)$$

$$= 0, \quad (\text{the composite}).$$

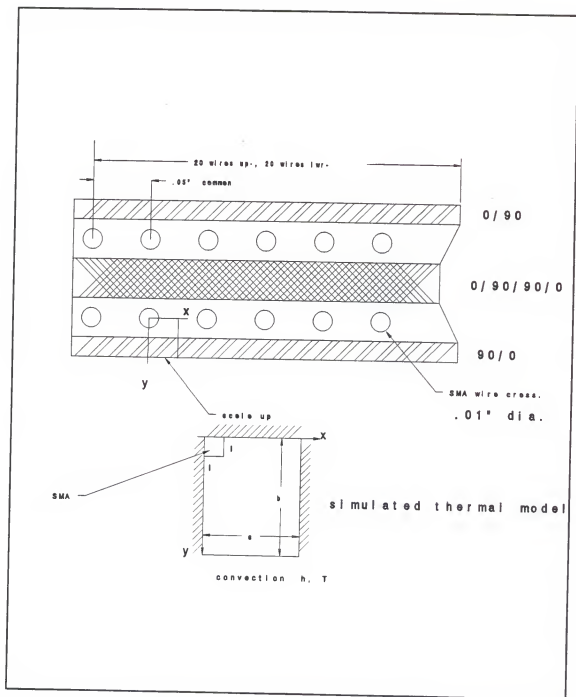


Figure 2.2. Cross section of a hybrid laminate and a thermal model

Choosing the following non-dimensional terms, we obtain

$$X = \frac{x}{l}, \quad Y = \frac{y}{l}, \quad \tau = \frac{t}{l^2} \frac{k_{cy}}{(\rho C_p)_c} \quad (2.3)$$

$$\theta = \frac{T - T_a}{A_f - T_a}, \quad \theta_{mf} = \frac{M_f - T_a}{A_f - T_a} \quad (2.4)$$

θ = range from 0 to 1;

x = range from 0 to a ;

y = range from 0 to b ;

t = real time (hr. or sec.);

τ = non-dimensional time;

M_f = Martensite final temperature;

A_f = Austenite final temperature;

T_a = ambient temperature.

$$K_x = \frac{k_x}{k_{cx}}, \quad K_y = \frac{k_y}{k_{cy}} \quad (2.5)$$

$$C = \frac{\rho C_p}{(\rho C_p)_c} \quad (2.6)$$

$$Q(\tau) = \frac{l^2 \rho_a}{l^2 k_{cy} (A_f - T_a)} \quad (2.7)$$

$k_x = k_w$, thermal conductivity in actuator (SMA) at 0° ,
 $k_x = k_{cx}$, thermal conductivity in composite at 0° ,
 $k_y = k_w$, thermal conductivity in actuator (SMA) at 90° ,
 $k_y = k_{cy}$, thermal conductivity in composite at 90° ,
 $C_p = C_{pw}$, heat capacity in actuator (SMA),
 $C_p = C_{pc}$, heat capacity in composite.

By substituting the previous terms in equation (2.1), the equation is converted to the non-dimensional equation

$$\frac{\partial}{\partial X} (K_x \frac{\partial \theta}{\partial X}) + \frac{\partial}{\partial Y} (K_y \frac{\partial \theta}{\partial Y}) + Q(\tau) = C \frac{\partial \theta}{\partial \tau} \quad (2.8)$$

the boundary conditions and initial conditions, according to Figure 2.2, are

$$\frac{\partial \theta}{\partial X} = 0, \text{ at } X=0, A, \text{ where } A = \frac{a}{l}. \quad (2.9)$$

$$\frac{\partial \theta}{\partial Y} = 0, \text{ at } y=0 \quad (2.10)$$

$$-\frac{\partial \theta}{\partial Y} = B_i \theta, \text{ at } y=B, \text{ where } B = \frac{b}{l} \quad (2.11)$$

$$\theta = 0, \text{ at } \tau = 0 \quad (2.12)$$

and

$$B_i = \frac{h l}{k_{cy}} = \text{Biot number}. \quad (2.13)$$

The Biot number represents the heat convection from the beam surface to the ambient air ($T_a = 70^\circ\text{F}$). The non-dimensional equation can be solved by the Finite Difference Method or by a commercially available thermal analysis package. The author used ANSYS to verify the transient thermal response for the experimental specimen.

For comparison purposes in thermal analysis, a verification experiment measuring the transient thermal response of using an experimental specimen is very important. Analysis of the said heat conduction equation (2.8) can explicitly show us the nondimensional temperature rise and fall during SMA wire activation-deactivation process Hawkins et al. [6]. The solution can also show that the required electric power can rapidly activate the beam, and the vibration control may be achieved in a proper time span. Theoretically, an electric impulse can quickly activate the hybrid beam ([6] at various Biot numbers) and at different beam constructions. However, the technique for deactivating a hybrid structure may pose a problem, because the ambient environment is potentially changeable that a cost-effective heat dissipation device can be difficult to design.

CHAPTER 3 THE SPECIMEN FABRICATION AND TESTING PLAN

3.1 Specimen Fabrication of SMA Hybrid Beam

The reason behind the use of SMA wires in composite laminates is its ability to increase stiffness in composite beams. The author used composite laminates because the SMA hybrid aluminum plate or hybrid steel plate, made with aluminum or steel mixed with the SMA wire, has too high a melting point and the properties of the wire are completely destroyed, because SMA no longer preserves its quality at the martensite phase or remembers its features at the austenite phase. The curing temperature for the graphite/epoxy composite is only 350°F (177°C), so the difference between room temperature and curing temperature (autoclave) is only about 250°F to 300°F (120°C to 150°C) [3]. Therefore, they are still on the safe side of SMA operating range, which is around 170°C, and the properties will scarcely be affected in the fabrication process.

In the experiments, we found some uncertainties in the properties of the hybrid beam before and after fabrication. For the first batch of specimens, the wire was fixed on the tool plate [6] and not strained to 5-6% as recommended by Rogers et al. [7]. Trial and error taught us not to

overstrain the wires, instead to permit them to resume the austenite phase first and cool before embedding in prepregs. The second batch of specimens were made by a modified wire-straining tool and fabrication tool, which can strain the wires to 10%, and this was found to be satisfactory.

3.1.1.1 Selection of Fabrication Tool

The tool materials and how they are set up are very important factors affecting the produced specimen. First, the author listed some important physical properties and mechanical properties of the Nitinol SMA. The following data are provided by the Precision Wire Company [8]:

3.1.1.1.1 Properties of Nitinol

Physical properties

Density.....	6.45 g/cm ³ , 0.234 lb/in ³
Electrical resistivity.....	76 microhm-cm (Martensite)
	82 microhm-cm (Austenite)
Coefficient of	$6.6 \times 10^{-6}/^{\circ}\text{C}$ (Martensite)
Thermal expansion	$11.0 \times 10^{-6}/^{\circ}\text{C}$ (Austenite)
Thermal Conductivity.....	0.17 watt/cm- $^{\circ}\text{C}$ (K_x)

Mechanical properties

Ultimate Tensile Strength..	125 ksi
Yield Strength	80 ksi (Austenite)
	10 ksi (Martensite)

Elongation.....	60 percent (Martensite)
	20 percent (Austenite)
Young's Modulus.....	3.5×10^6 psi (Martensite)
	11.0×10^6 psi (Austenite)
Hardness.....	42 HRA
Poisson's Ratio.....	0.33

Other factors

Stock size used (in shop)..	0.01" diameter wire
	(micrometer measured)
Cost/per foot.....	approximately \$1.31 (1992)
Martensite final (M_f)....	approximately 20°C
Austenite start (A_s)....	38°C (100°F)
Austenite final (A_f)....	130°F to 290°F

Thermal Expansion Coefficient of GF/Ep

$$\alpha_1 = .045 \times 10^{-6} / ^\circ\text{C}$$

$$\alpha_2 = 20.2 \times 10^{-6} / ^\circ\text{C}$$

The hybrid laminate specimen [0/90/SMA/0/90]_s, shown in Figure 3.1, is 2.87cm x 20cm beam (first batch) for the transient thermal test and the dynamic test.

The base tool plate and the Nitinol wire-straining frame (Figure 3.2) should be steel, because steel has approximately the same thermal expansion coefficient as that of the austenite SMA. Therefore, steel alloy with thermal expansion coefficient of $11 \times 10^{-6} / ^\circ\text{C}$ and aluminum alloy with

thermal expansion coefficient of $22 \times 10^{-6}/^{\circ}\text{C}$) were used as the tooling materials.

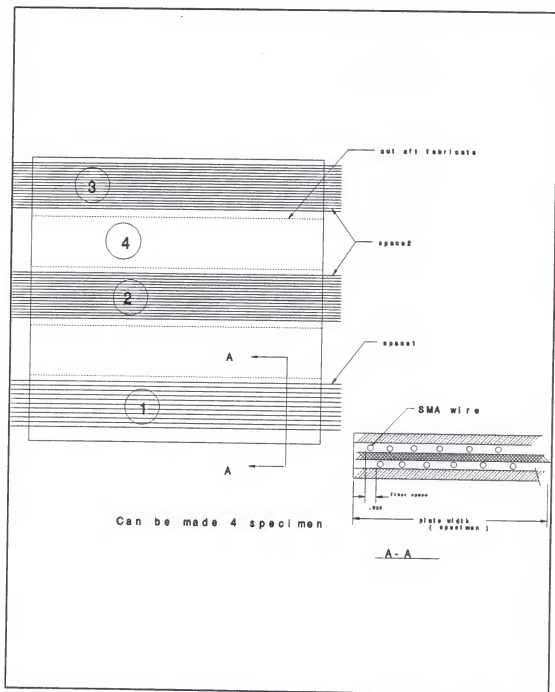


Figure 3.1. Specimen fabrication diagram (type 1 - no. 2,3; type 2 - no. 1)

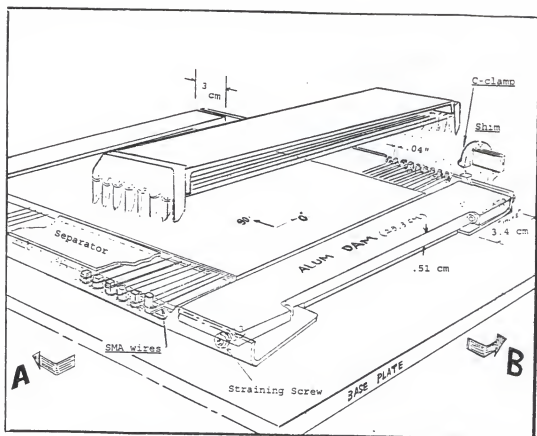


Figure 3.2. Perspective view of SMA wire-straining frame

3.1.2 Tool Design and Fabrication Procedure

The author used a 1.25 X 1.25 X 0.1" aluminum extruded L-shape beam, cutting teeth on it with a rotary hacksaw. The teeth are used for aligning SMA wires preparatory to burying the wires in the composite beam. Grinding and refining the teeth were done with a DREMEL miniature tool (large and small collet with various kinds of engraving bits or sanding bits to trim the teeth on the L-shape beam in Figure 3.2).

Two aluminum dams were cut to shape, and each was placed at the corner of the L-shape beam, forming a rectangular frame, as seen in Figure 3.2. Then, we aligned the four corners to drill through the L-shape beam and dams, Tapped the dams with internal threads for screw locking to strain the SMA wires before fabrication. Secondary base plates were cut and bonded to the right hand side of dams to fill the gap between the dams and the base plate.

The secondary base plate was trimmed to shape and put on the base plate to complete the basic frame assembly. Figures 3.2 and 3.3 show the perspective view and cross-sectional view. Each end of the dam was chamfered in order that a small adjusting wedge could be placed in it to strain the SMA wire to a specific elongation after the wire was wound around the small teeth of the L-shape beam. The author used compressed air to blow the metal crumbs away after trimming and sanding.

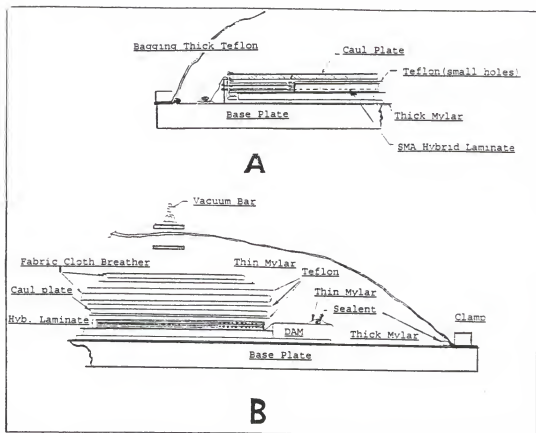


Figure 3.3. Specimen pre-curing bagging tool

The author used a 0.02"-thin aluminum separator to separate the upper and lower layers of SMA wires, as depicted in Figure 3.2 and Figure 3.3.

The caul plate must be made so that its edge could just fit against the L-shape beam to prevent cracking the tooth roots of the L-shape beam by excessive wire tension.

Finally, a thin sheet of mylar was placed on top of the whole frame and a release agent was sprayed on the mylar. Meanwhile, the whole frame and the SMA wires were cleaned with acetone. Then, a thick sheet of mylar was placed beneath the whole assembly. The Allen screw shown in Figure 3.2 can be adjusted to strain the wires which were ready for the embedding process.

3.1.3 First Batch Specimen Fabrication

The prepreg of GF/Ep uni-directional tape must be cleaned [9]. Any dirt, dust, or other foreign objects which come in contact with prepreg tape will cause voids within the hybrid composite laminates. Therefore, the base plate and wire-straining frame should be as clean as possible. The tool plate and the caul plate had to be sanded with number 200 or finer sandpaper until the surface was smooth with a dull shine.

The author covered the outside inch of the base plate with tissue or a wood frame before applying the mold release

agent. It is not desirable to have mold release agents on the outer inch of the base plate, for this area will be used to seal the vacuum bag on the base plate. The mold release agent was sprayed onto the base tool plate, both sides of the caul plate, the aluminum dams, and wire-straining frame. All of the sprayed pieces were placed in an oven and baked at 250°F (120°C) for approximately two hours.

Initially, before straining the wires between the opposite L-shapes, wire was wound on a hair-comb set (the same tooth size as the L-shape beams in Figure 3.2). Then, laid up the first two layers of GF/EP on thin mylar and the base plate, using a lamina cutting tool specially made to cut a lamina of a definite size. The wound wire was transferred from the hair comb set to the L-shape beam on top of the first two layers. Put the other six laminae on top of the wires. Transferred the upper layer SMA wires from another hair-comb set to the L-shape beam and placed the last two layers of laminae in position. This completed the lay-ups of the SMA hybrid composite laminate.

Next, the adhered instruments, such as the embedded thermocouple head or other connecting measuring devices, were cleaned with acetone and then calibrated.

Finally, bagging materials were wrapped on top of the wire-straining frame with the hybrid laminates for curing (Figure 3.3).

The fabricated hybrid laminate is a 20cm x 15cm rectangular laminate [0/90/SMA/0/90]_z (Figure 3.1), which then can be cut to the assigned specimen size. To do this:

- The SMA wire surface must be sanded (200 or finer grade) and cleaned with acetone after.
- A thermal-insulated coat may be required in order to shorten activation time for the SMA wire actuators.
- Spray release agent on the wires outside of the laminate for easy peeling off the bagging materials.
- A total of four specimens can be made. See Figure 3.1.

3.1.4 Second Batch Specimen Fabrication

It was decided that the wire straining frame for the first batch of specimens was not refined enough. Therefore, a new wire stretching tool was devised for more efficient fabrications. The new stretching tool and the new base plate/dam set for composite laminates are shown in Figure 3.4.

3.2 Specimen Testing Plan

- (1) The following items needed to be tested, either to verify the provided data [8] or to get more test information for the transient thermal response.

- Measuring Nitinol electric resistivity under the temperature ranging from 60°F to 220°F.
 - Measuring the heat conductivity of Nitinol and the whole specimen (which required a calorimeter)
- (2) The laminate beam must be clamped or simply supported at two ends. The modal test for the cantilever beam will be carried out for the first batch, type 1 only. Because the free end will be connected with electric jumper heads, the test data may not be accurate for the cantilever beam .

The author's test:

- The natural frequency
 - A. SMA hybrid laminated beam.
 - B. Gf/Ep laminated beam (no wires).
 - C. SMA hybrid beam with electric current at steady state beam surface temperature reaches austenite phase.
 - Damping coefficient with the above A, B, C conditions; Perkins [3] shows that SMA has lower electric resistance at -60°C.
- (3) The clamped support must be thermally insulated to assure that there is a minimum heat loss during the heating process. The insulation material may be polyurethane or some type of refractory felt. Another method is to apply an insulated pad while the hybrid laminate is activated, then remove the insulated pad at

the deactivation process or use airflow to cool down the hybrid laminate surface so the SMA wires can return to the martensite phase.

- (4) Electric current power supply:

The power supply should be impulse electric current, machine controlled manually. The diagram of Figure 2.1 shows the equipment of the wire connector, circuitry, the thermocouple, and the FFT dynamic response test devices [4-7].

3.3 Facilities for Specimen Fabrication, Testing

The facilities

- (1) Composite parts fabrication autoclave.
- (2) All the tooling materials and fiberglass/epoxy prepregs are available in shops.
- (3) SMA wire (300 feet total for first and second batch tests of SMA hybrid laminates).
- (4) Testing the natural frequency, and the damping (the data acquisition system in the structure laboratory).
- (5) Testing electric resistivity (a common multimeter).
- (6) An impulse electric current generator, to activate SMA wires.
- (7) Electric wire connecting devices, co-axial cables.

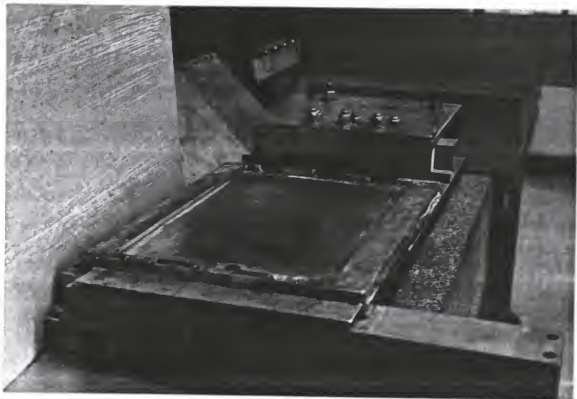


Figure 3.4. The L-shape beams with teeth, the base plate/Dam set, and the stretching tool at the far end.

CHAPTER 4 EXPERIMENT, ANALYSIS OF SPECIMEN TRANSIENT THERMAL RESPONSE

4.1 Analysis of Transient Thermal Response

The simulated thermal model is described in Figure 2.2. The x-axis is the width, and the y-axis is the depth of the SMA hybrid beam. Due to the symmetric wire and laminate combination, the small cell depicted in Figure 2.2 was used to verify the transient thermal response given by Hawkins et al. [6].

The simulated thermal model is used in predicting the temperature distribution (transient thermal response) in the said single cell of specimen type 1. By adjusting the DC power applied to the specimen, author could compare the ANSYS analysis results with the experimental results.

Using the ANSYS thermal analysis package, the author obtained the analysis results and printouts of (case 1a [6]) model and the specimen type 1 model. Diagrams of these plots of temperature distribution and the temperature-time can be seen in Figures 4.1, 4.2, and 4.3.

From the analysis results and plots, it was verified that the temperature inside the SMA hybrid composite laminate, as long as the laminate is thin compare to the

beam length, was constant and uniform at each time step (the temperature differences in diagrams were not much off from the SMA to the beam surface).

4.2 Experiment of Transient Thermal Response

The specimen for thermal response experiment was made from fiberglass prepreg with embedded SMA wires, which is described in the previous section. The facilities of testing were

- A K type (TT-K-36 SLE thermocouple wire, spot welded under 1.3 watt at the end), a SMP male connector(#1 style no.#10), a digital thermometer (model HHM59--K type)¹, and a thermocouple socket.
- A DC power source and a Triple output DC power supply 1660 (BK Precision Co.) were the power source for the activation of SMA wires.

The analysis tool for the transient thermal response is ANSYS. The geometry, density, and the thermal constants are listed as follows:

$$\begin{aligned}
 \rho &= 404.3 \text{ lb}_m/\text{ft}^3 && \text{(SMA wire)} \\
 l &= 0.005" = 1.27 \times 10^{-4} \text{ m} && \text{(SMA wire)} \quad [8] \\
 \rho_c &= 82 \times 10^{-6} \text{ ohm-cm} && \text{(SMA wire)} \quad [8] \\
 k_x &= 0.17 \text{ watt/cm/}^\circ\text{C} \text{ (thermal conductivity of SMA wire)} \\
 &\quad (9.82 \text{ BTU/hr/ft/}^\circ\text{F}) && [5] \\
 \rho_c &= 112.3 \text{ lb}_m/\text{ft}^3 && \text{(density of composite)} \quad [8] \\
 k_{cy} &= k_{cx} = k_x/15 \text{ (thermal conductivity of composite)} \quad [8] \\
 C_p &= 1757 \text{ joule/kg/}^\circ\text{K} = .3776 \text{ BTU/lb}_m/^\circ\text{F} \text{ (composite)} \quad [5] \\
 h &= 29.71 \text{ watt/m}^2/^\circ\text{K} = 5.232 \text{ BTU/ft}^2/^\circ\text{F} \text{ (composite)} \quad [5]
 \end{aligned}$$

¹Omega Technology, P.O. Box 4047, Stamford, CT 06907-0047

The experiment on SMA wire electric resistance to verify the electric resistivity provided by [8] and the connectivity of the wires inside the specimen was done at the laboratory (A common multimeter was used to measure the electric resistance). The specimen was the Type 1 plate with 20 SMA wires each on the upper layer and lower layers. Both the upper layer and lower layer wires at the first entry of the specimen were crimped. The cross section of the wire was $2A$ where A is a single wire cross-sectional area.

The calculated resistance

$$\rho_e = 76 \times 10^{-6} \text{ ohm cm} \quad (\text{martensite}) \quad [8]$$

$$A = \pi \times (0.005 \times 2.54)^2 = 5.067 \times 10^{-4} \text{ cm}^2$$

$$R = \rho_e / 2A = 0.075 \text{ ohm/cm}$$

There were 20 sets of wires in the specimen, each set is 22cm long. Therefore, $R_{\text{total}} = 0.075 \times 20 \times 22 = 33 \text{ ohm}$; the specimen test result is 34 ohm; and the error between the two data is $1/34$ or 2.9%. The result showed good agreement with calculated electric resistance.

The model dimension was measured from the specimen. The first batch test specimen (TYPE 1, SMA wire $V_f = 3.27\%$), and related data are listed in Table 4.1. The photograph of a real specimen is shown in Figure 4.5.

Table 4.1 Specimen data

TYPE 1	1.13"x7.88" , overstrained % SMA wires [0/90/SMA/0/90/90/0/SMA/90/0] FG/EP
TYPE 1 (base)	1.13"x7.88" , no SMA wire [0/90/0/90/90/0/90/0] FG/EP

The input data to generate the ANSYS plot in Figure 4.1 is listed in page 39, and the transient thermal response test/analysis comparison is in the Figure 4.4.

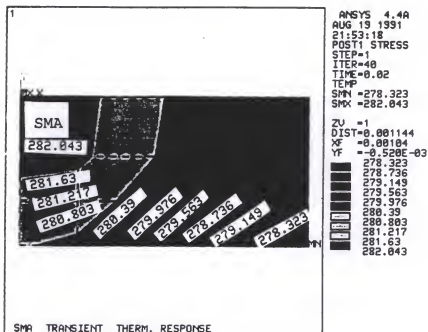


Figure 4.1. The temperature distribution from ANSYS result for (case 1a [6]) at $t = 0.02$ hr

$$A = a/l = 5.0, B = b/l = 2.5, l = 0.005''$$

A = width, B = depth

$$k_x = 9.82 \text{ Btu/hr/ft/}^\circ\text{F} \quad (\text{SMA})$$

$$\rho = 404 \text{ lbm/ft}^3 \quad (\text{SMA})$$

$$k_x = 0.655 \text{ Btu/hr/ft/}^\circ\text{F} \quad (\text{composite})$$

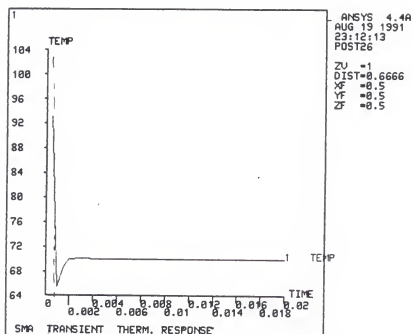
$$\rho = 112.3 \text{ lbm/ft}^3 \quad (\text{composite})$$

$$c = .3776 \text{ Btu/lbm/}^\circ\text{F} \quad (\text{composite})$$

$$T = 70^\circ\text{F} \quad (\text{ambient air})$$

$$h = 5.232 \text{ Btu/hr/ft}^2/\text{ft/}^\circ\text{F} \quad (\text{air convection})$$

$$q = 14471730 \text{ Btu/hr} \quad (\text{heat generation})$$



When blowing cool air across the beam surface, and $h = 5232 \text{ Btu/hr/ft}^2/\text{°F}$ (assumed). At $t = 0.0005 \text{ hr} = 2 \text{ sec}$, temperature drops fast.

Figure 4.2. The forced cooling of (case 1a [6]) from ANSYS

```

/PREP7
/TITLE, SMA TRANSIENT THERM. RESPONSE
KAN,-1
ET,1,55
KXX,1,9.82
dens,1,404.3
mptemp,1,70,172.4,187,215,256,300
mpdata,c,1,1,.108,.117,.18,.477,.126,.108
et,2,55
kxx,2,.655
DENS,2,112.3
C,2,.3776
N,1
N,2,-.00042
N,3,-.00073
N,4,-.00104
N,5,.00042
N,6,.00042,-.00042
N,7,.00042,-.00073
N,8,.00042,-.00104
N,9,.00125
N,10,.00125,-.00042
N,11,.00125,-.00073
N,12,.00125,-.00104
N,13,.00208
N,14,.00208,-.00042
N,15,.00208,-.00073
N,16,.00208,-.00104
type,1
mat,1
E,1,2,6,5
type,2
mat,2
e,2,3,7,6
e,3,4,8,7
E,5,6,10,9
EGEN,3,1,4
E,9,10,14,13
EGEN,3,1,7
ELIST
ITER,-40,1,1
time,.02
TUNIF,70.
KBC,1
KTEMP,-1
EC,3,2,5.232,70.,9,3
QE,1,14471730.
AFWRITE
FINISH
/INPUT,27
FINISH
/POST26
/SHOW,4107
DISP,2,12,TEMP
GRID,1
YLAB,TEMP
PLVAR,2

```

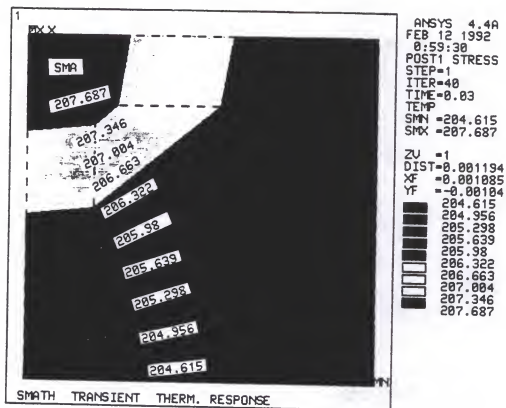


Figure 4.3. Thermal response of Type 1 specimen (first batch), $t = 0.03\text{hr}$, $I = 0.185\text{ amp}$.

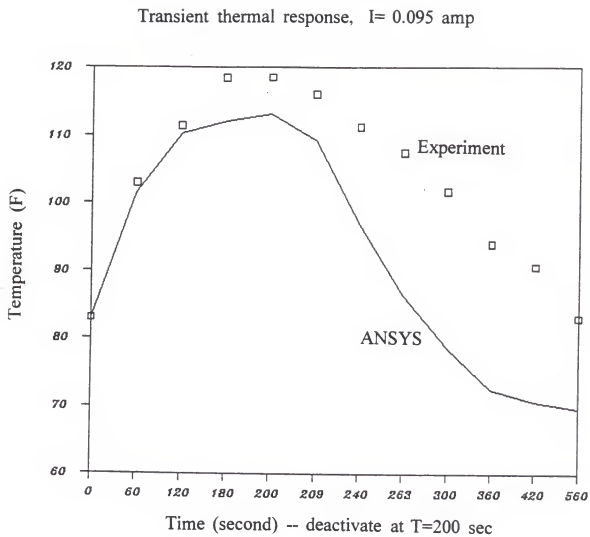


Figure 4.4. Thermal response of specimen (type 1), first batch. $I = 0.095$ amp.

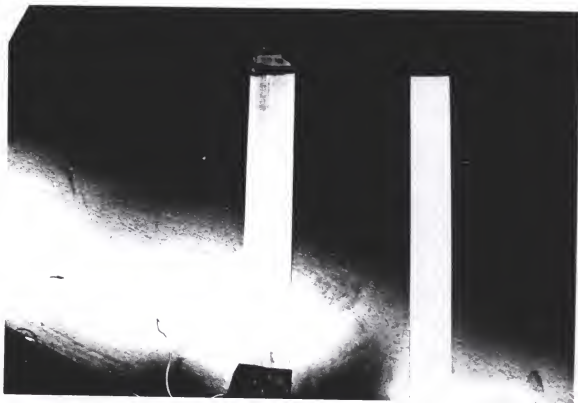


Figure 4.5. The first batch specimen (type 1) showing left end connected with wires for electric current.

CHAPTER 5
CONSTITUTIVE EQUATIONS OF SMA HYBRID
COMPOSITE LAMINATE

5.1 Stress/Strain in SMA Hybrid Composites

It is known that the conventional thin plate theory has been useful for predicting the stress/strain relations of the composite plate. The hygrothermal effects can also be calculated by using the conventional theories of composite plates to obtain ply strains and stresses, then, employing a failure criterion to determine whether or not failure will occur in a ply. The composite structure could be graphite /epoxy-Fiberglass/epoxy or combined Kevlar-graphite/epoxy laminate composed of orthotropic plies forming a homogeneous solid plate or beam.

The SMA hybrid composite is a totally different structure possessing composite plies with buried SMA wires. The SMA wire diameter is almost 25 to 30 times that of the reinforced fiber in a composite ply. By using the SMA wire, a new type of hybrid structure is formed with highly inhomogeneous properties and the SMA wires are often considered as inclusions in a composite structure. The SMA wires tend to shrink back to the austenite phase when activated by heating, which is why they must be strained

before curing. Thus, in this chapter, the stress/strain relation is still based on known theories, but the recovery stress will be emphasized in the following sections. The overall hybrid composite stiffness changes at different activation temperatures. At the activation temperature, the recovery stresses in SMA wires can create internal stresses at the interface of SMA and composite materials.

5.1.1 Thermal Strain of Laminate

The general expression of the strain in each lamina is given by

$$\begin{aligned}\epsilon_{ij} &= \epsilon_{ij}^M + \epsilon_{ij}^{th} \\ \epsilon_{ij} &= \epsilon_{ij}^M + \alpha_{ij} (T(t) - T_o)\end{aligned}\tag{5.1}$$

$$\theta(t) = (T(t) - T_o)$$

T_o = initial temperature before activation

$T(t)$ = transient temperature after activation.

According to the experimental results presented in Chapter 4, the temperature inside the hybrid laminate is fairly uniform at any time step. The strain of the plate containing the initial strain and curvature terms is represented by ϵ_{ij} . The subscript ij signifies the element in the column vector. The expression ϵ_{ij}^M is the mechanical strain of the K th layer which can produce stresses in each

ply, and α_{ij} is the thermal expansion coefficient of the K-th ply, which varies at different ply orientations. We can write (5.1) in matrix form as in (5.2) (see Agarwal [10]).

$$\begin{bmatrix} \epsilon_x^M \\ \epsilon_y^M \\ \gamma_{xy}^M \end{bmatrix}_K = \begin{bmatrix} \epsilon_x^o + ZK_x \\ \epsilon_y^o + ZK_y \\ \gamma_{xy}^o + ZK_{xy} \end{bmatrix} - \begin{bmatrix} \alpha_x^o \theta(t) \\ \alpha_y^o \theta(t) \\ \alpha_{xy}^o \theta(t) \end{bmatrix}_K \quad (5.2)$$

The extreme right bracket in (5.2) is the combined effect of recovery stress and thermal stress in a single lamina when SMA wires are embedded. We consider the recovery stress and induced ply stress in a global view at the moment. Time is represented by (t).

$$\begin{bmatrix} \sigma_x^M \\ \sigma_y^M \\ \tau_{xy}^M \end{bmatrix}_K = [\bar{Q}]_K^* \begin{bmatrix} \epsilon_x^M \\ \epsilon_y^M \\ \gamma_{xy}^M \end{bmatrix}_K ; [\bar{Q}]_K^* = [T]^T [Q^*]_K [T] \quad (5.3)$$

[T] = Transformation matrix

$$[Q^*]_K = (E_L^*, E_T^*, G_{LT}^*, \dots)$$

From reference [7]

$$E_L^* = E_m \frac{A_m}{A} + E_s \frac{A_s}{A} , \quad \begin{bmatrix} E_s = \text{SMA Young's modulus} \\ E_m = \text{comp. lamina modulus} \\ A_s = \text{SMA cross. area} \\ A_m = \text{comp. lamina cross.area} \end{bmatrix} \quad (5.4)$$

$$E_T^* = \frac{A E_{mT} E_{sT}}{A_m E_{sT} + A_s E_{mT}}, \quad E_{mT} = \text{transverse modulus} \quad (5.5)$$

$$\nu_{LT}^* = \nu_m \frac{A_m}{A} + \nu_s \frac{A_s}{A} \quad (5.6)$$

$$G_{LT}^* = \frac{A G_m G_s}{A_m G_s + A_s G_m} \quad (5.7)$$

Es: The SMA Young's modulus should be time dependent Es(t). It is not linear with respect to temperature from martensite to austenite phase, although it is linear from 100°F to 120°F during activation [1,2].

The above equation of lamina transverse stiffness properties could be modeled, according to Halpin-Tsai, Agarwal [10].

5.1.2 SMA Hybrid Laminate Strain

Therefore, from (5.2) to (5.7) we get

$$\begin{bmatrix} N_x \\ N_y \\ N_{xy} \end{bmatrix} = \int_{-h/2}^{h/2} \begin{bmatrix} \sigma_x^M \\ \sigma_y^M \\ \tau_{xy}^M \end{bmatrix} dz = [A^*] \begin{bmatrix} \epsilon_x^o \\ \epsilon_y^o \\ \gamma_{xy}^o \end{bmatrix} + [B^*] \begin{bmatrix} \kappa_x \\ \kappa_y \\ \kappa_{xy} \end{bmatrix} - \begin{bmatrix} N_x^{T^*} \\ N_y^{T^*} \\ N_{xy}^{T^*} \end{bmatrix} \quad (5.8)$$

$$\begin{bmatrix} M_x \\ M_y \\ M_{xy} \end{bmatrix} = \int_{-h/2}^{h/2} \begin{bmatrix} \sigma_x^M \\ \sigma_y^M \\ \tau_{xy}^M \end{bmatrix}_K z \, dz = [B^*] \begin{bmatrix} \epsilon_x^0 \\ \epsilon_y^0 \\ \gamma_{xy}^0 \end{bmatrix} + [D^*] \begin{bmatrix} \kappa_x \\ \kappa_y \\ \kappa_{xy} \end{bmatrix} - \begin{bmatrix} M_x^{T*} \\ M_y^{T*} \\ M_{xy}^{T*} \end{bmatrix} \quad (5.9)$$

The extreme right-hand term of (5.8) contains the thermal/recovery in-plane force N_x^{T*} and other terms; the extreme right hand term of (5.9) contains the thermal/recovery moment M_x^{T*} and other terms. The M_x^{T*} , M_y^{T*} , and M_{xy}^{T*} cease to exist if symmetric SMA lay-ups are formed.

$$\begin{aligned} [A^*] &= \int_{-h/2}^{h/2} [\bar{Q}]_K \, dz \\ [B^*] &= \int_{-h/2}^{h/2} [\bar{Q}]_K z \, dz \\ [D^*] &= \int_{-h/2}^{h/2} [\bar{Q}]_K z^2 \, dz \end{aligned} \quad (5.10)$$

$$\begin{bmatrix} A^* & B^* \\ B^* & D^* \end{bmatrix} \begin{bmatrix} \epsilon_x^0 \\ \epsilon_y^0 \\ \gamma_{xy}^0 \\ \kappa_x \\ \kappa_y \\ \kappa_{xy} \end{bmatrix} = \begin{bmatrix} N_x + N_x^{T*} \\ N_y + N_y^{T*} \\ N_{xy} + N_{xy}^{T*} \\ M_x + M_x^{T*} \\ M_y + M_y^{T*} \\ M_{xy} + M_{xy}^{T*} \end{bmatrix} \quad (5.11)$$

When the in-plane force and moment (external load) plus the thermal/recovery force and the boundary loads (SMA activation) as suggested by Agarwal [10] is applied on laminate, we are able to find the laminate strain as following.

$$\begin{bmatrix} \epsilon_x^o \\ \epsilon_y^o \\ \gamma_{xy}^o \\ \kappa_x \\ \kappa_y \\ \kappa_{xy} \end{bmatrix} = \begin{bmatrix} A^* & B^* \\ B^* & D^* \end{bmatrix}^{-1} \begin{bmatrix} N_x + N_x^{T*} \\ N_y + N_y^{T*} \\ N_{xy} + N_{xy}^{T*} \\ M_x + M_x^{T*} \\ M_y + M_y^{T*} \\ M_{xy} + M_{xy}^{T*} \end{bmatrix} \quad (\text{hybr. laminate strain})(5.12)$$

Note that in the column vector of previous equations or in the later equations, the superscript * of each term, represents laminate properties and the thermal/recovery stress change with respect to temperature. The temperature changes at each time step when the SMA wire in the laminate is activated or deactivated.

$$\begin{bmatrix} \sigma_x \\ \sigma_y \\ \tau_{xy} \end{bmatrix}_K (t) = [\bar{Q}]_K^* \begin{bmatrix} \epsilon_x^o \\ \epsilon_y^o \\ \gamma_{xy}^o \end{bmatrix} + z [\bar{Q}]_K^* \begin{bmatrix} \kappa_x \\ \kappa_y \\ \kappa_{xy} \end{bmatrix} \quad (5.13)$$

Therefore, due to the laminate strain, the Kth layer stress of (5.13) is primarily attributed to equation (5.14), which is the stress resultant of a 1-D beam. The symbols used in equation (5.14) are similar to those of equation (10) of Rogers et al. [7].

$$\begin{aligned}
 N_x^{T*} = & (1-K_r) \sum_{n=1}^N \sigma_r^{(n)} v_f^{(n)} (z_{n+1} - z_n) \\
 & + (1-K_\alpha) \sum_{n=1}^N \sigma_\alpha^{(n)} (1-v_f^{(n)}) (z_{n+1} - z_n) \\
 & + \sigma_o \sum_{n=1}^N (z_{n+1} - z_n) \quad (5.14)
 \end{aligned}$$

The N layers of hybrid laminate have recovery stresses which are intermingled with thermal stresses. With the additional boundary stresses, the stress resultants can be estimated as shown in equation (10) of Rogers et al. [7].

$$\begin{aligned}
 \sigma_r^{(n)} &= \text{recovery stress} \\
 K_r &= \text{nitinol boundary condition} \\
 \sigma_\alpha^{(n)} &= \text{Thermal stress} \\
 K_\alpha &= \text{thermal boundary condition} \\
 \sigma_o &= \text{Boundary stress}
 \end{aligned}$$

The thermal boundary condition $K_t = 0.77$ is for "rested" SMA hybrid composite beam, and the SMA boundary condition is $K_r = 0.71$ from the test results of Rogers et al. [7].

The term N_x^{T*} in equation (5.14) is the induced in-plane force in x-direction of a beam structure. The N_y^{T*} and the N_{xy}^{T*} will be presented in 2-D SMA hybrid plate structure, if there are no bending and twist moments induced by nonsymmetric activations. The equation (5.14) must be calculated prior to being inserted in equations (5.11) and (5.12) along with the applied external loads N_x , N_y and N_{xy} to obtain the hybrid laminate strain. Then, we obtain ply stresses at different time steps as described in equation (5.13).

The said expressions, however, are not adequate to determine what happens at the interface between each single SMA wire and the composite. Therefore, another approach is necessary to get N_x^{T*} and other terms. This includes looking into the internal stress distribution caused by SMA recovery stresses, which will be discussed in the next section.

The in-plane force, such as the N_x^{T*} , is the stiffening force in a beam structure. Because of the in-plane force, the stored elastic energy of a beam structure can increase tremendously.

5.2 Internal Stresses of SMA Hybrid Beam

The SMA wires generated large recovery stresses at activation, yet the internal stresses induced by the recovery stresses could not be found by conventional methods. Therefore, the sole objective of this section was to find compressive stresses and shear stresses attributable to the SMA wire activation.

Nomenclature

- C = cross-sectional width of composite strip
- r_s = SMA wire cross-section radius
- d_0 = SMA wire free shrinkage length (ref. to strain)
- σ_R = SMA recovery stress (uniform at cross section)
- σ_c = compressive stress of composite strip ($\sigma_c = \sigma_{zz}$)
- τ = shear stress of composite strip ($\tau = \tau_{xz}$)
- τ_0 = shear stress at SMA, composite interface

5.2.1 Stress Distribution at Interface

During activation, the SMA wires tend to shrink inside the laminated composite, but the composite prevents the SMA from recovering its original length ($L-d_0$). The stresses at each cross section tend to balance out one another under cantilevered boundary condition, as Figure 5.1 shows.

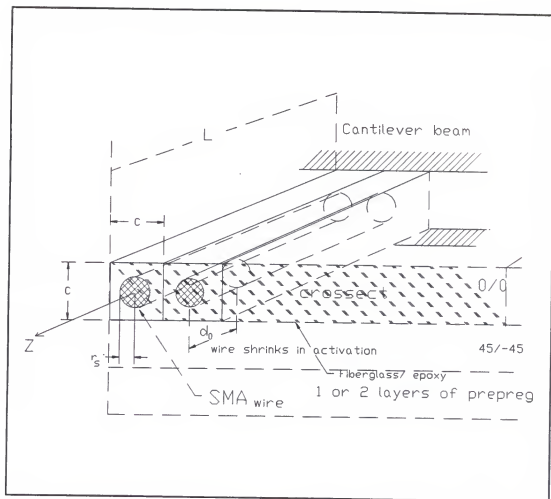


Figure 5.1. 3-D view of SMA hybrid composite beam at activation temperature

The SMA hybrid composite strip ($C \times C \times L$) in Figure 5.1 contains one or two layers of composite laminae (in this case, fiber orientation is along the SMA wire). Effective material properties are assumed homogenous but orthotropic in z, r, θ directions. The SMA wires with $r_s = 0.005$ " are all uniformly allocated in the composite beam; the two SMA wires

in Figure 5.1 are representative of still other wires not shown in the diagram.

Because the net in-plane force should be zero at any cross section ($z=z_0$) under cantilever boundary condition, the in-plane forces must balance each other between the SMA wire and the composite strip. The SMA is stretched by the composite strip and the composite strip is compressed due to the shear stress exerted by the SMA wire longitudinal interface (see Figure 5.1). (It should be noted that the in-plane force may not be zero under clamped-clamped or simply-supported boundary conditions.)

It is possible to use stress equilibrium equations (equations of motion) to find stresses in this region. According to Malvern [11, 1.1.2], the theories of elasticity and plasticity, which are based on the concept of continuous material, lead to quantitative predictions. These agree closely with experience over a wide range of conditions. Since the strip is continuous and is assumed to have no voids or flaws in the composite strip, we can use the equation of motion [11, p.668 (II.4.C10), (II.4.C11)] to solve the problem. Practically, Poisson's ratio could be ignored in beams.

Based on the above assumptions, the significant stresses in the strip region are σ_{zz} and τ_{xz} , which can be seen in Figure 5.2. (stress σ_{zz} will be dubbed σ_c and stress τ_{xz} will be called τ .) In the Figure 5.1 and 5.2, we pick

one composite strip containing one SMA wire, as a force equilibrium model. In this model, the interface between the SMA and the strip is shear stress τ_{rz} caused by the SMA wire shrinking effect (recovery stress).

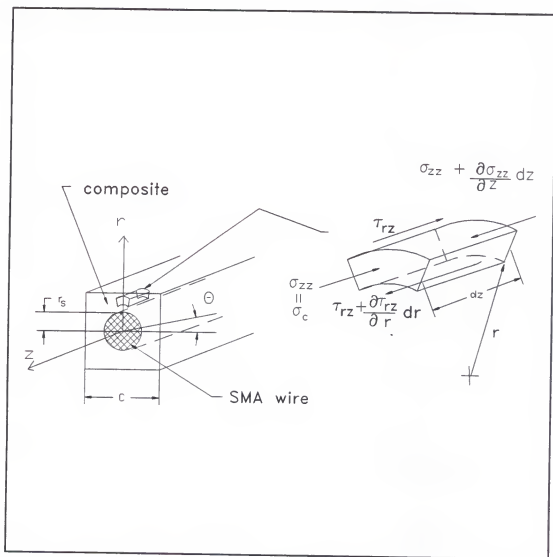


Figure 5.2. Stress diagram in strip at activation temperature.

The body forces and the inertia terms due to acceleration are negligible. By neglecting the stress terms σ_{rr} , $\sigma_{\theta\theta}$, $\tau_{r\theta}$, $\tau_{z\theta}$, the equations become

$$\frac{\partial \tau_{rz}}{\partial z} = 0 \quad (5.15)$$

$$\frac{\partial \tau_{rz}}{\partial r} + \frac{\partial \sigma_{zz}}{\partial z} + \frac{\tau_{rz}}{r} = 0 \quad (5.16)$$

At this point, there are only two non-trivial equations left. Equation (5.15) shows the following: $\tau_{rz} = f(r)$, the shear stress, induced by the SMA recovery stress, is constant along the z-axis, and it is only a function of r.

The second equation (5.16) can also be derived by the stress equilibrium diagram (Figure 5.2)

$$\begin{array}{c} \tau_{rz} \\ \longleftarrow \\ \sigma_{zz} = \sigma_c \longleftarrow \boxed{} \longrightarrow \sigma_c + \partial \sigma_c / \partial z \, dz \\ \longleftarrow \\ \tau_{rz} + \partial \tau_{rz} / \partial r \, dr \\ \longleftarrow dz \longrightarrow \end{array}$$

$$\text{set } \tau_{rz} = \tau ,$$

$$- (\tau + \partial\tau/\partial r \, dr) (r + dr) \, d\theta \, dz + \tau \, r \, d\theta \, dz = \\ (\sigma_c + \partial\sigma_c/\partial z \, dz) \, r \, d\theta \, dr - \sigma_c \, r \, d\theta \, dr$$

$$\therefore \frac{\partial \sigma_c}{\partial z} + \frac{\partial \tau}{\partial r} + \frac{\tau}{r} = 0 \quad (5.17)$$

Since $\tau = f(r)$, Equation (5.17) can be written as

$$\sigma_c(z, r) = \left(-\frac{\partial f(r)}{\partial r} - \frac{f(r)}{r} \right) z + C_0 \quad (5.18)$$

The shear stress distribution $\underline{f(r)}$ (τ_{rz}) is induced by the SMA recovery stress $\underline{\sigma_R}$. Therefore, by using the force balance diagram in Figure 5.3, we are able to find a relation between σ_R and τ_{rz} .

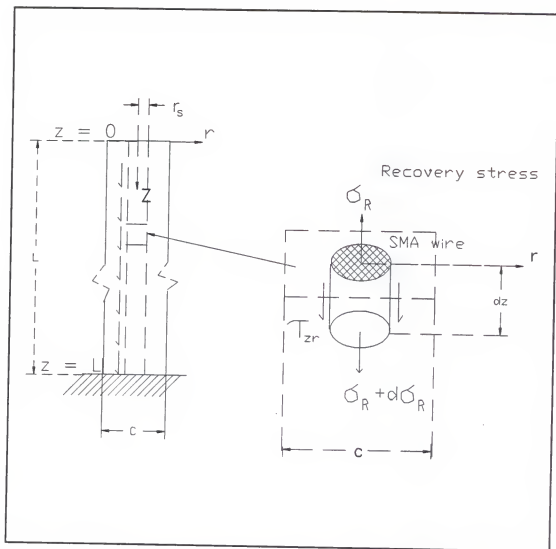


Figure 5.3. Recovery stress, shear stress diagram

Agarwal [10, (p.72,73)] cites the most quoted theory of stress transfer, the shear lag analysis. The SMA wire diameter (0.025 cm) is much bigger than the E-glass or the S-glass fiber diameter (0.001 cm = 10 μ m) Agarwal [10, p.17]. If the composite strip is treated as homogeneously

reinforced polymer matrix surrounding the SMA wire, the wire behaves as a fiber in the described shear lag principle. Also, Piggott et al. [12, (p.110,111 Fig 2,3)] showed the shear stress exerted on the matrix by the fiber under simply supported ends can be used as a base model applied in the force diagram shown in Figure 5.3.

$$\sigma_R \pi r_s^2 + 2\pi r_s \tau dz = (\sigma_R + d\sigma_R) \pi r_s^2$$

$$\therefore \frac{d\sigma_R}{dz} = \frac{2\tau}{r_s} \quad (5.19)$$

$$\sigma_R = \frac{2\tau}{r_s} z \quad (5.20)$$

The σ_R is known; it is dependent on temperature T and the initial pseudoelastic strain [2,3] before curing. So $\sigma_R = \sigma_{R0} * k$ ($0 < k < 1$), where k is the SMA wire slipping coefficient (depending on the matrix) and σ_{R0} is the recovery stress. (For conservative prediction, assume $k = 1$.)

We assume that $\tau = \tau_0$, which must be constant along the z direction in Eq (5.15), is also constant along the r direction. (Refer to Piggott [12] with modified assumptions.) This assumption is the most critical, because we know that usually it is the case that T decreases as r increases toward a free surface. If this is so, the equation

(5.18) becomes

$$\sigma_c = -\frac{\tau_0}{r} z + c_0 = \sigma_c(r, z) \quad (5.21)$$

The magnitude of σ_c (5.21) is half of σ_R at $r=r_s$, and c_0 is zero for the case of a cantilever beam. Thus, we use the force balance to equalize the SMA recovery force in the composite strip (see Figure 5.4). From (5.20), (5.21), $\sigma_c = -\sigma_R r_s / 2r$ with

$$\sigma' = \sigma_c / \sigma_R, \quad r' = r / r_s$$

$$\sigma' = -1/2r' \quad (1 \leq r' \leq s/r_s)$$

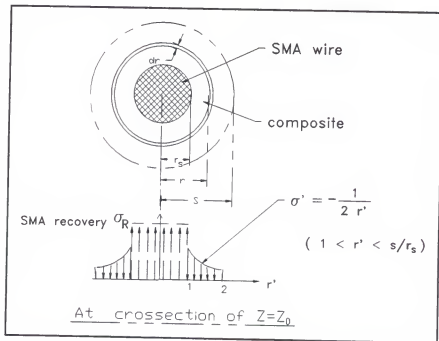


Figure 5.4. Compressive stress diagram in a strip

Therefore, from the force equilibrium

$$\begin{aligned}\sigma_R \pi r_s^2 &= \int_{r_s}^S \sigma_c 2\pi r dr \\ &= \int_{r_s}^S 2\pi \tau_0 dr\end{aligned}\tag{5.22}$$

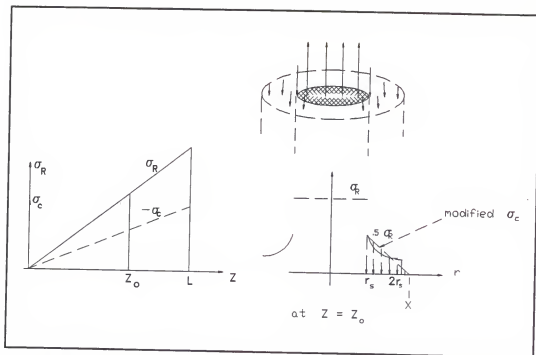
It follows that from equations (5.20), (5.21)

$$\underline{S} = 2 \underline{r}_s\tag{5.23}$$

For different laminae lay-up angle, with the SMA wire oriented as in Figure 5.1, the σ_c may alter at various ply constructions (c_0 not zero). The σ_c can depend on other factors in the realm of microstresses, such as fiber buckling strength, interlaminar shear strength, and matrix cracking strength of the composite.

The shear stress, τ , is actually not constant along the \underline{r} direction. As the \underline{r} increases, τ should decrease. (For a simplified solution at the macromechanical level, the Eq (5.23) and the σ' diagram in Figure 5.4 is sufficient.)

For a more realistic distribution of σ_c in the strip, we can approximate σ_c linearly along the \underline{r} direction as well as the \underline{z} direction (Figure 5.5). The diagram of σ' in Figure 5.4 actually contradicts the force equilibrium in Eq (5.22) if we include the rest of the curve of σ' beyond $r=2r_s$, which is not zero even at $r = \infty$. Therefore, we tend to single out the composite stress diagram at each small strip ($C \times C \times L$) as Figure 5.5 describes.

Figure 5.5. Modified σ_c distribution

With

$$\sigma_c = \left(-\frac{\tau_0}{(x-r_s)r_s} r + \frac{\tau_0 x}{(x-r_s)r_s} \right) z_0 \quad (r_s \leq r \leq x) \quad (5.24)$$

Again, using force balance at $\underline{z=z_0}$, we can find \underline{x} ,

$$\sigma_R \pi r_s^2 = \int_{r_s}^x \sigma_c 2\pi r dr \quad (r_s \leq r \leq x) \quad (5.22)$$

From (5.24) :

$$\frac{2\tau_0}{r_s} \pi r_s^2 = \int_{r_s}^x \left(-\frac{\tau_0}{(x-r_s)r_s} r + \frac{\tau_0 x}{(x-r_s)r_s} \right) 2\pi r dr$$

$$6 r_s^2 = 3 x^2 + 3 r_s x - 2x^2 - 2x r_s - 2r_s^2$$

$$x = \frac{1}{2} (\sqrt{33} - 1) r_s = 2.3723 r_s \quad (5.25)$$

Therefore, we substitute (5.25) back to (5.24) and get

$$\sigma_c = \left(\frac{1.7287}{r_s} - .7287 \frac{r}{r_s^2} \right) \tau_0 z_0 \quad (5.26)$$

This is the compressive stress at $z=z_0$. Putting (5.26) back into (5.18) to redistribute $\tau = f(r)$, we obtain

$$\tau_0 \left(\frac{1.7287}{r_s} - \frac{.7287}{r_s^2} r \right) = - \frac{d f(r)}{d r} - \frac{f(r)}{r} \quad (5.27)$$

The (5.27) should hold at any $z = z_0$ section. It is a typical O.D.E, which we can solve for

$f_H(r)$: homogeneous solution

$$f_H(r) = c_1/r$$

$f_p(r)$: particular solution

$$f_p(r) = (r^2/(4.1169 r_s^2) - .8284 r/r_s) \tau_0$$

with B.C. : $\tau = f(r_s) = \tau_0$

we obtain

$$\tau = (1.6215 \left(\frac{r_s}{r}\right) - 0.8644 \left(\frac{r}{r_s}\right) + 0.2429 \left(\frac{r}{r_s}\right)^2) \tau_0 \quad (r_s \leq r \leq x) \quad (5.28)$$

Checking Eq (5.28) at $r = 2.3723 r_s$ (the value of x), we have $\tau = 0.0001$, $\tau_0 \approx 0$, and $\tau = \tau_0$ at $r = r_s$ (checked)

Finally, the last part is how do we find constant L_0 .

From Eq (5.20) and Duerig [2, p.220 and p.222, Fig. 3] for Ni-Ti SMA, the initial strain is 6 %; so σ_R is about 400 Mpa (58 Ksi). We have found that the value varies with different SMA materials, so, from (5.20),

$$\begin{aligned} 58000 &= 2 \tau_0 / r_s L & (r_s = 0.005") \\ \tau_0 &= 145 / L \text{ psi.} \end{aligned} \quad (5.29)$$

Mohamed [13] also showed a formulation for calculating the SMA recovery stress as follows

$$\sigma_R(T, \epsilon) = \sigma_Y^{htp} \left(1 - \exp^{-K \left(\frac{T - A_s}{A_f - T} \right)} \right) \left(1 - \exp^{-N\epsilon} \right) \quad (5.30)$$

where

σ_R = recovery stress of SMA

σ_Y^{htp} = yield stress of SMA at A_f

K = constant analog to chemical reaction in austenite phase transform.

A_s = austenite starting temperature

A_f = austenite final temperature

N = number of crystallographically equivalent martensite variants.

ϵ = initial given strain

The features of the recovery stress of (5.30) are:

- (i) For a given strain, ϵ , σ_R is sensitive to temperature only within the range $A_s - A_f$.
- (ii) If σ_R achieves its maximum value at the A_f temperature, the equation (5.30) becomes

$$\sigma_R \text{ max.} = \sigma_Y^{htp} (1 - \exp^{-N\epsilon}) \quad (5.31)$$

- (iii) For temperatures higher than A_f , σ_R becomes sensitive only to initial strain ϵ .

The above can refer to Duerig et al. [2] in which the value of $N\epsilon$ can be found through cross-checking the above reference [2, p.220 - p.222, and Perkins, 3].

5.2.2 Micromechanics and Internal Stresses

If we combine (5.29) with (5.26) and (5.28), we get σ_c and τ in the hybrid composite. Then, we add them to the laminate hygrothermal residual stresses and in-plane stresses due to the static and dynamic loading. In this moment, the ply stresses derived from classic laminate theory can be calculated.

Finally, from the work of Chamis [14] and Guynn [15], microstress level can be checked at each layer of the hybrid laminate to see if any of them exceeds the allowable fiber strength and the allowable matrix strength. The formulations in Chamis [14] can predict the microstresses of tension, compression, and shear near the fiber/matrix or the matrix/matrix interface.

The Full clamp-clamp condition (Figure 5.7) creates the term N_x^* (section 5.1.2, Equation (5.18)) which is the in-plane force at a particular cross section of a clamped-clamped beam.

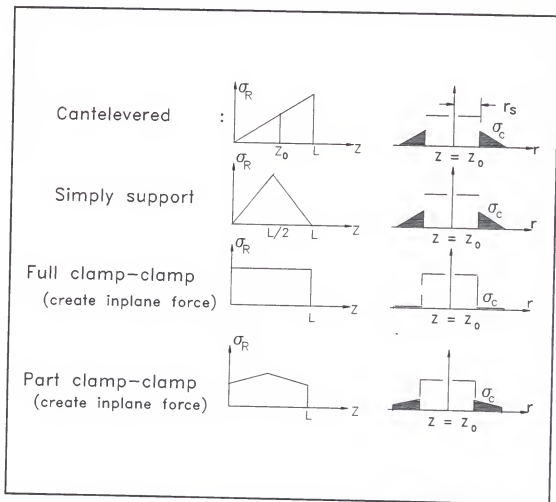


Figure 5.7. Four examples of internal stresses

The full clamp-clamp condition in Figure 5.7 is $\sigma_c = C_0$ or $\sigma_c = 0$, $\tau = \tau_0/r$ or $\tau = 0$; and the C_0 of Eq (5.21) depends on the boundary clamping device and the thermal conditions.

5.3 Dynamic Model of SMA Hybrid Laminate

The concept of using SMA in reinforced laminates was found in Rogers [1], Saunders et al. [5], and Rogers et al. [7]. The benefits of stiffening part of a structure are obvious in critical situations where resonances or acoustic noises impinge on the structure. SMA has the unique properties of promoting modulus variation and change recovery stresses.

5.3.1 General Dynamic Model

The governing equation of a symmetric SMA hybrid laminated plate can be derived by using the Ritz method or the energy variational principle, both mentioned in Saunders et al. [5] and Rogers et al. [7]. we assume that the structure is excited by a harmonic load. the general governing equation is described as :

$$\begin{aligned}
 & D_{11}^* \frac{\partial^4 W}{\partial X^4} + 4D_{16}^* \frac{\partial^4 W}{\partial X^3 \partial Y} + 2(D_{12}^* + 2D_{66}^*) \frac{\partial^4 W}{\partial X^2 \partial Y^2} \\
 & + 4D_{26}^* \frac{\partial^4 W}{\partial X \partial Y^3} + D_{22}^* \frac{\partial^4 W}{\partial Y^4} + \bar{N}_x \frac{\partial^2 W}{\partial X^2} + \bar{N}_y \frac{\partial^2 W}{\partial Y^2} \\
 & + 2\bar{N}_{xy} \frac{\partial^2 W}{\partial X \partial Y} + C_D \frac{\partial W}{\partial t} + \rho \frac{\partial^2 W}{\partial t^2} = q(x, y) e^{i\omega t}
 \end{aligned}$$

where

W = deflection function $W(x,y)$
 C_d = damping coefficient
 ρ = mass per unit area
 $q(x,y) e^{i\omega t}$ = external forcing function
 $N_x^* = N_x^{T*} = \text{SMA recovery stress resultant}$

This flexural equation can be expanded to handle the response of an asymmetric laminated plate. The $W(x,y)$ can be solved either by employing FEM or the Galerkin method, the choice depending on the boundary conditions.

5.3.2 Dynamic Model-Orthotropic Laminate (APT)

The orthotropic laminates are commonly used in many composite structures, and its SMA hybrid laminate can perform as active properties tuning (APT) elements. The hybrid structures are usually cantilever plates with linear vibration characteristics. Their flexural stiffness D_{ij} is the only temperature dependent term at the SMA activation and there are no in-plane forces.

$$D_{11}^* \frac{\partial^4 W}{\partial X^4} + 2(D_{12}^* + 2D_{66}^*) \frac{\partial^4 W}{\partial Y^4} + D_{22}^* \frac{\partial^4 W}{\partial Y^4} = -\rho \frac{\partial^2 W}{\partial t^2}$$

5.3.3 Dynamic Model-Orthotropic Laminate (ASET)

The governing equation of this type of structure is always under specially prescribed boundary condition such as hinged-simply support, clamped-clamped, and hinged-clamped conditions.

This means that

$$D_{11}^* \frac{\partial^4 W}{\partial X^4} + 2(D_{12}^* + 2D_{66}^*) \frac{\partial^4 W}{\partial Y^4} + D_{22}^* \frac{\partial^4 W}{\partial Y^4} + \bar{N}_x^* \frac{\partial^2 W}{\partial X^2} + \bar{N}_y^* \frac{\partial^2 W}{\partial Y^2} + 2\bar{N}_{xy}^* \frac{\partial^2 W}{\partial X \partial Y} = -\rho \frac{\partial^2 W}{\partial t^2}$$

For example, in a 1-D hybrid composite beam with a hinged simply-supported condition, the recovery stress resultant of SMA is not zero and the equation of motion can be described

$$D_{11} \frac{\partial^4 W}{\partial X^4} + \bar{N}_x^* \frac{\partial^2 W}{\partial X^2} = -\rho \frac{\partial^2 W}{\partial t^2}$$

The recovery stress resultant, combined effects of the thermal and prestressed condition, is present in the equation while the SMA is activated, and we assume

$$W = W(x) e^{i\omega t}$$

Then the natural frequency of the m th mode is

$$\omega_m = \frac{m\pi}{L} \sqrt{\frac{1}{\rho} \left(\frac{m^2 \pi^2 D_{11}}{L^2} + \bar{N}_x^* \right)}$$

Apparently, the natural frequency ω_m is higher than that of a beam which is not activated. The first or higher modes of natural frequencies can be shifted by heating the SMA wires in the hybrid composite beam to avoid resonance. It is expected that the vibration can be subdued by the activation or deactivation in SMA hybrid laminates.

CHAPTER 6
EXPERIMENTS OF SMA HYBRID LAMINATES
MODAL RESPONSE

6.1 Experiment Facilities

The equipment used in the testing are :

- LeCroy 8013A waveform recorder, a data acquisition device for dynamic response of structures, LeCroy Research System Corp.
- Hammer with force transducer, an impulse load on beams.
- Eddy current probe to measure beam vibration responses.
- K type(TT-K-36 SLE) thermocouple wire spot welded to the end to an SMP male connector (#1 style no. 10). Digital thermometer¹, Model HHM59, K type thermocouple socket.
- IBM PC-286 compatible, equipped with CATALYST/ASYST software which analyze the signal transmitted from the LeCroy 8013A wave form recorder. It creates dynamic response data in the time and frequency domains.
- DC power source, Triple Output DC Power Supply 1660 (BK Precision Co.) provides the SMA activation power.
- A 16.5 cm-thick granite slab as a foundation on which the impulse load hammer, eddy current probe, and all test

1 OMEGA Technologies Company, Box 4047, Stamford, CT 06907-0047.

facilities are set. There are several vibration isolators, made of hard rubber, placed under the slab to eliminate external noise signals.

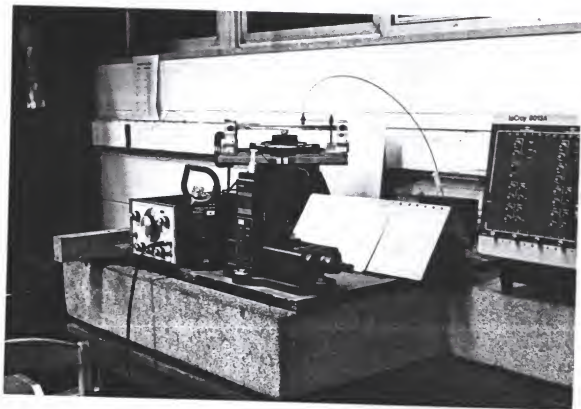


Figure 6.1. Experimental facilities including the LeCroy 8013a.

6.2 1st Batch of Specimen Test

The purpose of the test is to verify the theoretical prediction and to find the natural frequency and damping factor of the SMA hybrid laminate beam. The first batch of test specimens has two types of SMA hybrid laminated beams (Table 6.1), as well as two base laminated beams without SMA wires embedded. We will compare both the natural frequency and the damping factor of each SMA hybrid laminated beam to its base laminated beam at the room temperature (no activation) and the activation temperature.

Table 6.1 First batch (TYPE 1 , $V_f = 3.27\%$ SMA wire)


TYPE 1	1.13"x7.88", overstrained SMA wires [0/90/SMA/0/90/90/0/SMA/90/0] FG/EP
TYPE 1 (base)	1.13"x7.88", no SMA wire [0/90/0/90/90/0/90/0] FG/EP

(TYPE 2 , $V_f = 1.63\%$ SMA wire)

TYPE 2	1.1"x7.88" , overstrained SMA wire [0/90/SMA/0/90/90/0/90/0] FG/EP
TYPE 2 (base)	1.1"x7.88" , no SMA wire [0/90/0/90/90/0/90/0] FG/EP

With the Type 1, and Type 1 base cantilever beam under the test of impulse load, only the first mode natural frequency were recorded (Table 6.2).

Table 6.2 Natural Frequencies of cantilever beams

 <div style="display: inline-block; vertical-align: middle; margin-left: 10px;"> 5.88" → ----- cantilever beam </div>					
TYPE 1				TYPE 1 (base)	
I	V	Temp.	1st mode	Temp.	1st mode
0.	0.	R (75°F)	42 HZ	R (75°F)	41.5 HZ
.37 amp	24 volt	201°F (2 min)	47 HZ	////////	////////

The difference of first mode natural frequency for Type 1 and Type 1 base is not much. The reason may lie in the canceling effect of the stiffened wire embedded in the laminate minus the extra mass at the free end of the beam (crimped metal pieces and silver paint for SMA wire electric connection) under cantilever boundary condition.

The natural frequency for activated Type 1 is only slightly higher than non-activated Type 1 in Table 6.2, It appears that the beam has a very low SMA volume fraction (3.27 %).

The results of Type 1 beams under impulse load and Its first mode natural frequencies recorded at 76.6°F and 75°F, as well as the activated temperatures at 200.°F, 313°F can be seen in Tables 6.3 and 6.4.

Table 6.3 Natural frequency of clamped-clamped beam

<div style="text-align: center;"> </div>				
TYPE 1				
I	V	Temp.	1st mode	
0	0	76.6°F	319.4 HZ	
0	0	76.6°F	322.6 HZ	← higher clamp force
--	--	200.°F	322.0 HZ	

Table 6.4 Natural frequency of clamped-clamped beam

<div style="text-align: center;"> </div>							
TYPE 1					TYPE 1(base)		
I	V	Temp.	1st mode	ξ	Temp	1st mode	ξ
0	0	75.°F	336 HZ	.0095	79°F	307 HZ	.0186
.52	29v	313°F	324 HZ	.0088	263°F	300 HZ	.0323

 ξ : damping factor

hot air blowing

The conclusions to be drawn from the clamped-clamped beams (Tables 6.3 and 6.4):

- Higher clamping force gives higher natural frequency.
- Activated hybrid laminate beam has a slightly lower natural frequency. The most likely reason is that the SMA wires were overstrained (did not shrink back to the original austenite phase before straining), so their recovery stresses could not overcome the thermally induced beam compression. Therefore, the overall in-plane force $N_x^{T^*}$ is compressive. Proper choice of ply orientation in order to reduce effective thermal expansion may decrease the thermal stresses.
- The activated hybrid laminate beam has a lower damping factor than its non-activated phase, but the base beam

(without SMA wires) has a higher damping ratio at higher temperature than that of the low (room) temperature. [16]

It should be noted that the original test bed in the lab was designed only for cantilever beam tests. Some insert threads in the thick aluminum base plate would need to be retapped to hold the second vise in order to clamp the other end of the beam for clamped-clamped test. The insulation material between the beam and the vises is graphite (carbon) felt to prevent heat conduction from beam to vises. (The first batch test specimen did not have graphite felt insulator at the clamping location.)

The first batch specimens were not satisfactory and could not verify that an activated SMA hybrid laminated beam had a higher natural frequency than a non-activated SMA hybrid laminate beam. Some specific effects were found in the clamped-clamped test (Table 6.3) that showed that an activated SMA hybrid laminated beam has a little lower damping factor (ξ) when temperature increases. Compared with the base laminated beam (no SMA wire), the damping factor increases as temperature increases [16]. (The higher temperature on the base laminated beam is imposed by forced hot air.)

The first mode frequency response plots of the data from the first batch specimens (Table 6.4) are in Figures 6.4, 6.5, 6.6, and 6.7.

6.3 Calculated 1st Mode Natural Frequency

Table 6.2 lists the experimental data, that can be used to verify the theory.

(1) Cantilever beam: Type 1 (base)

First approach (simple lumped mass approach):

$$l = 5.88" , \quad t = 0.076" \text{ (8 layer GF/EP)}$$

$$[9] \quad m = 0.056 \times 1.8/1.61 \times \text{vol.} = 0.0354$$

$$* EI = 149.05 \text{ lb}_f \cdot \text{in}^2$$

$$\text{■} \text{-----} \bullet m \quad \delta = [l^2 / (3 EI)] \times P$$

$$\text{so, } K = (3 EI) / l^2$$

$$\omega = \sqrt{(K/m)} = \sqrt{(149.05 \times 32.2 \times 12) / (0.0354 \times 5.88^2)}$$

$$= 374.47 \text{ rad/sec} = \underline{59.6 \text{ HZ}}$$

Second approach (closed form solution):

$$l = 5.88" , \quad t = 0.076"$$

$$\rho = 0.056 \times 1.8/1.61 \times t = 0.005 \text{ lb}_m/\text{in}^2$$

$$* EI = 149.05 \text{ lb}_f \cdot \text{in}^2$$

$$[17] \quad \omega = 3.515 \sqrt{(EI) / (\rho l^4)}$$

$$= 345.04 \text{ rad/sec} = \underline{54.91 \text{ HZ}}$$

Third approach (ANSYS): $\omega = 59.1 \text{ HZ}$

* GENCOM2: a self-developed FORTRAN code for general laminate properties calculations (for hybrid laminate also)

Comparing the second approach with the test result ($\omega = 41.5$ HZ), we see that the error is about 24%. It clearly indicates that neither the clamping device nor the fabricated specimen had very good qualities, or there are measured errors. Therefore, further improvements in the specimen fabrication and testing method are crucial for future study on sandwich structures. The specimens are shown in Figure 6.2.

6.4 2nd Batch Specimen Test

The lay-up of Fiberglass/epoxy prepreg with the SMA wires is [90/SMA/0/0/SMA/90]; the 0 degree Fiberglass fiber direction is aligned to that of the SMA wire direction. Just as in the first batch specimens, the first layer is 20 wires, 20 wires down, width is 1.12", and volume fraction of the SMA in laminate is 6.37%.

The specimen is shown in Figure 6.3. The test results are seen in Figure 6.8, 6.9, and 6.10. We found that at the activation temperature the natural frequencies have changed for all three modes.

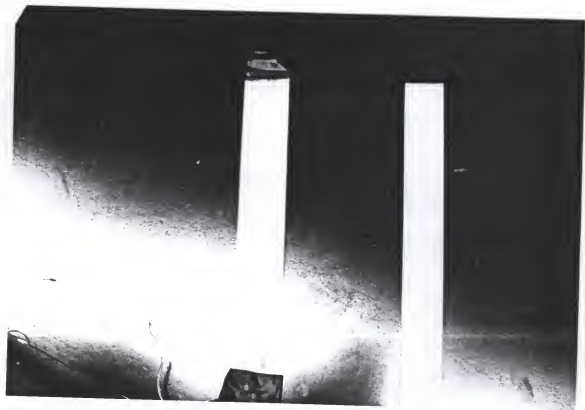


Figure 6.2. First batch specimens, Type 1 (left), Type 1 base (right)

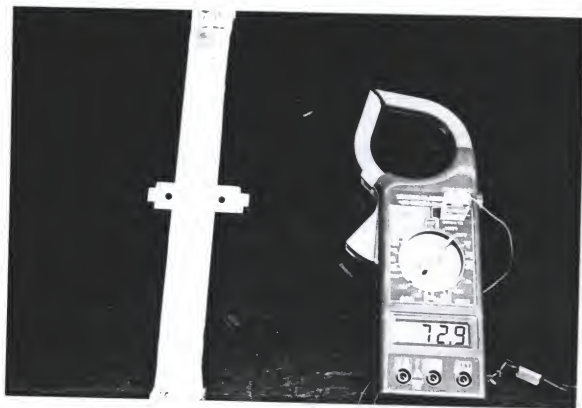


Figure 6.3. Second batch specimen, Type 1 (left)

Response of SMA hybrid beam (75°F) clamped-clamped

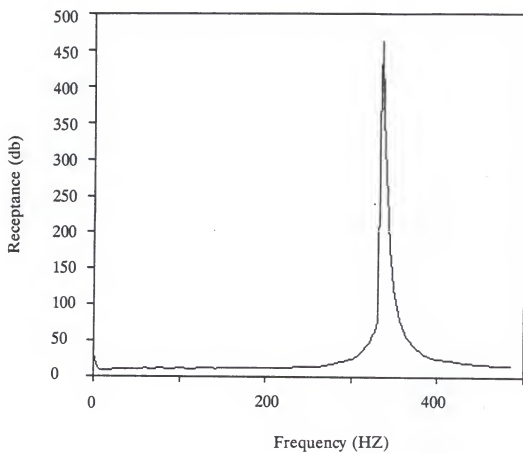


Figure 6.4. First mode natural frequency of Type 1 specimen

Response of SMA hybrid beam (313°F), clamped-clamped

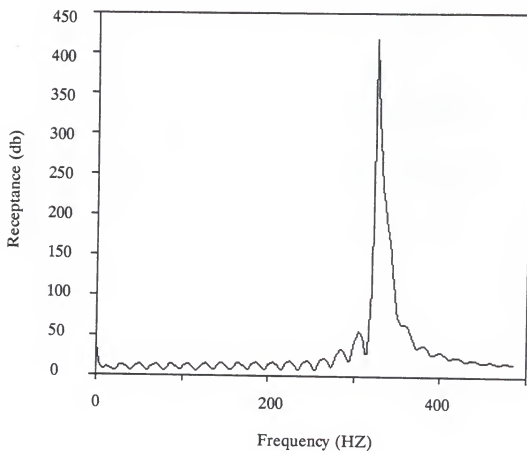


Figure 6.5. First mode natural frequency of Type 1 (activated)

Response of base beam (79°F) - no SMA wire

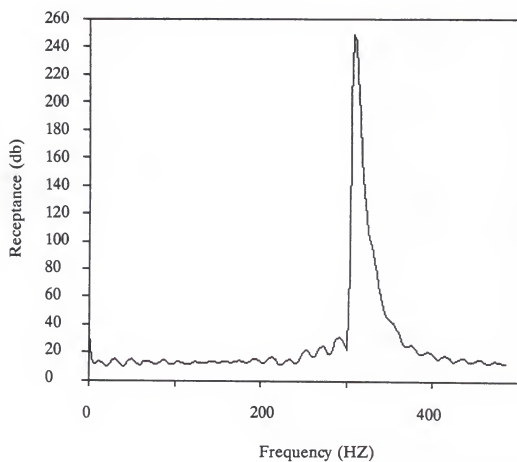


Figure 6.6. First mode natural frequency of Type 1 (base)

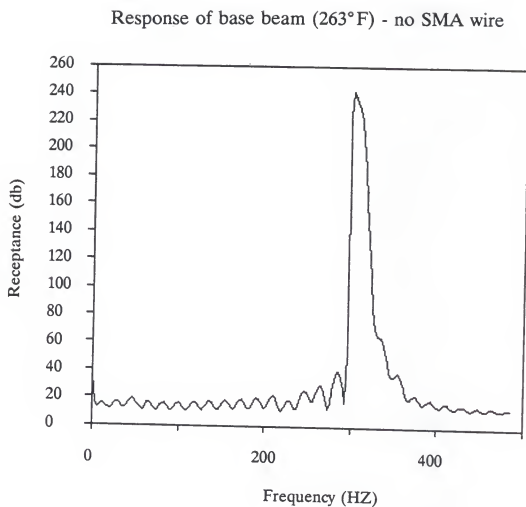


Figure 6.7. First mode natural frequency of Type 1 (base)

Second batch, Type 1 (73°F), clamped-clamped

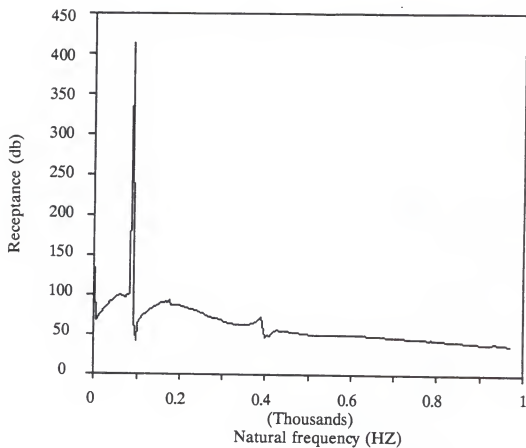


Figure 6.8. Frequency response at non-activation

Second batch, Type 1 (140.6°F), clamped-clamped

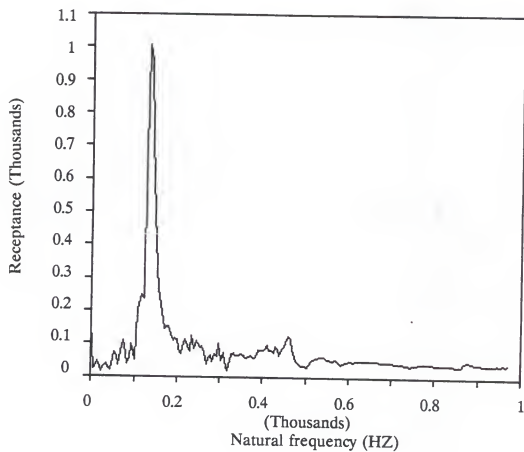


Figure 6.9. Frequency response at activation

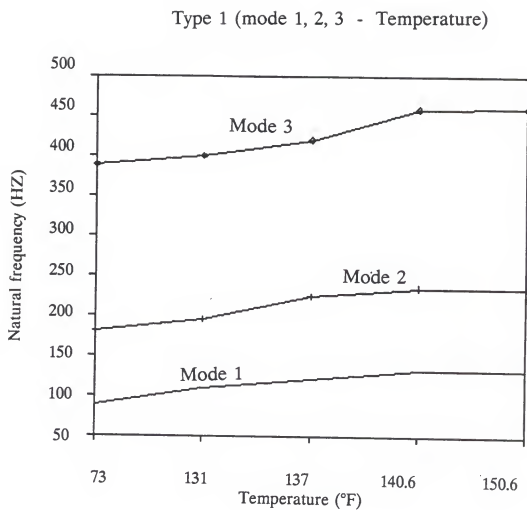


Figure 6.10. Natural frequency--Temperature plot of second batch specimen

CHAPTER 7 VIBRATION CONTROL OF SANDWICH BEAMS

Two kinds of vibration control techniques which are currently applied to reduce the problem. One is passive vibration control technique, the other is active vibration control technique. The emerging smart materials have created other ramifications in vibration control studies. Chapter 1 showed the unique abilities of smart materials to change material bulk modulus, stiffness, and so forth, when activated by electric current, by magnetic field, or by heating. The ability of SMA wire to change stiffness in a SMA hybrid laminated beam has been described in Chapter 6. There, the test results showed the potential of the hybrid material to shift the structure's natural frequencies. Thus, the resonant condition of vibration induced by impinging loads, sinusoidal loads, etc., could predictably be subdued by activating the SMA wires embedded in the composite structures. However, the test results in Chapter 6 also showed lower damping coefficients when the SMA hybrid laminated beam was fully activated. All the tests of SMA hybrid laminated beams were done under the clamp-clamp boundary condition. A simply-supported beam or a cantilever beam is often chosen as a candidate in practical vibration

problems. Still, the tests showed strong evidence of a structure-stiffening effect and the changing of damping properties.

In practical applications, simply supported beams and cantilever beams are commonly used. When a beam is fixed at two ends for a simply-supported case, or a helicopter rotor blade and a fan blade of a jet engine for cantilever beams, to name just a few. The simply-supported and cantilever beams require strength and bending rigidity to serve as sound structures. One of the best choices for a simply-supported beam construction is a sandwich beam. There are many advantages of using sandwich structures: (1) sandwich structures have great strength/weight ratio, (2) they have superior flexural rigidity/weight ratio, (3) the tailored composite skins perform excellently under various design requirements and, (4) the sandwich core, which is softer and weighs less, can be made out of good damping materials in order to reduce acoustic loading, or other applications. The bonding material can be film adhesive and spray-on primer which serve the purpose of join sandwich faces with core materials. Thicker core can be cut into smaller blocks then strung together to make curved sandwich panels.

The candidate sandwich panel in this chapter is a [12x1"] beam whose faces are E-glass/epoxy containing SMA wires with wire volume fraction 6.7% (each wire has 0.01" diameter). This adaptive structure may be activated by

electric current or by a direct heating process while vibration occurs.

7.1 Vibration Suppression in Structures

Vibration suppression is a very broad subject in which many techniques are available to achieve this purpose. Passive vibration control is a technology that uses extra mass-spring attached to the main structures or viscoelastic damping material on the structures. It requires predetermined dynamic system analysis and is an open loop control system. Active vibration control is essentially closed loop control to suppress mechanical vibration. It requires the effort in designing feed back control logic and the electronic devices in structure system such as a large space station. From surveying the research in these two control systems, the author found that the SMA hybrid sandwich structure possesses both abilities in passive vibration control and active vibration control.

7.1.1 Passive Vibration Control

To subdue vibration, one could use an added mass on a vibrating beam as a typical passive control scheme. It is an undamped dynamic vibration absorber which, according to Thomson [17] and Beards [18], can reduce structure vibration but extra viscous damping will have to be added to reduce vibration in general cases.

A case studied by Pierce et al. [19] uses the passive damping principle on a helicopter rotor, has a mass M and a single flap pendulum with m installed on the rotor to absorb vibration. This set-up would cut down shear force transfer to the rotor hub, and reduce the rotor deflection in flight. The mathematical model for the case is tedious to develop, and the method required trials and errors to locate the flap pendulum on the rotor to achieve ideal results. In addition, in real structures, the design for the installation of a flap pendulum on a helicopter rotor is difficult. An extra viscous damper may also be necessary for various loading conditions, not to mention the maintenance for the rotor with added pendulum in the long run.

In viscoelastic damping, composite materials have better damping quality than most monolithic materials [20], [21]. Short fiber composites have higher damping property than unidirectional fiber composites [22], [23] but inferior stiffness for the short fiber composite is inevitable. They are all fiber reinforced polymer materials, and the polymer is viscoelastic material which provides most of the damping factor. Therefore, using viscoelastic damping tape is more effective for increasing the damping property of modern structures. The damping tapes in structures can serve as dampers so that elastic vibration energy can be dissipated as heat (Jones [24], Sankar [25]). Also, in a large space truss whose bar elements were treated with segmented

constrained damping layers, the loss factor was tremendously increased -- an example of direct evidence of elastic energy dissipation in a structure.

The added mass damper could increase weight and not easy to apply to real structures. The viscoelastic damping treatment is easier to be bonded on structure, but may be peeled off by external disturbances. The sandwich structure has good damping core to be used for passive control in noise reduction or other purposes. If SMA hybrid laminates can combine the sandwich core become a property tunable structure, would it be more efficient to have this dual vibration control materials in one structure?

7.1.2 Active Vibration Control

In recent years, the active vibration control technique has appeared to provide more options to control mechanical vibrations. An example is the alteration of the stiffness of several bars of a cantilever truss under various modes of vibration (Onoda [26]). Onoda indicated that one of the control laws is to reduce the stiffness or increase the stiffness of a particular member of the truss by activating the attached piezoelectric actuator when the deflection of that member exceeds a threshold deformation. So, the member operates like a softener to absorb vibrational energy or a stiffener to reduce vibration. This unique device requires very special logic control circuitry, and the actuator tube connecting the adjacent truss members also demands accurate

tolerance control. The method is useful in space structures and many mechanical components.

In contrast to the complicated feed back control system, the SMA hybrid structure could be modeled as a simpler feed back control element with the passive damping core material added into it.

7.2 Equation of Motion of Sandwich Panel

In this section, the primary goal is to establish the principles of mechanics for sandwich panels with faces made of SMA hybrid composite laminate. A large flexible structure like a wind turbine, at random wind directions plus terrain variations, may face low-frequency vibrational problems. We are assuming that this flexible wind turbine is made of a sandwich panel which, in turn, vibrates with large amplitude. The structure is under elastic deformation when vibrates, and can cause large amplitude which creates geometric nonlinearity. There are normal or in-plane stresses in the core with constant thickness. The only significant stress in the core is the transverse shear. The face skins are thin compared to the core thickness and the upper skin is identical to the lower skin, and the face skins can only take the in-plane forces. The panel is assumed to have perfect bond between the skins and the core. This gives the most general case of kinematic assumptions.

7.2.1 Derivation of Equation of Motion

Assume this general case of a cantilevered sandwich panel, only one face is activated, erects the nonsymmetric activation model. Due to the variation of skin stiffness with temperature and time, the Young's modulus of SMA wire is denoted by $E_s(t)$. As in Chapter 5, Equation (5.4) could be linearized according to diagram in Rogers [1] giving the relation between the Young's modulus and temperature. Since the values $E_s(t)$ are different at activation and deactivation due to hysteresis effect (Duerig et al. [2] p.98), one can write:

At heating:

$$E_s(\Delta t) = 3.5 + 0.25 (\Delta T / \Delta t) \Delta t \quad (10^6 \text{ psi}) \quad (7.1)$$

$$E_s(\Delta t) = 24.13 + 3.10 (\Delta T / \Delta t) \Delta t \quad (\text{Gpa}) \quad T = ^\circ\text{C}$$

where, $\Delta T = 32^\circ\text{F}$, 17.78°C

At cooling after activation:

$$E_s(\Delta t) = 11.5 - 0.34 (\Delta T / \Delta t) \Delta t \quad (10^6 \text{ psi}) \quad (7.2)$$

$$E_s(\Delta t) = 79.29 - 4.22 (\Delta T / \Delta t) \Delta t \quad (\text{Gpa})$$

where, $\Delta T = 23.5^\circ\text{F}$, 13.07°C

$E_s(\Delta t)$ = SMA wire Young's modulus

ΔT = temperature range

Δt = time step (sec)

$\Delta T / \Delta t \propto f(I, V, \dot{G})$ (Chapter 2)

I = electric current

V = electric Voltage

\dot{G} = heat flux

We can approach the problem using energy variation to derive the equation of motion of sandwich panel. Only the strain energy of the SMA hybrid skins (upper and lower) and the transverse shear energy of the core are considered. We ignore flexural rigidities of the face skins because their thickness is very small compared to the core thickness. The recent research on nonlinear analysis of composites by Whitney and Leissa [27], Bai [28], and a collective work on geometrically nonlinear analysis by Chia [29], can serve as good models for deriving the equation of motion. The effects of skin stiffness variation at activation/deactivation will also be considered.

The displacement fields are assumed in the following form (from a 2-D plate approach):

Non-activation:

$$u(x, y, z, t) = u_0(x, y, t) + z \psi_x \quad (7.3)$$

$$v(x, y, z, t) = v_0(x, y, t) + z \psi_y \quad (7.4)$$

$$w(x, y, t) = w(x, y, t) \quad (7.5)$$

These assumptions lead to the conventional results found in such previously collected works as Whitney [30].

Activation mode: Upper skin deforms by heating and recovery stresses. If the core is an insulator to heat, the extra terms appearing in (7.6), (7.7) are small.

$$u(x, y, z, t) = u_0(x, y, t) + z \psi_x - f(x, t) \quad (7.6)$$

$$v(x, y, z, t) = v_0(x, y, t) + z \psi_y - g(y, t) \quad (7.7)$$

$$w(x, y, t) = w(x, y, t) \quad (7.5)$$

Where f and g represent the shrinkage of upper skin at activation (only at cantilever condition), the compression induced by SMA may be ignored if the base structure is stiff enough, thereby eliminate $f(x,t)$ and $g(y,t)$ at simply-supported boundary condition for $u=0$. From Figure 7.1,

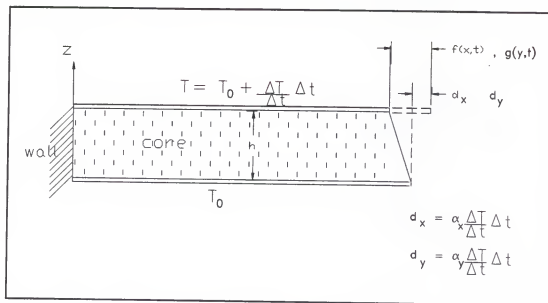


Figure 7.1. Cantilever panel-- extreme case of existing $f(x,t)$ and $g(y,t)$ due to upper skin activation

We introduce the core shear rotation due to upper skin activation (cantilever beam).

$$\begin{aligned} \psi_{sx}(x, t) &= \frac{f(x, t) - d_x}{h} \\ \psi_{sy}(y, t) &= \frac{g(y, t) - d_y}{h} \end{aligned} \quad (7.8)$$

where

$u_0(x, y, t)$ = panel neutral plane displacement in x-direction.

$v_0(x, y, t)$ = panel neutral plane displacement in y-direction.

$w(x,y,t)$ = panel neutral plane deflection in z-direction.

$\psi_x(x,y,t)$ = panel neutral plane rotation about y-axis.

$\psi_y(x,y,t)$ = panel neutral plane rotation about x-axis.

z = local normal direction to neutral plane of panel.

$f(x,t)$ = deformation of upper skin at activation in x-axis.

$g(y,t)$ = deformation of upper skin at activation in y-axis.

ψ_{sx} = core shear rotation due to upper skin activation
in x - direction.

ψ_{sy} = core shear rotation due to upper skin activation
in y - direction.

d_x = thermal expansion in x-direction.

d_y = thermal expansion in y-direction.

α_x = skin thermal expansion coefficient in x-direction.

α_y = skin thermal expansion coefficient in y-direction.

T_0 = ambient air temperature.

A diagram of the sandwich panel, shown in Figure 7.2, gives us a clearer description of the panel's longitudinal displacements and rotations. A long beam with cantilever or simply-supported boundary conditions under harmonic load will produce large amplitudes of vibration.

Figure 7.2 only shows the plane view of the sandwich panel from the y-direction; v_0 can not be shown in the diagram. Additionally, $\partial w / \partial y$ can not be shown except viewing from the x-direction, and ψ_x, ψ_y are briefly denoted as $\psi_{x,y}$.

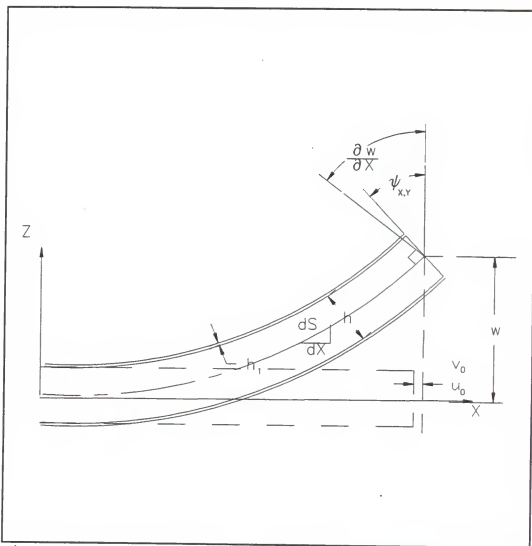


Figure 7.2 Large deformation of sandwich panel

The strains of skins can be expressed as

$$\epsilon_x^u = \frac{\partial u_0}{\partial x} - \frac{h}{2} \frac{\partial \psi_x}{\partial x} + \frac{1}{2} \left(\frac{\partial w}{\partial x} \right)^2 - \frac{\partial f(x, t)}{\partial x} \quad (7.9)$$

$$\epsilon_x^1 = \frac{\partial u_0}{\partial x} + \frac{h}{2} \frac{\partial \psi_x}{\partial x} + \frac{1}{2} \left(\frac{\partial w}{\partial x} \right)^2 \quad (7.10)$$

$$\epsilon_y^v = \frac{\partial v_0}{\partial y} - \frac{h}{2} \frac{\partial \psi_y}{\partial y} + \frac{1}{2} \left(\frac{\partial w}{\partial y} \right)^2 - \frac{\partial g(y, t)}{\partial y} \quad (7.11)$$

$$\epsilon_y^1 = \frac{\partial v_0}{\partial y} + \frac{h}{2} \frac{\partial \psi_y}{\partial y} + \frac{1}{2} \left(\frac{\partial w}{\partial y} \right)^2 \quad (7.12)$$

$$\gamma^u = \frac{\partial u_0}{\partial y} + \frac{\partial v_0}{\partial x} - \frac{h}{2} \left(\frac{\partial \psi_x}{\partial y} + \frac{\partial \psi_y}{\partial x} \right) + \left(\frac{\partial w}{\partial x} \frac{\partial w}{\partial y} \right) \quad (7.13)$$

$$\gamma^1 = \frac{\partial u_0}{\partial y} + \frac{\partial v_0}{\partial x} + \frac{h}{2} \left(\frac{\partial \psi_x}{\partial y} + \frac{\partial \psi_y}{\partial x} \right) + \left(\frac{\partial w}{\partial x} \frac{\partial w}{\partial y} \right) \quad (7.14)$$

The nonlinear parts of strains in (7.9) to (7.14) are owing to the nonlinear part of Lagrangean strain tensor in Fung [31]:

$$\begin{aligned} \epsilon_x &= \frac{\partial u}{\partial x} + \frac{1}{2} \left[\left(\frac{\partial u}{\partial x} \right)^2 + \left(\frac{\partial v}{\partial x} \right)^2 + \left(\frac{\partial w}{\partial x} \right)^2 \right] \\ \epsilon_y &= \frac{\partial v}{\partial y} + \frac{1}{2} \left[\left(\frac{\partial u}{\partial y} \right)^2 + \left(\frac{\partial v}{\partial y} \right)^2 + \left(\frac{\partial w}{\partial y} \right)^2 \right] \\ \gamma_{xy} &= \frac{1}{2} \left[\frac{\partial u}{\partial y} + \frac{\partial v}{\partial x} + \left(\frac{\partial u \partial u}{\partial x \partial y} + \frac{\partial v \partial v}{\partial x \partial y} + \frac{\partial w \partial w}{\partial x \partial y} \right) \right] \end{aligned}$$

Since the second order terms like $\left(\frac{\partial u}{\partial x} \right)^2$ etc are small compared with $\left(\frac{\partial w}{\partial x} \right)^2$, we ignore them.

The core transverse shear strains are

$$\gamma_{xz}^c = \psi_x - \psi_{sx} + \frac{\partial w}{\partial x} \quad (7.15)$$

$$\gamma_{yz}^c = \psi_y - \psi_{sy} + \frac{\partial w}{\partial y} \quad (7.16)$$

According to the asymmetrical skin laminated sandwich panel at activation (upper skin stiffness change) and compared to [28], we find

skin strains expressed

$$[\epsilon^u]^T = [\epsilon_x^u \quad \epsilon_y^u \quad \gamma^u]$$

in (7.9) to (7.14) as

$$[\epsilon^l]^T = [\epsilon_x^l \quad \epsilon_y^l \quad \gamma^l]$$

Neutral-plane strain (which causes bending by coupling stiffness), and sandwich panel curvature κ are expressed as

$$[\bar{\epsilon}]^T = \left[\frac{\partial u_0}{\partial x} + \frac{1}{2} \left(\frac{\partial w}{\partial x} \right)^2 \quad \frac{\partial v_0}{\partial y} + \frac{1}{2} \left(\frac{\partial w}{\partial y} \right)^2 \quad \frac{\partial u_0}{\partial y} + \frac{\partial v_0}{\partial x} + \left(\frac{\partial w}{\partial x} \frac{\partial w}{\partial y} \right) \right]$$

$$[\kappa]^T = \left[\frac{\partial \psi_x}{\partial x} - \frac{\partial \psi_{sx}}{\partial x} \quad \frac{\partial \psi_y}{\partial y} - \frac{\partial \psi_{sy}}{\partial y} \quad \frac{\partial \psi_y}{\partial x} + \frac{\partial \psi_x}{\partial y} \right]$$

Also according to equations (5.3) to (5.11) in Chapter 5, total strain energy of the sandwich panel is expressed as

$$V = \frac{1}{2} \int_0^a \int_0^b [\epsilon^u]^T \begin{bmatrix} \bar{A}_{11} & \bar{A}_{12} & \bar{A}_{13} \\ \bar{A}_{21} & \bar{A}_{22} & \bar{A}_{23} \\ \bar{A}_{31} & \bar{A}_{32} & \bar{A}_{33} \end{bmatrix} [\epsilon^u] dx dy$$

$$\begin{aligned}
& + \frac{1}{2} \int_0^a \int_0^b [\epsilon^1]^T \begin{bmatrix} A_{11} & A_{12} & A_{13} \\ A_{21} & A_{22} & A_{23} \\ A_{31} & A_{32} & A_{33} \end{bmatrix} [\epsilon^1] dx dy \\
& + \frac{1}{2} \int_0^a \int_0^b [\bar{\epsilon} \quad \kappa]^T \begin{bmatrix} B^* \\ D^* \end{bmatrix} [\kappa] dx dy \\
& + \frac{1}{2} \int_0^a \int_0^b \int_{-\frac{h}{2}}^{\frac{h}{2}} [\gamma_{xz}^c \quad \gamma_{yz}^c] \begin{bmatrix} G_{13} & 0 \\ 0 & G_{23} \end{bmatrix} \begin{bmatrix} \gamma_{xz}^c \\ \gamma_{yz}^c \end{bmatrix} dz dy dx \quad (7.17)
\end{aligned}$$

\bar{A}_{ij} , A_{ij} , B^* , D^* are the laminated plate stiffness properties. The superscripts u , l , c indicate upper, lower, core. The superscript * means skin is activated, where

$$\bar{A}_{ij}^* : \sum_{n=1}^N \bar{Q}_{ij}^n (z_n - z_{n-1}) \quad N = \text{upper skin layer number}$$

* : skin at activation

$$A_{ij}^* : \sum_{n=1}^N \bar{Q}_{ij}^n (z_n - z_{n-1}) \quad N = \text{lower skin layer number}$$

$$B_{ij}^* : \begin{bmatrix} B_{11}^* & B_{12}^* & B_{13}^* \\ B_{21}^* & \dots & \dots \\ \dots & \dots & \dots \end{bmatrix}, \quad B_{11}^* = \sum_{n=1}^N \frac{1}{2} \bar{Q}_{11} (z_n^2 - z_{n-1}^2) \dots\dots\dots$$

$$D_{ij}^* : \begin{bmatrix} D_{11}^* & D_{12}^* & D_{13}^* \\ D_{21}^* & \dots & \dots \\ \dots & \dots & \dots \end{bmatrix}, \quad D_{11}^* = \sum_{n=1}^N \frac{1}{3} \bar{Q}_{11} (z_n^3 - z_{n-1}^3) \dots\dots\dots$$

G_{13} : core transeverse shear stiffness at xz plane
 G_{23} : core transeverse shear stiffness at yz plane
 Q_{11} etc. are function of E_s defined as eq. (1), (2)

We could also express the equation in the following equation
 (7.18)

$$\begin{aligned} V = & \frac{1}{2} \int_0^a \int_0^b [N_x^u \quad N_y^u \quad N_{xy}^u] \cdot \begin{bmatrix} \epsilon_x^u \\ \epsilon_y^u \\ \gamma^u \end{bmatrix} dy \, dx \\ & + \frac{1}{2} \int_0^a \int_0^b [N_x^l \quad N_y^l \quad N_{xy}^l] \cdot \begin{bmatrix} \epsilon_x^l \\ \epsilon_y^l \\ \gamma^l \end{bmatrix} dy \, dx \\ & + \frac{1}{2} \int_0^a \int_0^b [\bar{M}_x \quad \bar{M}_y \quad \bar{M}_{xy}] \cdot \begin{bmatrix} \frac{\partial (\psi_x - \psi_{sx})}{\partial x} \\ \frac{\partial (\psi_y - \psi_{sy})}{\partial y} \\ \frac{\partial \psi_x}{\partial y} + \frac{\partial \psi_y}{\partial x} \end{bmatrix} dy \, dx \end{aligned}$$

$$+ \frac{1}{2} \int_0^a \int_0^b [q_x^c \ q_y^c] \begin{bmatrix} \gamma_{xz}^c \\ \gamma_{yz}^c \end{bmatrix} dy \, dx \quad (7.18)$$

The kinetic energy form could be derived as follows,
from (7.5), (7.6), (7.7)

$$u_u = u_0 - \frac{h}{2} \psi_x - f(x, t)$$

$$u_1 = u_0 + \frac{h}{2} \psi_x$$

$$v_u = v_0 - \frac{h}{2} \psi_y - g(y, t)$$

$$v_1 = v_0 + \frac{h}{2} \psi_y$$

$$w = w(x, y, t)$$

$$T^u = \frac{1}{2} \int_0^a \int_0^b \rho_0 h_1 (\dot{u}_u^2 + \dot{v}_u^2 + \dot{w}^2) \, dy \, dx \quad (7.19)$$

$$T^1 = \frac{1}{2} \int_0^a \int_0^b \rho_0 h_1 (\dot{u}_1^2 + \dot{v}_1^2 + \dot{w}^2) \, dy \, dx \quad (7.20)$$

$$T^c = \frac{1}{2} \int_0^a \int_0^b \rho_c h (\dot{u}_0^2 + \dot{v}_0^2 + \dot{w}^2) \, dy \, dx \quad (7.21)$$

where, ρ_0 is SMA hybrid laminate skin density (lb/in³)

where, ρ_c is sandwich core density (lb/in³)

Therefore, total kinetic energy of sandwich panel is:

$$T = T^u + T^l + T^c \quad (7.22)$$

External work can be expressed due to a transverse uniform loading q_0 , as

$$W = -\frac{1}{2} \int_0^a \int_0^b q_0 w \, dy \, dx \quad (7.23)$$

Thus, employing the variational principle minimizing the total energy, we have the following

$$\begin{aligned} U &= -T + V + W \\ \delta U &= -\delta T + \delta V + \delta W = 0 \end{aligned} \quad (7.24)$$

From Appendix A (A.25), (A.26), (A.27), (A.28), we assume that under simply-supported or cantilever boundary conditions, beams are under cylindrical bending (1-D static condition). Because we ignore the coupling stiffness effect of upper, and lower skins at activation, and there are no nonlinear part containing $N_x^{u,1}$ in the (A.28), we have the following governing equations

$$2 A_{11} \left(\frac{\partial^2 u_0}{\partial x^2} + \frac{\partial w}{\partial x} \frac{\partial^2 w}{\partial x^2} - \frac{1}{2} \frac{\partial^2 f}{\partial x^2} \right) = 0 \quad (7.25)$$

$$A_{11} \left(\frac{\partial^2 u_0}{\partial x^2} + \frac{\partial w}{\partial x} \frac{\partial^2 w}{\partial x^2} - \frac{h}{2} \frac{\partial^2 \psi_x}{\partial x^2} - \frac{\partial^2 f}{\partial x^2} \right) + G_{13} \left(\psi_x - \psi_{sx} + \frac{\partial w}{\partial x} \right) = \frac{D_{11}}{h} \frac{\partial^2 (\psi_x - \psi_{sx})}{\partial x^2} \quad (7.26)$$

$$G_{13} \left(\psi_x - \psi_{sx} + \frac{\partial w}{\partial x} \right) = \frac{D_{11}}{h} \frac{\partial^2 (\psi_x - \psi_{sx})}{\partial x^2} \quad (7.27)$$

$$G_{13} h \left(\frac{\partial \psi_x}{\partial x} - \frac{\partial \psi_{sx}}{\partial x} + \frac{\partial^2 w}{\partial x^2} \right) + q_0 = 0 \quad (7.28)$$

The above equations of motion are able to lead to the same conclusion as Whitney [30] if we neglect (7.25), (7.26) and preserve the bending equations (7.27), (7.28). The ψ_{sx} varies in different materials and is often negligible.

7.2.2 Simply-Supported Sandwich Beam

An example case of sandwich beam under uniform loading condition (static) has been solved by Whitney [30]

$$\psi_x = - \frac{q_0}{24D_{11}} (4x^3 - 6Lx^2 + L^3) \quad (7.29)$$

$$w = \frac{q_0 x}{24D_{11}} [x^3 - 2Lx^2 + L^3 + \frac{12D_{11}}{G_{13}h} (L-x)] \quad (7.30)$$

where q_0 is the uniform load on a sandwich beam.

7.2.3 Cantilever Sandwich Beam (static)

Case 1:

A cantilever beam, under uniform loading, q_0 , can be solved by using (7.27), (7.28) equations along with the cantilever boundary conditions.

$$\psi_x = -\frac{q_0 x^3}{6D_{11}} + \frac{q_0 L x^2}{2D_{11}} - \frac{q_0 L^2 x}{2D_{11}} \quad (7.31)$$

$$w = \frac{q_0 x^4}{24D_{11}} - \frac{q_0 L x^3}{6D_{11}} + \left(\frac{q_0 L^2}{4D_{11}} - \frac{q_0}{2G_{13}h} \right) x^2 + \frac{q_0 L}{G_{13}h} x \quad (7.32)$$

detailed procedures for getting solutions can be found in Appendix B.

Case 2:

A cantilever beam, under concentrated load P at the tip, can be solved by (7.27), and the slightly different Equation (7.28) along with the boundary conditions. See Appendix B for details.

$$\psi_x = \frac{Px^2}{2D_{11}} - \frac{PLx}{D_{11}} \quad (7.33)$$

$$w = \frac{PLx^2}{2D_{11}} - \frac{Px^3}{6D_{11}} + \frac{Px}{G_{13}h} \quad (7.34)$$

7.3 Vibration Analysis of Sandwich Beam

The applications of composite materials have been spread from the aerospace engineering in the early 1960 to the automobile industry, marine engineering, sporting goods, and some other commercial applications. We have found many research papers in composite structures, mostly related to laminated beams and plates or shells but very few of them are associated with the studies of sandwich structures.

Journal papers surveyed by Kapania and Rakesh [32], [33], have shown evidence of applying Classical Laminate Theory (CLT) on thin plate analysis at early stages of applications on composites. The classical theory, which ignores the effect of transverse shear deformation, may not exactly describe the kinematics of relatively thick plates, however. It can underpredict the deflections and overpredict the natural frequencies of thick plates. This is especially true when transverse shear moduli (interlaminar shear moduli) of laminated composite beams and plates are very low as compared to in-plane tensile moduli.

Therefore, shear effects are crucial in composite laminates. Following the classical laminate theory, two categories in the shear deformation theory have been developed. One is the first-order theory and the other is the higher-order theory. The first-order theory, the well-

known Reissner-Mindlin theory, was developed by Reissner [34] and Mindlin [35]. More extensive work by Yang, Norris, and Stavsky [36] and by Whitney, and Pagano [37], following the earlier Mindlin theory, has worked well for laminated beams and plates analysis in predicting deflections, natural frequencies, and buckling loads. The higher-order theory, a more sophisticated idea, considers through-the-thickness stress response, such as σ_z , τ_{xz} , in regions of discontinuities at the boundaries. Thus, the higher-order theory gives more accurate results than CLT or Mindlin's theory. However, the theory requires much higher computing costs and this made it impractical. To overcome this limitation, Reddy [38] has made some progress to make this theory more applicable.

The survey work in [32], [33] also mentioned numerous other research on vibration of composite beams and plates. We found references in section 7.1 referred to this special topic, in particular a paper on the dynamic behavior of composites and sandwich plates by Bert [39]. The papers pertained to symmetrically laminated plates and linear vibration problems using the first-order or the higher-order approach. The solution methodologies involve the analytical closed form solution as well as the approximate numerical method by Galerkin and Rayleigh-Ritz, and numerical techniques such as FEM method.

In recent years, there are considerable amounts of research on the unsymmetric laminated composites (with non-zero B matrix). The reasons of this particular research are: 1) providing a built-in self-damping mechanism when subjected to dynamic excitations, 2) the results of fabrication error in orienting different plies of a structure component, 3) for aeroelastic tailoring to control mode shapes and frequencies of lifting surfaces or 4) to analyze the dynamic characteristics of the unparalleled activations of smart materials embedded in composites or sandwich structures, such as the sandwich beam, made of SMA hybrid composite skins and soft core. The upper skin is stiffer at full activation than the lower skin, indicating that $B_{11} \neq 0$. Some analytical approaches to unsymmetric laminates were presented by Whitney [40] and vibration analysis in unsymmetric composite plates by Jensen [41] have laid a solid foundation in solving the two governing equations as shown in (A.27), (A.28) in Appendix A.

Selection of the first-order shear deformation theory as the assumption of sandwich panel's displacement field, described in section 7.1, is appropriate because of the panel's fairly soft core and the fact that the thin SMA hybrid laminated skins have good bonding force with the core. The higher-order theory may not fit for unprecedented thermal activation and combined core deformations.

A long and flexible beam or a sandwich beam can incur large-amplitude vibration, which leads to nonlinear vibration problems, so its nonlinear governing equations require special technique to obtain fairly good results. The researches in this particular area can be found in Kapania & Raciti [42]. They applied the FEM technique to obtain the nonlinear governing equations, then use the multiple-scale method to solve the nonlinear ordinary differential equation. In our case, however, the governing equations of sandwich beam have already been obtained in section 7.1.

Reviewing the work by Bhimaraddi [43] [44] and Eslami & Kandil [45] [46] has helped the author to solve a group of nonlinear partial differential equations. The method assigns two known admissible functions for w , ψ_x which satisfy the structure boundary conditions. Then applying Galerkin method transforms the nonlinear governing equations into a nonlinear ordinary differential equation which take the form as $\ddot{s} + a_1\dot{s} + a_2s^2 + a_3s^3 = q$. The final step is to use multiple-scale technique to solve this nonlinear ordinary differential equation for free vibration analysis.

The latest research shows that the study of vibrations are mostly related to the analysis of composite beams, plates, shells of solid laminates. There are very few reports dealing with sandwich structures, especially in the study of sandwich beams with embedded smart materials. The nonlinear vibration problems of the SMA hybrid sandwich beam

will be studied for different boundary conditions in the following subsections.

7.3.1 Solution of Simply-Supported Beam

The nonlinearity induced by the unsymmetric laminate of the sandwich skins is expressed in appendix A, (A.18), (A.19) and (A.22). The two simultaneous governing equations (A.27), (A.28) ($u_0 = 0$, preserving the $\partial/\partial x(N_x^u \partial w/\partial x) + \partial/\partial x(N_x^l \partial w/\partial x)$ in (A.28)), with the substitution of (A.22) to (A.15), become

$$-G_{13}h \left(\psi_x + \frac{\partial w}{\partial x} \right) + D_{11} \frac{\partial^2 \psi_x}{\partial x^2} + B_{11} \frac{\partial w}{\partial x} \frac{\partial^2 w}{\partial x^2} = I \psi_x \quad (7.35)$$

$$\begin{aligned} G_{13}h \left(\frac{\partial \psi_x}{\partial x} + \frac{\partial^2 w}{\partial x^2} \right) + \frac{3}{2} (\bar{A}_{11} + A_{11}) \left(\frac{\partial w}{\partial x} \right)^2 \frac{\partial^2 w}{\partial x^2} \\ + \frac{h}{2} (A_{11} - \bar{A}_{11}) \left(\frac{\partial \psi_x}{\partial x} \right) \frac{\partial^2 w}{\partial x^2} \\ + \frac{h}{2} (A_{11} - \bar{A}_{11}) \left(\frac{\partial^2 \psi_x}{\partial x^2} \right) \frac{\partial w}{\partial x} \\ + (N_x^{*u} + N_x^{*l}) \frac{\partial^2 w}{\partial x^2} = (2\rho_0 h_1 + \rho_c h) \ddot{w} + q_0 \end{aligned} \quad (7.36)$$

two nonlinear partial differential equations, where

N_x^{*u} Applied in-plane load due to SMA wire
recovery stress in upper skin (lb/in)

N_x^{*l} Applied in-plane load due to SMA wire
recovery stress in lower skin (lb/in)

I Bending rotational inertia (usually the
term is very small)

Equation (7.36) could be expressed as

$$\frac{\partial \psi_x}{\partial x} = -\frac{\partial^2 w}{\partial x^2} + \frac{q_0}{G_{13}h} + \frac{2\rho_0 h_1 + \rho_c h}{G_{13}h} \ddot{w} - \frac{(N_x^{*u} + N_x^{*l})}{G_{13}h} \frac{\partial^2 w}{\partial x^2} + (\text{Non-linear terms}) \quad (7.36a)$$

Boundary condition (simply-supported)

$$\underline{x=0}$$

$$w = 0 \quad (7.37a)$$

$$\partial \psi_x / \partial x = 0 \quad (7.37b)$$

$$\underline{x=L}$$

$$w = 0 \quad (7.37c)$$

$$\partial \psi_x / \partial x = 0 \quad (7.37d)$$

We could assume the admissible functions as

$$w = S(t) \sin(\alpha x) \quad (7.38)$$

$$\psi_x = (-S(t)/L) \cos(\alpha x) \quad (7.39)$$

$$\alpha = n\pi/L$$

$$n = 1, 2, 3, \dots$$

$$S(t) = \text{flexural amplitude}$$

Equations (7.38) and (7.39) satisfy boundary conditions described in Equations (7.37a), (7.37b), (7.37c), and (7.37d). Take the derivative of (7.35) with respect to x then add (7.36). Insert (7.36a) in $D_{11} \partial / \partial x (\partial \psi_x / \partial x)$ of Equation (7.35), we obtain

$$\begin{aligned}
D_{11} \frac{\partial^2}{\partial x^2} \left(-\frac{\partial^2 w}{\partial x^2} + \frac{q_0}{G_{13}h} + \frac{2\rho_0 h_1 + \rho_c h}{G_{13}h} \ddot{w} - \frac{(N_x^{*u} + N_x^{*i})}{G_{13}h} \frac{\partial^2 w}{\partial x^2} \right) \\
+ B_{11} \frac{\partial}{\partial x} \left(\frac{\partial w}{\partial x} \frac{\partial^2 w}{\partial x^2} \right) + \frac{3}{2} (\bar{A}_{11} + A_{11}) \left(\frac{\partial w}{\partial x} \right)^2 \frac{\partial^2 w}{\partial x^2} \\
+ \frac{h}{2} (A_{11} - \bar{A}_{11}) \left(\frac{\partial \psi_x}{\partial x} \right) \frac{\partial^2 w}{\partial x^2} + \frac{h}{2} (A_{11} - \bar{A}_{11}) \left(\frac{\partial^2 \psi_x}{\partial x^2} \right) \frac{\partial w}{\partial x} \\
+ (N_x^{*u} + N_x^{*i}) \frac{\partial^2 w}{\partial x^2} + q_0 = I \frac{\partial^3 \psi_x}{\partial t^2 \partial x} + (2\rho_0 h_1 + \rho_c h) \frac{\partial^2 w}{\partial t^2}
\end{aligned} \quad (7.40)$$

Note that the shear effect and the in-plane load effect are included in $D_{11}\partial^2/\partial x^2$ term. Ignore the nonlinear part in $D_{11}\partial^2/\partial x^2$ (...). Then substitute (7.38), (7.39) in (7.40) and apply Galerkin method for (7.40) with weighing function $\sin(\alpha x)$. The Equation for the simply-supported vibration beam (Figure 7.3) becomes:



$$\alpha = n\pi/L$$

Figure 7.3. The simply-supported beam

$$\begin{aligned}
\int_0^L \left\langle -s \left[D_{11} \left(1 + \frac{(N_x^{*u} + N_x^{*i})}{G_{13}h} \right) \alpha^4 + (N_x^{*u} + N_x^{*i}) \alpha^2 \right] \sin^2 \alpha x \right. \\
+ B_{11} (\alpha^4 \sin^3 \alpha x - \alpha^4 \cos^2 \alpha x \sin \alpha x) s^2 \\
- \frac{3}{2} (\bar{A}_{11} + A_{11}) s^3 \alpha^4 \cos^2 \alpha x \sin^2 \alpha x - \frac{h}{2} (A_{11} - \bar{A}_{11}) \frac{s^2}{L} \alpha^3 \sin^3 \alpha x \\
+ \frac{h}{2} (A_{11} - \bar{A}_{11}) \frac{s^2}{L} \alpha^3 \cos^2 \alpha x \sin \alpha x \left. \right\rangle dx + \int_0^L q_0 \sin \alpha x \, dx \\
= \int_0^L \left[\frac{I\alpha}{L} + (2\rho_0 h_1 + \rho_c h) + \frac{D_{11} (2\rho_0 h_1 + \rho_c h)}{G_{13}h} \alpha^2 \right] \sin^2 \alpha x \, dx
\end{aligned} \quad (7.41)$$

$$\begin{aligned}
& -s \left[D_{11} \left(1 + \frac{N_x^{*u} + N_x^{*1}}{G_{13}h} \right) \alpha^4 + (N_x^{*u} + N_x^{*1}) \alpha^2 \right] \frac{L}{2} + \\
& s^2 \left(\frac{2}{3} \alpha^3 B_{11} - \frac{h\alpha^2}{3L} (A_{11} - \bar{A}_{11}) \right) - s^3 \left(\frac{3\alpha^4 L}{16} (\bar{A}_{11} + A_{11}) \right) \\
& + \frac{2q_0 L}{n\pi} = \ddot{s} \left[(2\rho_0 h_1 + \rho_c h) \left(1 + \frac{D_{11}}{G_{13}h} \alpha^2 \right) + \frac{I\alpha}{L} \right] \frac{L}{2}
\end{aligned} \quad (7.41a)$$

Eliminating the inertia term, we obtain a static problem of external uniform load q_0 over span of L . For free vibrational analysis, we delete q_0 , and (7.41a) could be simply expressed as

$$a_1 \ddot{s} + a_2 s + a_3 s^2 + a_4 s^3 = 0 \quad (7.42)$$

where

$$a_1 = (2\rho_0 h_1 + \rho_c h) \left(1 + \frac{D_{11}}{G_{13}h} \alpha^2 \right) + \frac{I\alpha}{L} \quad (7.42a)$$

$$a_2 = D_{11} \left(1 + \frac{N_x^{*u} + N_x^{*1}}{G_{13}h} \right) \alpha^4 + (N_x^{*u} + N_x^{*1}) \alpha^2 \quad (7.42b)$$

$$a_3 = \left(\frac{h\alpha^2}{3L} (A_{11} - \bar{A}_{11}) - \frac{2}{3} B_{11} \alpha^3 \right) \frac{2}{L} \quad (7.42c)$$

$$a_4 = \frac{3\alpha^4 L}{16} (\bar{A}_{11} + A_{11}) \frac{2}{L} \quad (7.42d)$$

(7.42) can also be expressed as

$$\ddot{s} + \omega^2 s + \frac{a_3}{a_1} s^2 + \frac{a_4}{a_1} s^3 = 0 \quad (7.43)$$

$$\omega^2 = \frac{D_{11} \left(1 + \frac{N_x^{*u} + N_x^{*l}}{G_{13}h}\right) \alpha^4 + (N_x^{*u} + N_x^{*l}) \alpha^2}{(2\rho_0 h_1 + \rho_c h) \left(1 + \frac{D_{11}}{G_{13}h} \alpha^2\right) + \frac{I\alpha}{L}} \quad (7.43a)$$

Equation (7.43) is Duffing equation without the damping term. The current methods of treating (7.43) include Newton-Raphson approach like Singh & Rao [47], the finite element in time (FET) method of Baughan & Hong [48], the finite element method of Hou & Yuan [49] and the multiple scale technique in Bhimaraddi [43], [44].

The cubic nonlinearity described in $(a_4/a_1)s^3$ is a stiffening factor as the vibration amplitude becomes large enough, or this term can also be used to describe a softening factor if (a_4/a_1) is negative. This phenomenon can be found in Cartwell [50], and Schmidt & Tondl [51], all of whom investigate some parametrically excited systems or coupled nonlinear vibration systems.

7.3.1.1 Case study of linear vibration

The nonlinear vibration response for a nonactivated SMA sandwich beam or its two-faces-activated case is determined by (7.43) but with $a_3=0$, since $A_{11} = \bar{A}_{11}$, $B_{11} = 0$ (the case is equivalent to a symmetric condition). Therefore, (7.43) becomes

$$\ddot{s} + \omega^2 s + (a_4/a_1)s^3 = 0 \quad (7.44)$$

If we use Whittney's equation (10.69) [30, p. 280] for the simply-supported boundary condition, we get the linear eigen value characteristic equations defined in (7.45), (7.46) are

$$-(D_{11} \frac{n^2 \pi^2}{L^2} + G_{13} h) A_n - G_{13} h \frac{n \pi}{L} B_n = -I \omega_n^2 A_n \quad (7.45)$$

$$-G_{13} h \frac{n \pi}{L} A_n - G_{13} h \frac{n^2 \pi^2}{L^2} B_n = -\rho \omega_n^2 B_n \quad (7.46)$$

$$\begin{bmatrix} (D_{11} \frac{n^2 \pi^2}{L^2} + G_{13} h) - I \omega_n^2 & G_{13} h \frac{n \pi}{L} \\ G_{13} h \frac{n \pi}{L} & G_{13} h \frac{n^2 \pi^2}{L^2} - \rho \omega_n^2 \end{bmatrix} \begin{bmatrix} A_n \\ B_n \end{bmatrix} = 0 \quad (7.47)$$

which is equivalent to the solution of (7.44) without the s^3 term, in other words, to the solution of small amplitude A.

For Mode 1 :

$$n=1, \text{ wvf} = 6.7\%$$

$$D_{11} = 2264.4 \text{ lb}_f \text{ in} = 2264.4 \times 12 \text{ slug in}^2 / \text{sec}^2$$

$$L = 12 \text{ in}$$

$$G_{13} = 600 \text{ lb}_f / \text{in}^2 = 600 \times 12 \text{ slug} / \text{in sec}^2$$

$$h = 0.2 \text{ in}$$

$$I = 2\rho_0 h_1 \times ((2h_1 + h)/2)^2 = 2.6 \times 10^{-5} (\text{lb}_m \text{ in}^3) \\ = 2.6 \times 10^{-5} / 32.2 (\text{slug in}^3)$$

for wvf=6.7%, 1 SMA hybrid layer at both top & bottom face of the sandwich beam

$$\rho = 2 \times \rho_0 h_1 + \rho_c x h = 2.675 \times 10^{-3} (\text{lb}_m / \text{in}^2) \\ = 2.675 \times 10^{-3} / 32.2 (\text{slug/in}^2)$$

G_{13} is shear modulus of (XUS 46218.00) which is blue

closed cell extruded polystyrene foam, produced by Dow Chemical Company.

Dimensional compatibility is very crucial for dimensional characteristic equation in eigen value calculation, from (7.47) we get $\omega_1 = 817.8$ rad/sec. We could also use Whittney [30] eq.(10.72), (10.73) to get the eigen value, for 1st mode ($n = 1$)

$$\omega_1 = \omega_1^* \sqrt{1 - \frac{B\pi^2}{1+B\pi^2}}$$

$$\omega_1^* = \frac{\pi^2}{L^2} \sqrt{\frac{D_{11}}{\rho}} \quad , \quad B = \frac{D_{11}}{G_{13}hL^2}$$

$$\omega_1^* = \frac{\pi^2}{12^2} \sqrt{\frac{2264.4 \times 32.2 \times 12}{2.675 \times 10^{-3}}} = 1239.57 \frac{\text{rad}}{\text{sec}}$$

Where, $\omega_1 = 1239.57 \times 0.6599 = \underline{817.99}$ rad/sec (both face activated condition without in-plane forces) comparing the above approaches to the linear solution of (7.44) at null amplitude to thickness ratio ($A/h = 0$), namely 818.4 rad/sec, from which we conclude that the Galerkin method is accurate enough. This solution of nonlinear modal analysis of (7.43), (7.44) is based on Bhimaraddi [43] eq.(18) $\underline{\omega_N = \omega_1[1+b_1A^2+b_2A^4+b_3A^6] + O(\epsilon^6)}$ et al. All the procedure is coded in Gencom2 for even further analysis of damped and forced dynamic response.

7.3.2 Damped System under Harmonic Excitation

The nonlinear vibration model, illustrated in the previous section, is merely for the study of undamped free vibration. It has inherent features of increased natural frequencies with respect to higher vibrational amplitude (A/h) under the prescribed condition. Our primary goal, in this section, is to excite the known nonlinear model with a harmonic load to find the dynamic response in either the time domain or the frequency domain.

The physical model is a sandwich beam of composite faces with SMA wires embedded, and the sandwich core is a good damping materials. All the properties of the model were mentioned in the previous sections. This damped system, however, is not a viscously damped but a hysteretically damped system. The rationale is based on the fact that the composite material with polymer matrix follows the elastic-viscoelastic correspondence principle (its moduli can be expressed as complex moduli). In view of [22] and [52], the governing equation is (7.42) with a harmonic forcing term added on the right hand side. The equation becomes

$$\ddot{s} + \omega^2 s + d_2 \dot{s}^2 + d_3 s^3 = \epsilon q' \cos \Omega t \quad (7.48)$$

where ω^2 , d_2 , d_3 , were defined in equation (7.43a) and (7.42a - 7.42d), ϵ is small, and $q' = 4q_0/(\pi a_1 h)$ (#/slug in) as indicated in (7.41a). Ω is forcing frequency (rad/sec), t

is time step, and s is nondimensional amplitude (A/h). Since $\underline{1}$ is very small and \underline{L} is large for long beam, (7.42a) can be simplified as

$$a_1 = (2\rho_0 h_1 + \rho_c h) \left(1 + \frac{\bar{D}_{11}}{G_{13}h} \alpha^2\right) \quad (7.48a)$$

We then apply the correspondence principle from [53] and [54],

$$\bar{G}_{13} = G_{13} + i \eta_c G_{13} \quad (7.48a)$$

$$\bar{D}_{11} = D_{11} + i \eta_b D_{11} \quad (7.48b)$$

$$(A_{11} - \bar{A}_{11})^* = (A_{11} - \bar{A}_{11}) + i \eta_e (A_{11} - \bar{A}_{11}) \quad (7.48c)$$

$$B_{11}^* = B_{11} + i \eta_d B_{11} \quad (7.48d)$$

$$(A_{11} + \bar{A}_{11})^* = (A_{11} + \bar{A}_{11}) + i \eta_a (A_{11} + \bar{A}_{11}) \quad (7.48e)$$

where η_b , η_a , η_d , η_e are the loss factors for the composite laminate [54], $i = \sqrt{-1}$, the values of η_b , η_a , η_d , η_e are approximately $.2 \eta_m$ [η_m (loss factor of epoxy matrix) = .015], core η_c is approximately .12. Therefore, the known values of loss factor can be substituted in the following expressions,

$$\omega^2 = \frac{\bar{D}_{11} \left(1 + \frac{N_x^{*u} + N_x^{*1}}{G_{13}h}\right) \alpha^4 + (N_x^{*u} + N_x^{*1}) \alpha^2}{a_1} \quad (7.49)$$

$$d_2 = \bar{a}_2 / a_1 \quad (7.50)$$

$$\bar{a}_2 = \left(\frac{h\alpha^2}{3L} (A_{11} - \bar{A}_{11})^* - \frac{2}{3} B_{11}^* \alpha^3 \right) \frac{2}{L} \quad (7.50a)$$

$$d_3 = \bar{a}_3 / a_1 \quad (7.51)$$

$$\bar{a}_3 = \frac{3\alpha^4 L}{16} (\bar{A}_{11} + A_{11}) \cdot \frac{2}{L} \quad (7.51a)$$

From (7.48a), the real part and imaginary part can be expressed as

$$e_1 = (2\rho_0 h_1 + \rho_c h) \left(1 + \frac{(1 + \eta_b \eta_c) D_{11} G_{13} \alpha^2}{(G_{13}^2 + \eta_c^2 G_{13}^2) h} \right) \quad (7.52)$$

$$e_2 = (2\rho_0 h_1 + \rho_c h) \frac{(\eta_b - \eta_c) D_{11} G_{13} \alpha^2}{(G_{13}^2 + \eta_c^2 G_{13}^2) h} \quad (7.52a)$$

From (7.49), the real part and imaginary part of numerator can be expressed as

$$e_3 = D_{11} \left(1 + \frac{(1 + \eta_b \eta_c) G_{13} (N_x^{*u} + N_x^{*l})}{(G_{13}^2 + \eta_c^2 G_{13}^2) h} \right) \alpha^4 + (N_x^{*u} + N_x^{*l}) \alpha^2 \quad (7.53)$$

$$e_4 = (\eta_b D_{11} + \frac{(\eta_b - \eta_c) D_{11} G_{13} (N_x^{*u} + N_x^{*l})}{(G_{13}^2 + \eta_c^2 G_{13}^2) h}) \alpha^4 \quad (7.53a)$$

with

$$\omega^2 = e^5 + i e_6$$

$$e_5 = (e_1 e_3 + e_2 e_4) / (e_1^2 + e_2^2)$$

$$e_6 = (e_1 e_4 - e_2 e_3) / (e_1^2 + e_2^2)$$

from (7.50a), (7.51a), we get

$$\bar{a}_2 = a_{21} + i a_{22}$$

$$\bar{a}_3 = a_{31} + i a_{32}$$

$$a_{21} = \left(\frac{h\alpha^2}{3L} (A_{11} - \bar{A}_{11}) - \frac{2}{3} B_{11} \alpha^3 \right) \frac{2}{L}$$

$$a_{22} = \left(\eta_e \frac{h\alpha^2}{3L} (A_{11} - \bar{A}_{11}) - \eta_d \frac{2}{3} B_{11} \alpha^3 \right) \frac{2}{L}$$

$$a_{31} = \frac{3\alpha^4}{8} (\bar{A}_{11} + A_{11})$$

$$a_{32} = \eta_a \frac{3\alpha^4}{8} (\bar{A}_{11} + A_{11})$$

$$d_2 = (a_{21}e_1 + a_{22}e_2) / (e_1^2 + e_2^2) +$$

$$i (e_1 a_{22} - e_2 a_{21}) / (e_1^2 + e_2^2) = e_7 + i e_8$$

$$d_3 = (a_{31}e_1 + a_{32}e_2) / (e_1^2 + e_2^2) +$$

$$i (e_1 a_{32} - e_2 a_{31}) / (e_1^2 + e_2^2) = e_9 + i e_{10}$$

Therefore, the nonlinear ordinary differential equation (7.48), with its amplitude s , follows the correspondence principle also can be expressed as below (see [55]).

$$s = X + i Y$$

We substitute this expression into eq (7.48)

$$\begin{aligned} & (\ddot{X} + i\ddot{Y}) + (e_5 + ie_6)(X + iY) + (e_7 + ie_8)(X + iY)^2 + \\ & (e_9 + ie_{10})(X + iY)^3 = \epsilon q' \cos \Omega t \end{aligned}$$

(7.54)

Separation of the real and imaginary parts in equation (7.53) gives

real part

$$\ddot{X} + e_5 X - e_6 Y + e_7 (X^2 - Y^2) - 2e_8 XY + e_9 (X^3 - 3XY^2) + e_{10} (Y^3 - 3X^2Y) = (\epsilon e_1 q''') / (e_1^2 + e_2^2) \cos \Omega t \quad (7.54a)$$

imaginary part

$$\ddot{Y} + e_5 X + e_6 Y + e_8 (X^2 - Y^2) + 2e_7 XY - e_9 (Y^3 - 3YX^2) + e_{10} (X^3 - 3Y^2X) = (-\epsilon e_2 q''') / (e_1^2 + e_2^2) \cos \Omega t \quad (7.54b)$$

where $q''' = 4q_0 / (\pi h)$

Solving (7.54a) and (7.54b) system of highly nonlinear and coupled equations with assumed initial conditions, as

$$X(0) = \dot{X}(0) = Y(0) = \dot{Y}(0) = 0 \quad (7.55)$$

we obtained the calculated dynamic response under harmonic excitation. However, there is no analytical solution for the system of equations and it is necessary to use numerical method to find solutions.

Using the higher order Runge-Kutta approach to obtain the time response of the physical model, we insert the prescribed SMA sandwich beam model in (7.54a), (7.54b) and (7.55) then apply ode45 (fixed time step) of MATLAB to get the response plot as shown from Figures 7.11 to 7.13. The

real part \underline{X} is the physical nondimensional amplitude-time response at a specific excited frequency. The frequency response could also be obtained by FFT (fast fourier transform) over the calculated time response.

7.3.3 Analysis of Nonlinear Vibration

The analytical results for sub-section 7.3.1 and 7.3.2 will be discussed in this sub-section. We will discuss the free vibration of two SMA hybrid sandwich beam models with different SMA wire volume fraction in each beam in the next sub-sections. Results of a complete analysis of the forced responses of the two SMA sandwich beam models are discussed in the sub-section 7.3.3.3 after the free vibration analysis.

7.3.3.1 Free Vibration of Short Beam

The nonlinear frequencies (1st mode) of SMA hybrid sandwich beam (s.s) for a short beam model are described as

Model 1 : $L = 12"$

width = 1"

Three SMA volume fractions 6.7%, 10%, 16% were calculated by the multiple scale method, and the diagrams are plotted with three different core depths. In Figure 7.4 $(wvf) = 0.16$, Figure 7.5 $(wvf) = 0.1$, Figure 7.6 $(wvf) = 0.067$ there are three groups of curves represent the three beams with core depths 0.2", 0.4", 0.6" as typical analytical Model 1 cases.

Each group has three curves where

Dash dot line (_._._) : nonactivated SMA hybrid beam

Dashed line (-----) : upper face activated beam

Solid line (————) : both faces activated

A : free vibration amplitude of the midpoint of beam

All the plots were calculated under the assumption of no recovery force effect (pure simply supported B.C); the results checked with reference [56]. The same pattern of nonlinear frequency curves is shown for the cubic and quadratic terms stiffening effects while A/h is larger than 0.1. The linear natural frequencies (A/h smaller than 0.1) of SMA hybrid sandwich beams for three different core depths in Figure 7.4 to Figure 7.6 show that higher volume fractions of SMA gave lower natural frequencies for Model 1 sandwich beams. But the differences between activation and non- activation are more obvious. Especially, the upper-face or lower-face activated condition at large A/h showed nonlinear frequencies lower than nonactivated condition.

However, the recovery force (N_x) does appear in the hinged-hinged boundary condition. The beam length in the x-direction does not change ($u_0 = 0$) under this particular boundary condition. The activated SMA wires tend to shrink back to the original austenite state but are constrained by hinged end support, and large in-plane forces are induced by SMA wires which are embedded in the composite laminated faces (fiber glass/epoxy).

Figure 7.7 gives the analytical results of Model 1 beam with SMA volume fraction 0.067 as in Figure 7.6 , but the diagram clearly shows the increase of natural frequencies under the effect of in-plane forces produced by SMA recovery forces in the same beams as in Figure 7.6 . This is the hinged-hinged boundary condition, and the in-plane forces 90#/in are estimated under the volume fraction of SMA representing 20 wires (0.01 OD) at recovery stress 58 ksi, inserted in 2 plies of fiber-glass prepreg. Each wire creates approximately 4.5 bounds of force.

7.3.3.2 Free Vibration of Long Beam

The nonlinear frequencies (1st mode) of SMA hybrid sandwich beam (s.s) for a long beam model described as

Model 2 : L = 120"

width = 1"

Two SMA volume fractions 6.7%, 16% were calculated by the multiple scale method, and the diagrams are plotted with three different core depths. In Figure 7.8 (wvf) = 0.16, Figure 7.9 (wvf) = 0.067 , Figure 7.10 (wvf) = 0.067 , in-plane force effect. There are three groups of curves, in each figure, representing the three beams with core depths 0.2", 0.4", 0.6" as typical analytical Model 2 cases. Each group has three curves

Dash dot line(-._-.-) : nonactivated SMA hybrid beam

Dashed line (-----) : upper face activated beam

Solid line (——) : both faces activated

A : free vibration amplitude of the midpoint of beam
The inplane force (45#/in) in the face sheet of the sandwich beams of Figure 7.10 was assumed value, it is due to the possible slippage of wires if the ends at boundary fixing devices are not tight enough.

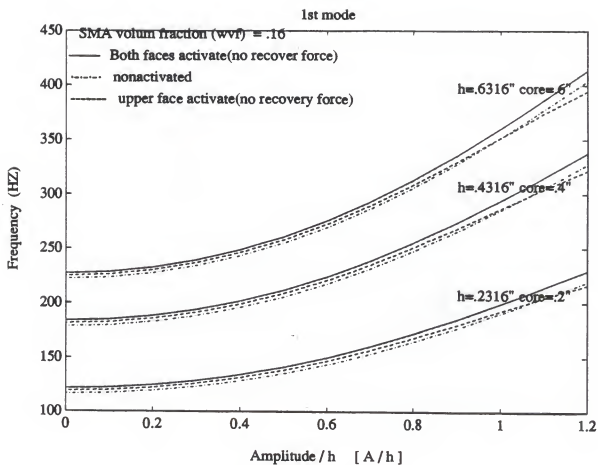


Figure 7.4 Free vibration nonlinear frequency of Model 1
(wvf) = 16%

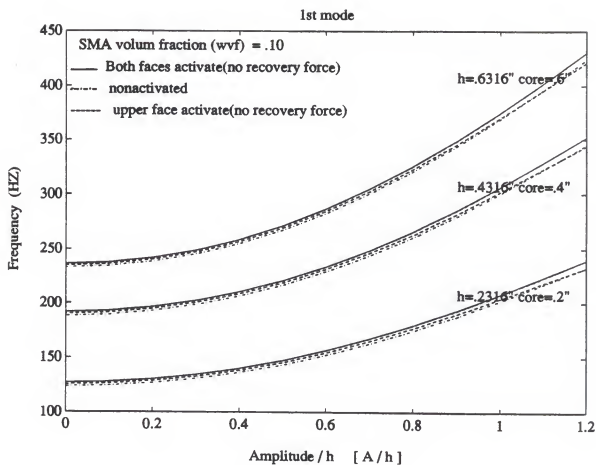


Figure 7.5. Free vibration of nonlinear frequency Model 1
(wvf) = 10%

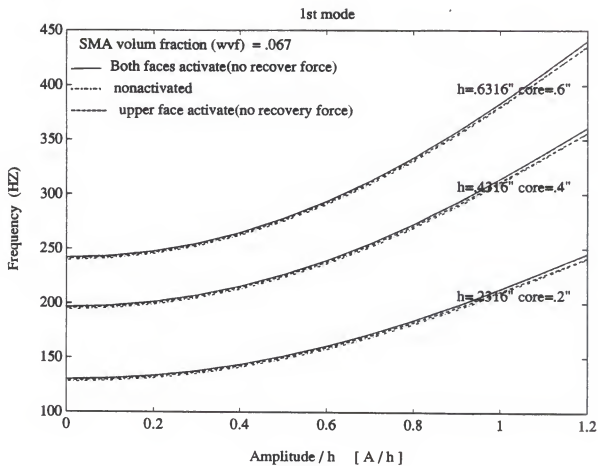


Figure 7.6. Free vibration of nonlinear frequency Model 1
 (wvf) = 6.7%

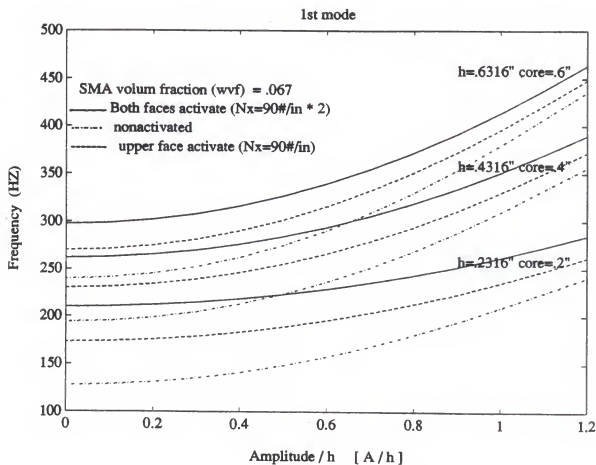


Figure 7.7. Free vibration of nonlinear frequency Model 1
(wvf) = 6.7% (inplane forces effect)

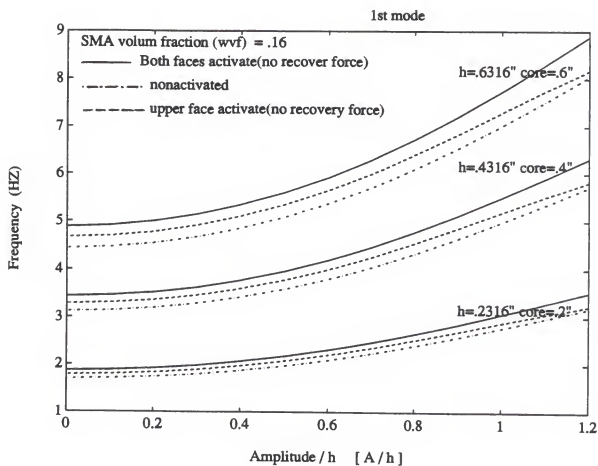


Figure 7.8 Nonlinear frequency of Model 2 (wvf)=16%

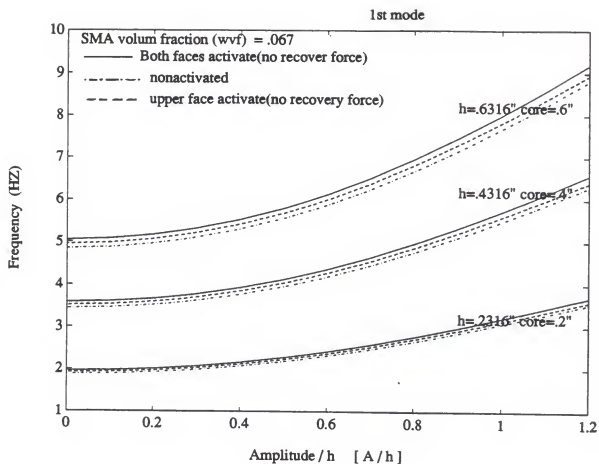


Figure 7.9 Nonlinear frequency of Model 2 (wvf)=6.7%

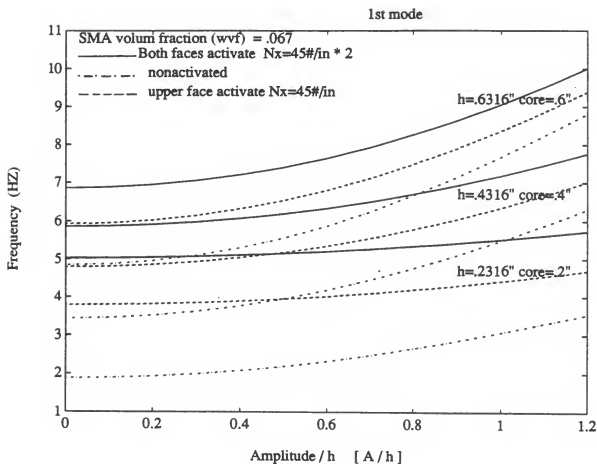


Figure 7.10 Nonlinear frequency of Model 2 (wvf)=6.7%
(inplane force effect)

In comparison to Figure 7.6 and Figure 7.7 , Figure 7.9 and Figure 7.10 manifest greater differences in recovery stress (in-plane force) effects. The design of SMA hybrid sandwich beam could utilize the said effects in vibration suppression for short and long beams, and adding the good damping effect of sandwich core materials also reduces acoustic noise in many applications.

Due to the fact that design of structure components seeks to obtain lighter weight and lower stress levels, a smaller SMA volume fraction (but not smaller than 3%) in the laminate is recommended. The internal stresses induced in laminates, while the wires are activated, can be decreased if a lower volume fraction of SMA wires are embedded.

7.3.3.3 Dynamic Response of SMA Sandwich Beam

The dynamic responses of the simply-supported beam, described in the sub-section 7.3.2, are calculated and plotted in the following Figure 7.11, 7.12, 7.13.

Each diagram has an upper section and a lower section; the upper represents the time response, and the lower is its response in the frequency domain under a particular excitation frequency.

The text "omega" at the left side of each diagram is the harmonic forcing frequency. The y-label " A/h "

represents the "(deflection of middle point of the beam) / (thickness of the core)."

In Figure 7.11, the time response of a long beam, under the harmonic excitation ($\omega=0.6366$ HZ = 4 rad/sec) at the beam center; showing vibrational amplitudes of this beam's center at the nonactivated ($N_x^u=N_x^{*1}=0$) and the activated ($N_x^u=N_x^{*1}=45\#/in$) condition. We use 4th/5th order Runge-Kutta-Fehlberg method to calculate the time response of Equation (7.54a) and (7.54b) from $t_0=0.0$ second to $t_f=6.0$ seconds. Totally 1024 time steps were taken and each time interval were fixed. Use of the Hanning window on these two steady-state responses, we can apply fast fourier transform (FFT) to transform dynamic responses from time domain (upper diagram) to frequency domain (lower diagram). The lower diagram shows response amplitudes of these nonactivated and activated beams, it also show the excited frequency and the natural frequency of each condition. From the lower diagram, the nonactivated beam's response has two peaks; one is at $\omega=.6366$ HZ and the other is at beam's natural frequency which can be cross-checked in Figure 7.10. The activated beam's response also possess two peaks where one peak is at excited frequency and the other peak is at the natural frequency, which is found compatible to that of Figure 7.10.

In Figure 7.12, responses of the same beam (model 2), under the harmonic excitation ($\omega=3.183$ HZ = 20 rad/sec); at the same nonactivated/activated conditions and solution

methods. Because the excited frequency is close to the nonactivated beam's natural frequency, the beat phenomenon happens for this nonactivated beam. The lower diagram shows that the natural frequency increases for this nonactivated beam as the beam's vibrational amplitude increases. The diagram also has two major peaks and other small peaks in frequency domain. This phenomenon may be resulted from its nonlinear behavior at near-resonance occurrence. Also, the activated beam's vibrational amplitude has two peaks represent the excited frequency and its natural frequency.

In Figure 7.13, the same nonactivated and activated conditions for this long beam were under near-resonance excitation which is close to the natural frequency of this activated beam. The solid line is the time response for activated beam, the response also shows beat phenomenon. The two peaks of solid line, in frequency domain, represent both the excited frequency and natural frequency. The natural frequency is about 6 HZ, greater than 5 HZ depicted in Figure 7.10, which is due to its increasing vibrational amplitude.

Apparently, under this harmonic excitation ($\omega = 5.013\text{HZ}$), we can deactivate the activated beam by cooling it. The beam transforms back to nonactivated condition as the dashed line represents in Figure 7.13. This is how we can tune the structure to shift its natural frequency.

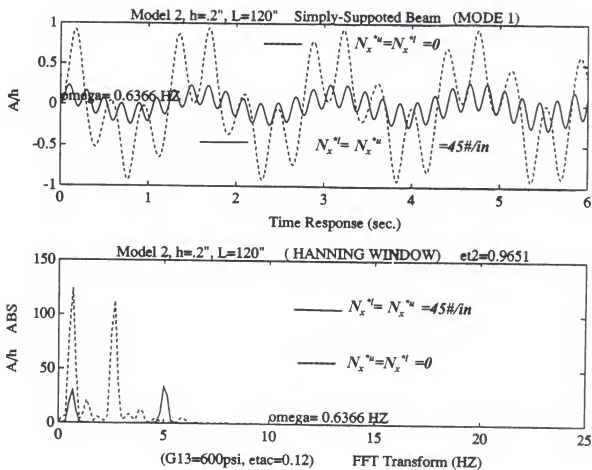


Figure 7.11. Dynamic response of Model 2 ($q=.1$)

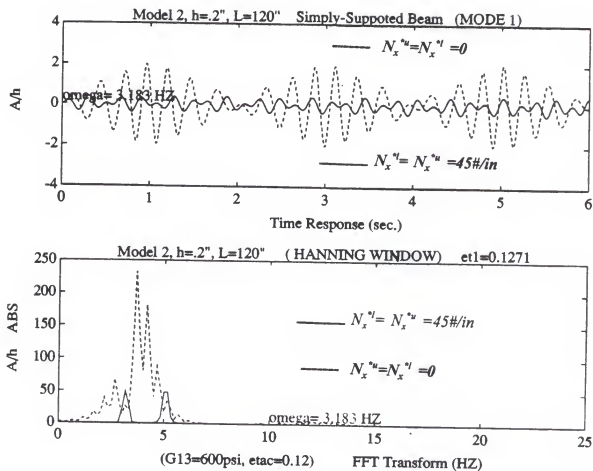


Figure 7.12. Dynamic response of Model 2 ($q=.1$)

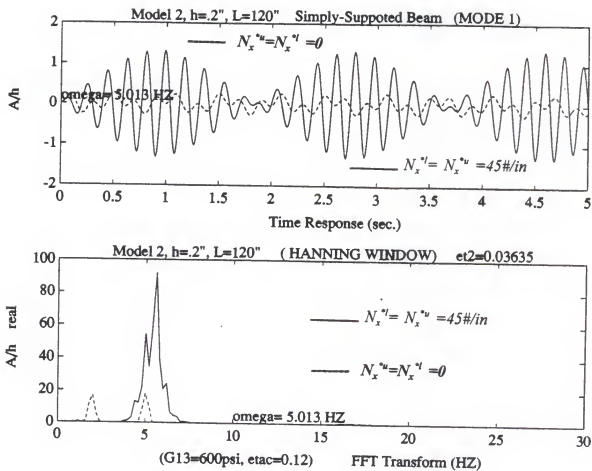


Figure 7.13. Dynamic response of Model 2 ($\alpha=.1$)

CHAPTER 8

CONCLUSION AND FUTURE WORK

The current problems in dealing with the vibration control of structures are primarily attributable to two concerns. One is to reduce the stress level in structural or mechanical parts when the vibration occurs by methods such as damping to reduce the vibrational amplitude to achieve longer operational life; the second is to control the modal response of structures. Using SMA in the composite structure is part of the solution to both problems.

8.1 Conclusion of Current Study

There are five major research areas in this dissertation. They are:

- Heat conduction, transient thermal response

We can make a structure stiffer or more flexible by adding or dissipating a small amount of thermal energy. Chapter 1, Chapter 2, and Chapter 4 describe SMA properties and the transient thermal response with test comparisons and analyses so that the activation/deactivation process in hybrid structures can be analyzed.

- Stress-strain relations of SMA hybrid composites

We have to deal with this problem with care because of

its complexity. In a composite plate, the stress-strain relations must combine with the internal stresses induced by the SMA wires. This is complicated by the two distinct behaviors of SMA at the two different material phases, hot and cold, which has generated the special term, recovery stress, due to initial straining before embedding into the structure. The author used a simple modeling approach to achieve near-uniform internal stress distribution in composite laminate (0° fiber alignment using SMA wires as a first case). We can simply use classical laminate theory plus internal stress distribution analysis to estimate the laminate strength during the activation/deactivation. This approach is still in the scope of macromechanics.

- Making of SMA hybrid composites

The fabrication of even a simple SMA laminate beam of four to eight layers is tedious work, especially in the tooling for SMA wire pre-straining and fixing which has many more procedures than that of plain laminates. The description of this is in Chapter 3.

- Testing of specimens

This is another time-consuming process for SMA hybrid structures. The boundary conditions for the hybrid structures must be compatible with theoretical assumptions. The experimenter must avoid data errors and imperfect specimens which can make the comparison impossible. The

experiments described in Chapter 4 and Chapter 6 show different levels of complexities.

- Dynamic behavior of SMA hybrid structures

The equation of motion of a sandwich beam in general has extended to the first order nonlinear approach. The assumptions are based on large deformation theory and the hinged support (hinged-simply supported) boundary condition which could be modeled conservatively as a beam or a panel fastened to a base structure.

This particular hinged support beam case can also be applied to a 2-D sandwich panel. We just add more related terms in the 2-D governing equations, and the admissible functions can be obtained in like fashion.

Basically, we used the natural frequency shifting method, an open loop control system, to suppress vibrations. The stiffening effect is greater for a sandwich panel with a thicker core (diagrams in Chapter 7) even without the recovery stress effect. This is even more valid for softer face sheets.

The application of SMA hybrid structure with a cantilever boundary condition is also possible. We can use active property tuning (APT) to increase its flexural stiffness to control the static deflection or buckling strength. Another approach for modal control of a rotating cantilever structure such as a large rotating wind turbine could be active strain energy tuning (ASET).

8.2 Future Study of SMA Hybrid Structures

Suggestions for future study include:

- Use in short fiber composites and other materials.

The base composite material may not have to be uni-directional fiber-reinforced composites. They can be short fiber (SMC) panels, plain epoxy, and plastics. Although, coating of SMA wires might be required for better bonding with base composite materials.

- Prediction of microstresses in SMA hybrid composites.

SMA hybrid structures may have higher internal stresses with higher wire volume fraction, especially at a cantilever boundary condition as depicted in last few diagrams in the Chapter 5. The σ_c , τ_{xz} (composite's compressive stress and shear stress) combined with the hygrothermal effect of the laminate can generate very complicated problems in micro-crack, resulting in local failure at the microstress level. The shear stress and peeling stress at the bonding interfaces between the face laminates and sandwich core may cause debonding at the activation. Large amplitude vibrations of a sandwich beam may obtain stronger bonding force by using high performance film adhesives. In the study of fracture problems, the activation of SMA wires in composites may result in the closure of small cracks.

- The use of SMA wires in woven composite.

Stitching method is potentially very helpful to forestall delamination and improve dynamic properties simultaneously. In these cases, the modeling of the hybrid structure's stiffness, strength, microstress is very critical.

- Other potential applications.

In modal analysis, using SMA to control low frequency vibrations of long flexible beams or panels made of hybrid composites could be very important.

Using SMA as both sensor and actuator in more advanced closed loop vibration control devices for long flexible structures.

Using SMA in structures for acoustic noise control.

And, in configuration problems, using SMA in structures to control the geometric shapes.

APPENDIX A
THE EQUATION OF MOTION OF SANDWICH PANEL

The variational principle of (7.24) in Chapter 7 will be derived in details as the following:

$$\begin{aligned}
 \delta T = & \frac{1}{2} \int_0^a \int_0^b \rho_0 h_1 \delta (\dot{u}_u^2 + \dot{v}_u^2 + \dot{w}^2) dy dx \\
 & + \frac{1}{2} \int_0^a \int_0^b \rho_0 h_1 \delta (\dot{u}_1^2 + \dot{v}_1^2 + \dot{w}^2) dy dx \\
 & + \frac{1}{2} \int_0^a \int_0^b \rho_c h \delta (\dot{u}_0^2 + \dot{v}_0^2 + \dot{w}^2) dy dx
 \end{aligned} \tag{A.1}$$

For example, taking the upper skin velocity in x-dir. we get

$$\begin{aligned}
 \frac{1}{2} \int_0^a \int_0^b \rho_0 h_1 \delta \dot{u}_u^2 dy dx &= \rho_0 h_1 \int_0^a \int_0^b \dot{u}_u \delta \dot{u}_u dy dx \\
 &= \rho_0 h_1 \int_0^a \int_0^b \frac{\partial u_u}{\partial t} \frac{\partial}{\partial t} (\delta u_u) dy dx \\
 &= \rho_0 h_1 \int_0^a \int_0^b \left(\frac{\partial u_u}{\partial t} \delta u_u \Big|_0^1 - \frac{\partial^2 u_u}{\partial t^2} \delta u_u \right) dy dx \\
 \delta u_u(0) &= \delta u_u(t_1) = 0
 \end{aligned} \tag{A.2}$$

assumed that the
same fasion for

$$\delta \dot{u}_1^2, \delta \dot{v}_u^2, \delta \dot{v}_1^2$$

Therefore,

$$\delta T = \int_0^a \int_0^b \left(-\rho_0 h_1 \ddot{u}_u \delta u_u - \rho_0 h_1 \ddot{u}_1 \delta u_1 - \rho_0 h_1 \ddot{v}_u \delta v_u - \rho_0 h_1 \ddot{v}_1 \delta v_1 - 2\rho_0 h_1 \ddot{w} \delta w - \rho_c h \ddot{u}_0 \delta u_0 - \rho_c h \ddot{v}_0 \delta v_0 - \rho_c h \ddot{w} \delta w \right) dy dx \quad (\text{A.3})$$

since,

$$\begin{aligned} \ddot{u}_u \delta u_u &= \left(\ddot{u}_0 + \frac{h}{2} \ddot{\psi}_x - \ddot{f} \right) (\delta u_0 + \frac{h}{2} \delta \psi_x - \delta f) \\ \ddot{u}_1 \delta u_1 &= \left(\ddot{u}_0 - \frac{h}{2} \ddot{\psi}_x \right) (\delta u_0 - \frac{h}{2} \delta \psi_x) \\ \ddot{v}_u \delta v_u &= \left(\ddot{v}_0 + \frac{h}{2} \ddot{\psi}_y - \ddot{g} \right) (\delta v_0 + \frac{h}{2} \delta \psi_y - \delta g) \\ \ddot{v}_1 \delta v_1 &= \left(\ddot{v}_0 - \frac{h}{2} \ddot{\psi}_y \right) (\delta v_0 - \frac{h}{2} \delta \psi_y) \end{aligned}$$

After several manipulations, (A.3) is

$$\begin{aligned} \delta T = \int_0^a \int_0^b & \left[\left(-(2\rho_0 h_1 + \rho_c h) \ddot{u}_0 + \rho_0 h_1 \ddot{f} \right) \delta u_0 \right. \\ & \left(-(2\rho_0 h_1 + \rho_c h) \ddot{v}_0 + \rho_0 h_1 \ddot{g} \right) \delta v_0 \\ & \left(-(2\rho_0 h_1 + \rho_c h) \ddot{w} \right) \delta w \\ & \left(-\frac{\rho_0 h_1 h^2}{2} \ddot{\psi}_x - \frac{\rho_0 h_1 h}{2} \ddot{f} \right) \delta \psi_x \\ & \left(-\frac{\rho_0 h_1 h^2}{2} \ddot{\psi}_y - \frac{\rho_0 h_1 h}{2} \ddot{g} \right) \delta \psi_y \\ & \left(-\rho_0 h_1 \ddot{u}_0 - \frac{\rho_0 h_1 h}{2} \ddot{\psi}_x - \rho_0 h \ddot{f} \right) \delta f \\ & \left. \left(-\rho_0 h_1 \ddot{v}_0 - \frac{\rho_0 h_1 h}{2} \ddot{\psi}_y - \rho_0 h \ddot{g} \right) \delta g \right] dy dx \quad (\text{A.4}) \end{aligned}$$

From Chapter 7, equation (7.23), we get

$$\delta W = -\frac{1}{2} \int_0^a \int_0^b q_0 \delta w dy dx \quad (\text{A.5})$$

From Chapter 7, equation (7.18), we also can apply the variational principle to get

$$\begin{aligned} \delta V = & -\frac{1}{2} \int_0^a \int_0^b \left[\frac{\partial N_x^u}{\partial x} (\delta u_0) + \frac{h}{2} \frac{\partial N_x^u}{\partial x} (\delta \psi_x) + \left(\frac{\partial}{\partial x} N_x^u \frac{\partial w}{\partial x} \right) (\delta w) + \frac{\partial N_x^u}{\partial x} (\delta f) \right] dy dx \\ & + \frac{1}{2} \int_0^b \left(N_x^u \delta u_0 + \frac{h}{2} N_x^u \delta \psi_x + N_x^u \frac{\partial w}{\partial x} \delta w + N_x^u \delta f \right) dy \end{aligned}$$

$$\begin{aligned} -\frac{1}{2} \int_0^a \int_0^b \left[\frac{\partial N_y^u}{\partial y} (\delta v_0) + \frac{h}{2} \frac{\partial N_y^u}{\partial y} (\delta \psi_y) + \left(\frac{\partial}{\partial y} N_y^u \frac{\partial w}{\partial y} \right) (\delta w) + \frac{\partial N_y^u}{\partial y} (\delta g) \right] dy dx \\ + \frac{1}{2} \int_0^a \left(N_y^u \delta v_0 + \frac{h}{2} N_y^u \delta \psi_y + N_y^u \frac{\partial w}{\partial y} \delta w + N_y^u \delta g \right) dx \end{aligned}$$

$$\begin{aligned} -\frac{1}{2} \int_0^a \int_0^b \left[\frac{\partial N_x^l}{\partial x} (\delta u_0) + \frac{h}{2} \frac{\partial N_x^l}{\partial x} (\delta \psi_x) + \left(\frac{\partial}{\partial x} N_x^l \frac{\partial w}{\partial x} \right) (\delta w) + \frac{\partial N_x^l}{\partial x} (\delta f) \right] dy dx \\ + \frac{1}{2} \int_0^b \left(N_x^l \delta u_0 + \frac{h}{2} N_x^l \delta \psi_x + N_x^l \frac{\partial w}{\partial x} \delta w + N_x^l \delta f \right) dy \end{aligned}$$

$$\begin{aligned} -\frac{1}{2} \int_0^a \int_0^b \left[\frac{\partial N_y^l}{\partial y} (\delta v_0) + \frac{h}{2} \frac{\partial N_y^l}{\partial y} (\delta \psi_y) + \left(\frac{\partial}{\partial y} N_y^l \frac{\partial w}{\partial y} \right) (\delta w) + \frac{\partial N_y^l}{\partial y} (\delta g) \right] dy dx \\ + \frac{1}{2} \int_0^a \left(N_y^l \delta v_0 + \frac{h}{2} N_y^l \delta \psi_y + N_y^l \frac{\partial w}{\partial y} \delta w + N_y^l \delta g \right) dx \end{aligned}$$

$$\begin{aligned}
& -\frac{1}{2} \int_0^a \int_0^b \left[\frac{\partial N_{xy}^u}{\partial y} (\delta u_0) + \frac{\partial N_{xy}^u}{\partial x} (\delta v_0) + \frac{h}{2} \frac{\partial N_{xy}^u}{\partial y} (\delta \psi_x) + \frac{h}{2} \frac{\partial N_{xy}^u}{\partial x} (\delta \psi_y) + \right. \\
& \left. \left(\frac{\partial}{\partial x} N_{xy}^u \frac{\partial w}{\partial y} + \frac{\partial}{\partial y} N_{xy}^u \frac{\partial w}{\partial x} \right) (\delta w) \right] dy dx + \frac{1}{2} \int_0^b \left(N_{xy}^u \delta v_0 + \frac{h}{2} N_{xy}^u \delta \psi_y + N_{xy}^u \frac{\partial w}{\partial y} \delta w \right) dy \\
& + \frac{1}{2} \int_0^a \left(N_{xy}^u \delta u_0 + \frac{h}{2} N_{xy}^u \delta \psi_x + N_{xy}^u \frac{\partial w}{\partial x} \delta w \right) dx
\end{aligned}$$

$$\begin{aligned}
& -\frac{1}{2} \int_0^a \int_0^b \left[\frac{\partial N_{xy}^l}{\partial y} (\delta u_0) + \frac{\partial N_{xy}^l}{\partial x} (\delta v_0) + \frac{h}{2} \frac{\partial N_{xy}^l}{\partial y} (\delta \psi_x) + \frac{h}{2} \frac{\partial N_{xy}^l}{\partial x} (\delta \psi_y) + \right. \\
& \left. \left(\frac{\partial}{\partial x} N_{xy}^l \frac{\partial w}{\partial y} + \frac{\partial}{\partial y} N_{xy}^l \frac{\partial w}{\partial x} \right) (\delta w) \right] dy dx + \frac{1}{2} \int_0^b \left(N_{xy}^l \delta v_0 + \frac{h}{2} N_{xy}^l \delta \psi_y + N_{xy}^l \frac{\partial w}{\partial y} \delta w \right) dy \\
& + \frac{1}{2} \int_0^a \left(N_{xy}^l \delta u_0 + \frac{h}{2} N_{xy}^l \delta \psi_x + N_{xy}^l \frac{\partial w}{\partial x} \delta w \right) dx
\end{aligned}$$

$$\begin{aligned}
& -\frac{1}{2} \int_0^a \int_0^b \left[\frac{\partial \bar{M}_x}{\partial x} (\delta \psi_x - \delta \psi_{sx}) + \frac{\partial \bar{M}_y}{\partial y} (\delta \psi_y - \delta \psi_{sy}) + \frac{\partial \bar{M}_{xy}}{\partial x} (\delta \psi_y) \right. \\
& \left. + \frac{\partial \bar{M}_{xy}}{\partial y} (\delta \psi_x) \right] dy dx + \frac{1}{2} \int_0^b \bar{M}_x (\delta \psi_x - \delta \psi_{sx}) + \bar{M}_{xy} \delta \psi_y dy \\
& + \frac{1}{2} \int_0^a \bar{M}_y (\delta \psi_y - \delta \psi_{sy}) + \bar{M}_{xy} \delta \psi_x dx
\end{aligned}$$

$$\begin{aligned}
& + \frac{1}{2} \int_0^a \int_0^b \left[q_x^c (\delta \psi_x - \delta \psi_{sx}) + q_y^c (\delta \psi_y - \delta \psi_{sy}) - \left(\frac{\partial q_x^c}{\partial x} + \frac{\partial q_y^c}{\partial y} \right) \delta w \right] dy dx \\
& + \frac{1}{2} \int_0^b q_x^c \delta w dy + \frac{1}{2} \int_0^a q_y^c \delta w dx
\end{aligned}$$

(A.6)

Since the activation term in (A.4) is not accelerating quickly enough, we ignore

$$\begin{aligned} \ddot{f} \text{ term, } (\ddot{f} = h \ddot{\psi}_{sx}) \\ \ddot{g} \text{ term, } (\ddot{g} = h \ddot{\psi}_{sy}) \end{aligned}$$

Therefore, from (A.4), (A.5), and (A.6), we have the line integrals representing the boundary conditions of the panel. Then we collect the terms having the same variation terms as δu_0 , δv_0 , and so forth, in the double integrals. We conclude

$$\underline{\delta u_0 \text{ term} = 0}$$

$$\left(\frac{\partial N_x^u}{\partial x} + \frac{\partial N_x^l}{\partial x} \right) + \left(\frac{\partial N_{xy}^u}{\partial y} + \frac{\partial N_{xy}^l}{\partial y} \right) = (2\rho_0 h_1 + \rho_c h) \ddot{u}_0 \quad (\text{A.7})$$

$$\underline{\delta v_0 \text{ term} = 0}$$

$$\left(\frac{\partial N_{xy}^u}{\partial x} + \frac{\partial N_{xy}^l}{\partial x} \right) + \left(\frac{\partial N_y^u}{\partial y} + \frac{\partial N_y^l}{\partial y} \right) = (2\rho_0 h_1 + \rho_c h) \ddot{v}_0 \quad (\text{A.8})$$

$$\underline{\delta \psi_x \text{ term} = 0}$$

$$\begin{aligned} \frac{h}{2} \left[\left(\frac{\partial N_x^u}{\partial x} + \frac{\partial N_x^l}{\partial x} \right) + \left(\frac{\partial N_{xy}^u}{\partial y} + \frac{\partial N_{xy}^l}{\partial y} \right) \right] + \\ \left(\frac{\partial M_x}{\partial x} + \frac{\partial M_{xy}}{\partial y} \right) - q_x^c = \frac{\rho_0 h_1 h^2}{2} \ddot{\psi}_x \end{aligned} \quad (\text{A.9})$$

$$\underline{\delta\psi_y \text{ term} = 0}$$

$$\frac{h}{2} \left[\left(\frac{\partial N_{xy}^u}{\partial x} + \frac{\partial N_{xy}^l}{\partial x} \right) + \left(\frac{\partial N_y^u}{\partial y} + \frac{\partial N_y^l}{\partial y} \right) \right] + \left(\frac{\partial M_{xy}}{\partial x} + \frac{\partial M_y}{\partial y} \right) - q_y^c = \frac{\rho_0 h_1 h^2}{2} \ddot{\psi}_y \quad (\text{A.10})$$

$$\underline{\delta\psi_{sx} \text{ term} = 0} \quad , \quad (\delta\psi_{sx} = (1/h) \delta f)$$

$$h \left(\frac{\partial N_x^u}{\partial x} \right) - \frac{\partial \bar{M}_x}{\partial x} + q_x^c = \rho_0 h_1 h \ddot{u}_0 + \frac{\rho_0 h_1 h^2}{2} \ddot{\psi}_x \quad (\text{A.11})$$

$$\underline{\delta\psi_{sy} \text{ term} = 0} \quad , \quad (\delta\psi_{sy} = (1/h) \delta g)$$

$$h \left(\frac{\partial N_y^u}{\partial y} \right) - \frac{\partial \bar{M}_y}{\partial y} + q_y^c = \rho_0 h_1 h \ddot{v}_0 + \frac{\rho_0 h_1 h^2}{2} \ddot{\psi}_y \quad (\text{A.12})$$

$$\underline{\delta w \text{ term} = 0}$$

$$\begin{aligned} \frac{\partial}{\partial x} (N_x^u \frac{\partial w}{\partial x}) + \frac{\partial}{\partial y} (N_y^u \frac{\partial w}{\partial y}) + \frac{\partial}{\partial y} (N_{xy}^u \frac{\partial w}{\partial x}) + \frac{\partial}{\partial x} (N_{xy}^u \frac{\partial w}{\partial y}) \\ \frac{\partial}{\partial x} (N_x^l \frac{\partial w}{\partial x}) + \frac{\partial}{\partial y} (N_y^l \frac{\partial w}{\partial y}) + \frac{\partial}{\partial y} (N_{xy}^l \frac{\partial w}{\partial x}) + \frac{\partial}{\partial x} (N_{xy}^l \frac{\partial w}{\partial y}) \\ + \frac{\partial q_x^c}{\partial x} + \frac{\partial q_y^c}{\partial y} + q_0 = (2\rho_0 h_1 + \rho_c h) \ddot{w} \end{aligned} \quad (\text{A.13})$$

Assuming 1-D beam model, we ignore $N_y^{u,1}$, $N_{xy}^{u,1}$ terms.

In the meantime,

we assume \ddot{u}_0 , \ddot{v}_0 , $\ddot{\psi}_x$, $\ddot{\psi}_y$, $g = 0$

So, we only have 4 equations (A.7), (A.9), (A.11), (A.13) left, they become

$$\frac{\partial N_x^u}{\partial x} + \frac{\partial N_x^l}{\partial x} = 0 \quad (\text{A.14})$$

$$\frac{\partial \bar{M}_x}{\partial x} + \frac{\partial \bar{M}_{xy}}{\partial y} - q_x^c = 0 \quad (\text{A.15})$$

$$h \frac{\partial N_x^u}{\partial x} - \frac{\partial \bar{M}_x}{\partial x} + q_x^c = 0 \quad (\text{A.16})$$

$$\begin{aligned} \frac{\partial}{\partial x} (N_x^u \frac{\partial w}{\partial x}) + \frac{\partial}{\partial x} (N_x^l \frac{\partial w}{\partial x}) + \frac{\partial q_x^c}{\partial x} + q_0 \\ = (2\rho_0 h_1 + \rho_c h) \ddot{w} \end{aligned} \quad (\text{A.17})$$

In Chapter 7, equations (7.9) - (7.17), we are able to derive the following expression

$$\begin{aligned} \frac{\partial N_x^u}{\partial x} = & \bar{A}_{11} \left(\frac{\partial^2 u_0}{\partial x^2} - \frac{h}{2} \frac{\partial^2 \psi_x}{\partial x^2} - \frac{\partial^2 f}{\partial x^2} + \frac{\partial w}{\partial x} \frac{\partial^2 w}{\partial x^2} \right) \\ & + \bar{A}_{21} \left(\frac{\partial^2 v_0}{\partial x \partial y} - \frac{h}{2} \frac{\partial^2 \psi_y}{\partial x \partial y} + \frac{\partial w}{\partial y} \frac{\partial^2 w}{\partial y \partial x} - \frac{\partial g}{\partial x \partial y} \right) \\ & + \bar{A}_{31} \left(\frac{\partial^2 u_0}{\partial x \partial y} + \frac{\partial^2 v_0}{\partial x^2} - \frac{h}{2} \frac{\partial^2 \psi_x}{\partial x \partial y} - \frac{h}{2} \frac{\partial^2 \psi_y}{\partial x^2} \right. \\ & \quad \left. + \frac{\partial w}{\partial y} \frac{\partial^2 w}{\partial x^2} + \frac{\partial w}{\partial x} \frac{\partial^2 w}{\partial x \partial y} \right) \end{aligned} \quad (\text{A.18})$$

The \bar{A}_{ij} terms are the upper skin stiffness in activation, and the A_{ij} terms are the lower skin stiffness.

$$\begin{aligned}
\frac{\partial N_x^1}{\partial x} = & A_{11} \left(\frac{\partial^2 u_0}{\partial x^2} + \frac{h}{2} \frac{\partial^2 \psi_x}{\partial x^2} + \frac{\partial w}{\partial x} \frac{\partial^2 w}{\partial x^2} \right) \\
& + A_{21} \left(\frac{\partial^2 v_0}{\partial x \partial y} + \frac{h}{2} \frac{\partial^2 \psi_y}{\partial x \partial y} + \frac{\partial w}{\partial y} \frac{\partial^2 w}{\partial y \partial x} \right) \\
& + A_{31} \left(\frac{\partial^2 u_0}{\partial x \partial y} + \frac{\partial^2 v_0}{\partial x^2} + \frac{h}{2} \frac{\partial^2 \psi_x}{\partial x \partial y} + \frac{h}{2} \frac{\partial^2 \psi_y}{\partial x^2} \right. \\
& \quad \left. + \frac{\partial w}{\partial y} \frac{\partial^2 w}{\partial x^2} + \frac{\partial w}{\partial x} \frac{\partial^2 w}{\partial x \partial y} \right)
\end{aligned} \tag{A.19}$$

$$\begin{aligned}
\frac{\partial N_{xy}^u}{\partial y} = & \bar{A}_{13} \left(\frac{\partial^2 u_0}{\partial x \partial y} - \frac{h}{2} \frac{\partial^2 \psi_x}{\partial x \partial y} - \frac{\partial^2 f}{\partial x \partial y} + \frac{\partial w}{\partial y} \frac{\partial^2 w}{\partial x \partial y} \right) \\
& + \bar{A}_{23} \left(\frac{\partial^2 v_0}{\partial y^2} - \frac{h}{2} \frac{\partial^2 \psi_y}{\partial y^2} + \frac{\partial w}{\partial y} \frac{\partial^2 w}{\partial y^2} - \frac{\partial^2 g}{\partial y^2} \right) \\
& + \bar{A}_{33} \left(\frac{\partial^2 u_0}{\partial y^2} + \frac{\partial^2 v_0}{\partial x \partial y} - \frac{h}{2} \frac{\partial^2 \psi_y}{\partial x \partial y} - \frac{h}{2} \frac{\partial^2 \psi_x}{\partial y^2} \right. \\
& \quad \left. + \frac{\partial w}{\partial x} \frac{\partial^2 w}{\partial y^2} + \frac{\partial w}{\partial y} \frac{\partial^2 w}{\partial x \partial y} \right)
\end{aligned} \tag{A.20}$$

$$\begin{aligned}
\frac{\partial N_{xy}^1}{\partial y} = & A_{13} \left(\frac{\partial^2 u_0}{\partial x \partial y} + \frac{h}{2} \frac{\partial^2 \psi_x}{\partial x \partial y} + \frac{\partial w}{\partial y} \frac{\partial^2 w}{\partial x \partial y} \right) \\
& + A_{23} \left(\frac{\partial^2 v_0}{\partial y^2} + \frac{h}{2} \frac{\partial^2 \psi_y}{\partial y^2} + \frac{\partial w}{\partial y} \frac{\partial^2 w}{\partial y^2} \right) \\
& + A_{33} \left(\frac{\partial^2 u_0}{\partial y^2} + \frac{\partial^2 v_0}{\partial x \partial y} + \frac{h}{2} \frac{\partial^2 \psi_y}{\partial x \partial y} + \frac{h}{2} \frac{\partial^2 \psi_x}{\partial y^2} \right. \\
& \quad \left. + \frac{\partial w}{\partial x} \frac{\partial^2 w}{\partial y^2} + \frac{\partial w}{\partial y} \frac{\partial^2 w}{\partial x \partial y} \right)
\end{aligned} \tag{A.21}$$

In the same fashion, by using (7.11 - 7.17), we get

$$\begin{aligned}
\frac{\partial \bar{M}_x}{\partial x} = & \frac{\partial}{\partial x} \left[D_{11} \left(\frac{\partial \psi_x}{\partial x} - \frac{\partial \psi_{sx}}{\partial x} \right) + D_{21} \left(\frac{\partial \psi_y}{\partial y} - \frac{\partial \psi_{sy}}{\partial y} \right) + \right. \\
& \quad \left. D_{31} \left(\frac{\partial \psi_y}{\partial x} + \frac{\partial \psi_x}{\partial y} \right) + B_{11} \left(\frac{\partial u_0}{\partial x} + \frac{1}{2} \left(\frac{\partial w}{\partial x} \right)^2 \right) \right. \\
& \quad \left. + B_{21} \left(\frac{\partial v_0}{\partial y} + \frac{1}{2} \left(\frac{\partial w}{\partial y} \right)^2 \right) + B_{31} \left(\frac{\partial u_0}{\partial y} + \frac{\partial v_0}{\partial x} + \frac{\partial w}{\partial x} \frac{\partial w}{\partial y} \right) \right]
\end{aligned} \tag{A.22}$$

$$\begin{aligned}
\frac{\partial \bar{M}_{xy}}{\partial y} = \frac{\partial}{\partial y} [& D_{13} \left(\frac{\partial \psi_x}{\partial x} - \frac{\partial \psi_{sx}}{\partial x} \right) + D_{23} \left(\frac{\partial \psi_y}{\partial y} - \frac{\partial \psi_{sy}}{\partial y} \right) + \\
& D_{33} \left(\frac{\partial \psi_y}{\partial x} + \frac{\partial \psi_x}{\partial y} \right) + B_{13} \left(\frac{\partial u_0}{\partial x} + \frac{1}{2} \left(\frac{\partial w}{\partial x} \right)^2 \right) \\
& + B_{23} \left(\frac{\partial v_0}{\partial y} + \frac{1}{2} \left(\frac{\partial w}{\partial y} \right)^2 \right) + B_{33} \left(\frac{\partial u_0}{\partial y} + \frac{\partial v_0}{\partial x} + \frac{\partial w}{\partial x} \frac{\partial w}{\partial y} \right)]
\end{aligned} \quad (A.23)$$

$$q_x^c = G_{13} h \gamma_{xz}^c = G_{13} h (\psi_x - \psi_{sx} + \frac{\partial w}{\partial x}) \quad (A.24)$$

Assuming the $\bar{A}_{ij} = A_{ij}$, $B_{ij} = 0$, at a moderate activation, no resultant shear $N_{xy}^{u,1}$, no twisting term as \bar{M}_{xy} in 1-D beam, substituting (A.18), (A.19), (A.22), (A.23), (A.24) into the previous equations of motion (A.14), (A.15), (A.16), (A.17). We conclude that in (A.18), all $\bar{A}_{21}(\dots)$ terms in the bracket are eliminated for the 1-D beam case. Same as in (A.19), all $A_{21}(\dots)$ are eliminated. The SMA lay-up in laminate is considered the same as the orthotropic laminates mentioned in Chapter 5. Then, the \bar{A}_{31} in (A.18), and the A_{31} in (A.19) are zeros, too. Thus, Equation (A.14) becomes

$$2 A_{11} \left(\frac{\partial^2 u_0}{\partial x^2} + \frac{\partial w}{\partial x} \frac{\partial^2 w}{\partial x^2} - \frac{1}{2} \frac{\partial^2 f}{\partial x^2} \right) = 0 \quad (A.25)$$

Since, ignoring the sandwich beam twisting moment \bar{M}_{xy} ,

(A.23) could be eliminated,

and

$$D_{11}^* \frac{\partial \psi_{sx}}{\partial x} = \frac{D_{11}^*}{h} \frac{\partial f}{\partial x}$$

$D_{21}(\dots)$ and $D_{31}(\dots)$ in (A.22) are eliminated for the 1-D case. Therefore, (A.15), (A.16), (A.17) becomes

$$G_{13}(\psi_x - \psi_{sx} + \frac{\partial w}{\partial x}) = \frac{D_{11}^*}{h} \frac{\partial^2 \psi_x}{\partial x^2} - \frac{D_{11}^*}{h^2} \frac{\partial^2 f}{\partial x^2} \quad (\text{A.26})$$

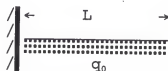
$$\begin{aligned} A_{11} \left(\frac{\partial^2 u_0}{\partial x^2} + \frac{\partial w}{\partial x} \frac{\partial^2 w}{\partial x^2} - \frac{h}{2} \frac{\partial^2 \psi_x}{\partial x^2} - \frac{\partial^2 f}{\partial x^2} \right) + G_{13}(\psi_x - \psi_{sx} + \frac{\partial w}{\partial x}) \\ = \frac{D_{11}^*}{h} \frac{\partial^2 \psi_x}{\partial x^2} - \frac{D_{11}^*}{h^2} \frac{\partial^2 f}{\partial x^2} \end{aligned} \quad (\text{A.27})$$

$$\begin{aligned} G_{13} h \left(\frac{\partial \psi_x}{\partial x} - \frac{\partial \psi_{sx}}{\partial x} + \frac{\partial^2 w}{\partial x^2} \right) \\ + \frac{\partial}{\partial x} (N_x^u \frac{\partial w}{\partial x}) + \frac{\partial}{\partial x} (N_x^l \frac{\partial w}{\partial x}) + q_0 = (2\rho_0 h_1 + \rho_c h) \ddot{w} \end{aligned} \quad (\text{A.28})$$

The $f(x,t)$ and $g(y,t)$ are very small and can be treated as perturbed terms; additionally, they are different in various kinds of SMA composites.

APPENDIX B
CANTILEVER SANDWICH BEAM

Case 1:



A cantilever beam under uniform loading q_0 with governing equations

$$G_{13} (\psi_x - \psi_{sx} + \frac{\partial w}{\partial x}) = \frac{D_{11}}{h} \frac{\partial^2 (\psi_x - \psi_{sx})}{\partial x^2} \quad (\text{B.1})$$

and

$$G_{13} h \left(\frac{\partial \psi_x}{\partial x} - \frac{\partial \psi_{sx}}{\partial x} + \frac{\partial^2 w}{\partial x^2} \right) + q_0 = 0 \quad (\text{B.2})$$

For simplicity, we define $\psi_x - \psi_{sx}$ by $\underline{\psi}_x$, so equations (B.1), (B.2) become

$$G_{13} (\underline{\psi}_x + \frac{\partial w}{\partial x}) = \frac{D_{11}}{h} \frac{\partial^2 \underline{\psi}_x}{\partial x^2} \quad (\text{B.1})$$

and

$$G_{13} h \left(\frac{\partial \underline{\psi}_x}{\partial x} + \frac{\partial^2 w}{\partial x^2} \right) + q_0 = 0 \quad (\text{B.2})$$

Boundary conditions are

at $\underline{x=0}$,

$$w=0 \quad , \quad \psi_x=0 \quad (B.3)$$

$$D_{11} \partial \psi_x / \partial x = -q_0 L^2 / 2 \quad (B.4)$$

$$G_{13} h (\psi_x + \partial w / \partial x) = q_0 L \quad (B.5)$$

and at $\underline{x=L}$,

$$\partial \psi_x / \partial x = 0 \quad (M_x = 0) \quad (B.6)$$

$$\psi_x + \partial w / \partial x = 0 \quad (\text{shear} = 0) \quad (B.7)$$

Integration of eq. (B.2) and using boundary condition (B.5) we obtain

$$G_{13} h (\psi_x + \frac{\partial w}{\partial x}) = -q_0 x + q_0 L \quad (B.8)$$

Substitution of eq. (B.8) into (B.1) leads to

$$\begin{aligned} D_{11} \frac{\partial^2 \psi_x}{\partial x^2} &= -q_0 x + q_0 L \\ D_{11} \frac{\partial \psi_x}{\partial x} &= -\frac{q_0 x^2}{2} + q_0 L x + C_2 \end{aligned} \quad (B.9)$$

The second eq. of (B.9) is obtained by integrating the first eq. of (B.9) and from boundary condition (B.6), we get $C_2 = -q_0 L^2 / 2$. Then, substituting the second equation of (B.9) and C_2 into (B.2), we obtain

$$\begin{aligned} \frac{\partial^2 w}{\partial x^2} &= -\frac{q_0}{G_{13} h} + \frac{q_0 x^2}{2 D_{11}} - \frac{q_0 L x}{D_{11}} + \frac{q_0 L^2}{2 D_{11}} \\ \frac{\partial w}{\partial x} &= -\frac{q_0}{G_{13} h} x + \frac{q_0 x^3}{6 D_{11}} - \frac{q_0 L x^2}{2 D_{11}} + \frac{q_0 L^2}{2 D_{11}} x + C_3 \end{aligned} \quad (B.10)$$

Based on the boundary condition (B.3), the second equation of (B.9) becomes

$$\psi_x = -\frac{q_0 x^3}{6D_{11}} + \frac{q_0 L x^2}{2D_{11}} - \frac{q_0 L^2}{2D_{11}} x + \delta \quad (\text{B.11})$$

The term δ is ψ_{sx} (the core shear rotation due to activation).

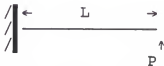
For the deflection $w(x)$, we substitute (B.10) and (B.11) into boundary condition (B.7). This leads to

$$C_3 = q_0 L / G_{13} h$$

and

$$w = \frac{q_0 x^4}{24D_{11}} - \frac{q_0 L x^3}{6D_{11}} + \left(\frac{q_0 L^2}{4D_{11}} - \frac{q_0}{2G_{13}h} \right) x^2 + \frac{q_0 L}{G_{13}h} x + \delta x \quad (\text{B.12})$$

Case 2:



For a cantilever beam under concentrated load P at the tip, the governing equations are

$$G_{13} \left(\psi_x + \frac{\partial w}{\partial x} \right) = \frac{D_{11}}{h} \frac{\partial^2 \psi_x}{\partial x^2} \quad (\text{B.13})$$

$$G_{13} h \left(\frac{\partial \psi_x}{\partial x} + \frac{\partial^2 w}{\partial x^2} \right) = 0 \quad (\text{B.14})$$

The boundary conditions are

$$\underline{x=0}$$

$$w = 0, \quad \psi_x = 0 \quad (\text{B.15})$$

$$D_{11} \partial \psi_x / \partial x = -PL \quad (\text{B.16})$$

$$\underline{x=L}$$

$$\partial \psi_x / \partial x = 0 \quad (\text{B.17})$$

$$\psi_x + \partial w / \partial x = P/G_{13}h \quad (\text{B.18})$$

integrate (B.14)

$$G_{13}h \left(\psi_x + \partial w / \partial x \right) = C_1 \quad (\text{B.19})$$

and substitute into (B.13), it becomes

$$\psi_x = C_1 x^2 / 2D_{11} + C_2 x \quad (\text{B.20})$$

which satisfies the boundary condition (B.15). Using the boundary condition (B.17), we obtain $C_2 = -C_1 L / D_{11}$.

Therefore, ψ_x can be expressed as

$$\psi_x = \left(x^2 / 2D_{11} - Lx / D_{11} \right) C_1 \quad (\text{B.21})$$

Substituting (B.21) into (B.14) we obtain

$$\begin{aligned}\frac{\partial^2 w}{\partial x^2} &= \left(\frac{L}{D_{11}} - \frac{x}{D_{11}} \right) C_1 \\ \frac{\partial w}{\partial x} &= \left(\frac{Lx}{D_{11}} - \frac{x^2}{2D_{11}} \right) C_1 + C_4\end{aligned}\tag{B.22}$$

From eqs (B.21), (B.22) and the boundary condition (B.18), we get

$$C_4 = P / G_{13}h\tag{B.23}$$

take the derivative of eq (B.21) with respect to x and apply the boundary condition (B.16) to derive

$$C_1 = P\tag{B.24}$$

Finally, we substitute the boundary condition (B.15) and eqs (B.23), (B.24) back into eqs (B.21), (B.22) with the integration of the second eq of (B.22), and conclude the following:

$$\psi_x = \frac{Px^2}{2D_{11}} - \frac{PLx}{D_{11}} - \delta\tag{B.25}$$

$$w = \frac{PLx^2}{2D_{11}} - \frac{Px^3}{6D_{11}} + \frac{Px}{G_{13}h} + \delta x\tag{B.26}$$

The term δ is ψ_{sx} (the core shear rotation due to the sandwich beam activation).

REFERENCES

- [1] Rogers, C.A., Introduction to Smart Materials and Structures. Selected Papers Presented at the U.S. Army Research Office Workshop on Smart Materials, Structures, and Mathematical Issues, pp. 17-26, Virginia Polytechnic Inst. and State U., Blacksburg, VA, September 15-16, 1988.
- [2] Duerig, T.W., K.N. Melton, D. Stockel, and C.M. Wayman, Engineering Aspects of Shape Memory Alloys, Butterworth-Heinemann, Ltd., London, 1990.
- [3] Perkins, J., Shape Memory Effect in Alloys, International Symposium on Shape Memory Effect and Applications, Toronto, 1975.
- [4] Rogers C.A., and Barker, D.K., Experimental Studies of Active Strain Energy Tuning of Adaptive Composites, p. 2234, Fig. 9., A Collection of Technical Papers of AIAA/ASME/ASCE/AHS/ASC 31st Structures, Structural Dynamics and Materials Conference, Long Beach, CA, April 2-4, 1990.
- [5] Saunders W.R., Robertshaw H.H., and Rogers C.A., Experimental Studies of Structural Acoustic Control for a Shape Memory Alloy Composite Beam, p. 2274, Fig. 8., AIAA/ASME/ASCE/AHS/ASC 31st Structures, Structural Dynamics and Materials Conference, Long Beach, CA, April 2-4, 1990.
- [6] Hawkins L.E., Vick, B., and Rogers, C.A., An Investigation of the Transient Thermal Response of Shape Memory Alloy Composite Beam, p. 1972, AIAA/ASME/ASCE/AHS/ASC 31st Structures, Structural Dynamics and Materials Conference, Long Beach, CA, April 2-4, 1990.
- [7] Rogers, C.A., Liang, C., and Jia, J., Behavior of Shape Memory Alloy Reinforced Composite Plates, Part I: Model Formulation and Control Concepts, p.2011, AIAA/ASME/ASCE/AHS/ASC 31st Structures, Structural Dynamics and Materials Conference, Long Beach, CA, April 2-4, 1990.

- [8] Technical data manual by Precision Wire Corporation (formerly US NITINOL), P.O. Box 767, Rancho Ruidoso, Alto, NM 88321, 1990.
- [9] Sun, C.T., Fabrication of Fiber-Reinforced Composite Plates, Manual from EAS6242 Advanced Composite I, Dr. C.T. Sun, Dept. of Aerospace, Mechanics & Eng. Science. U of Florida, Gainesville, 1987.
- [10] Agarwal, B.D., and Broutman, L.J., Analysis and Performance of Fiber Composites, John Wiley & Sons, NY, 1980
- [11] Malvern, L.E., Introduction to the Mechanics of a Continuous Medium, Prentice-Hall, Engelwood Cliffs, NJ, 1969.
- [12] Piggott, M.R., Mechanical Interactions in the Interfacial Region of Fibre Reinforced Thermosets, from Composite Interfaces, Proceedings of the First International Conference on Composite Interfaces (ICCI-1), Cleveland, OH, 1986.
- [13] Mohamed, H.A., Determination of The Recovery Stresses Developed by Shape Memory Alloys, contract no. W-7405-eng-48, UC-Berkeley, 1978.
- [14] Chamis, C.C., Simplified Composite Micromechanics for Predicting Microstresses, research contract no. NASA-TM-87295, UF NAS 1.15:87295, 1986
- [15] Guynn, E.G., Micromechanics of Composite Laminate Compression Failure, (NASA-CR-183179), research contract no. UF NAS 1.26:183179, 1988
- [16] Nashif, A.D., Jones, David I.G., and Henderson, J P., Vibration Damping, John Wiley and Sons, NY, 1985.
- [17] Thomson, W.T., Theory of Vibration with Applications, 3rd edition, Prentice-Hall, Englewood Cliffs, NJ, 1981
- [18] Beards C.F., Vibration Analysis and Control System Dynamics, University of London and John Wiley & Sons, NY, 1981.
- [19] Pierce, G.A., Nabil, M., and Hamouda, H., Helicopter Vibration Suppression Using Simple Pendulum Absorber on the Rotor Blade, NASA contract report 3619, UF NAS 1.26:3619, 1982.

- [20] Bush, H.G., and Mikulas, M.M., Some Design Considerations for Large Space Structures, AIAA Journal, 16:352-359, 1978.
- [21] Gibson, R.F., Vibration Damping Characteristics of Graphite/Epoxy Composites for Large Space Structures, NASA Conference Publication 2215, 1984
- [22] Sun, C.T., and Wu, J.K., Internal Damping of Short-Fiber Reinforced Polymer Matrix Composites, Computers and Structures, 20:391-400, 1985.
- [23] Sun, C.T., and Wu, J.K., Prediction of Material Damping in Randomly Oriented Short Fiber Polymer Matrix Composites, J. Reinforced Plastics and Composites, 4:262-272, 1985.
- [24] Jones, D.I.G., Design of Constrained Layer Treatments for Broad Temperature Damping, Shock and Vibration Bulletin, 44:(5)1-12, 1974.
- [25] Sankar, B.V., Deshpande, A.S., and Sun, C.T., Constrained Layer Damping of Large Space Structures, 33rd SDM conference, U of Florida, Gainesville, 1992.
- [26] Junjiro, Onoda, Vibration Suppression by Variable-Stiffness Members, AIAA Journal 29:977-983, 1991.
- [27] Whitney, J.M., and Leissa, A.W., Analysis of Heterogeneous Anisotropic Plates, J. Applied Mechanics, 36:261-266, 1969.
- [28] Bai, C.M., and Sun, C.T., Nonlinear Flexural Vibration of Sandwich Plates Subjected to In-Plane Forces, 2nd International Conference on Sandwich Construction, U of Florida, Gainesville, 1992.
- [29] Chia, C.Y., Nonlinear Analysis of Plates, McGraw-Hill, NY, 1980.
- [30] Whitney, J.M., Structural Analysis of Laminated Anisotropic Plates, Materials Lab., AFWAL, Technomic Publishing Co., Cleveland, OH, 1987.
- [31] Fung, Y.C., Foundations of Solid Mechanics, Prentice-Hall, Englewood Cliffs, NJ, 1965.
- [32] Kapania, R.K., and Raciti, S., Recent Advances in Analysis of Laminated Beams and Plates, Part I: Shear Effects and Buckling, AIAA Journal, 27:(7)923-934, 1989.

- [33] Rakesh, K.K, and Stefano, R., Recent Advances in Analysis of Laminated Beams and Plates, Part II: Vibrations and Wave Propagation, AIAA Journal, 27:(7)935-946, 1989.
- [34] Reissner, E., The Effect of Transverse Shear Deformation on the Bending of Elastic Plates, J. Applied Mechanics. 12:69-77, 1945.
- [35] Mindlin, R.D., Influence of Rotatory Inertia and Shear on Flexural Motions of Isotropic, Elastic Plates, J. Applied Mechanics 18:336-343, 1951.
- [36] Yang, P.C., Norris, C.H., and Stavsky, Y., Elastic Wave Propagation in Heterogenous Plates, International J. Solids and Structures, 2:665-684, 1966.
- [37] Whitney, J.M., and Pagano, N.J., Shear Deformation in Heterogeneous Anisotropic Plates, J. Applied Mechanics, 37:1031-1036, 1970.
- [38] Reddy, J.N., A Simple Higher-Order Theory for Laminated Composites, J. of Applied Mechanics, 51:745-752, 1984.
- [39] Bert, C.W., Research on Dynamic Behavior of Composite and Sandwich Plates, Shock and Vibration Digest, 17:3-15, 1985.
- [40] Whitney, J.M., Bending-Extensional Coupling in Laminated Plates under Transverse Loading, J. Composite Materials, 3:20-28, 1969.
- [41] Jensen, D.W., and Crawley, E.F., Frequency Determination Technique for Cantilevered Plates with Bending-Torsion Coupling, AIAA Journal, 22:415-420, 1984.
- [42] Kapania, R.K., and Raciti, S., Nonlinear Vibrations of Unsymmetrically Laminated Beams, AIAA Journal, 27:201-211, 1989.
- [43] Bhimaraddi, A., Nonlinear Flexural Vibrations of Rectangular Plates Subjected to In-Plane Forces Using a New Shear Deformation Theory, Elsevier Applied Science Publishers Ltd., NY, 1987.
- [44] Bhimaraddi, A., Nonlinear Free Vibration Analysis of Composite Plate with Initial Imperfections and In-Plane Loading, Internatl. J. Solids Structures, 25:(1)33-43, 1989.

- [45] Eslami, H., and Kandil, O.A., Nonlinear Forced Vibration of Orthotropic Rectangular Plates Using the Method of Multiple Scales, *AIAA Journal*, 27:(7)955-960, 1989.
- [46] Eslami, H., and Kandil, O.A., Two-Mode Nonlinear Vibration of Orthotropic Plates Using a Method of Multiple Scales, *AIAA Journal*, 27:(7)961-967, 1989.
- [47] Singh, G, and Rao, G.V., Analysis of The Nonlinear Vibration of Unsymmetrically Laminated Composite Beams, *AIAA Journal*, 29:(10)1727-1735, 1991.
- [48] Bauchau, O.A., and Hong, C.H., Nonlinear Response and Stability Analysis of Beams Using Finite Elements in Time, *AIAA Journal*, Vol. 26:(9)1135-1142, 1988.
- [49] Hou, J.W., and Yuan, J.Z., Calculation of Eigenvalue and Eigenvector Derivatives for Nonlinear Beam Vibration, *AIAA journal*, 26:872-880, 1988.
- [50] Cartwell, M., Introduction to Linear, Parametric and Nonlinear Vibration, U of Aberdeen, T.J. Press (Padstow) Ltd, Padstow, Cornwall, Great Britain, 1990.
- [51] Schmidt, G., and Tondl, A., Nonlinear Vibration, Cambridge University Press, Cambridge, 1986.
- [52] Gibson, R.F., Chaturvedi, S.K., and Sun, C.T., Complex Moduli of Aligned Discontinuous Fiber-Reinforced Polymer Composites, *J. Materials Science*, 17:3499-3509, 1982.
- [53] Suarez, S.A., Ginson, R.F., Sun, C.T., and Chaturvedi, S.K., The Influence of Fiber Length and Fiber Orientation on Damping and Stiffness of Polymer Composite Materials, Conference on Experimental Mechanics, Las Vegas, June, 1985.
- [54] Sun, C.T., and Wu, J.K., Prediction of Material Damping of Laminated Polymer Matrix Composites, *J. Material Science*, 22:1006-1012, 1987.
- [55] Sun, C.T., Rao, V.S., and Sankar, B.V., Passive Damping of Prestressed Composite Structures, *Acta Mechanica Solida Sinica (English Edition)*, 5:(3), 1992.
- [56] Rajagopal S. V., Singh G., Rao Y. S. Large Deflection and Nonlinear Vibration of Multilayered Sandwich Plates, *AIAA Journal*, 25:(1)130-133, 1987.

BIOGRAPHICAL SKETCH

Chin Hai Lee was born in Taiwan, Republic of China. He received the B.S. degree in Aerospace engineering at Chun Cheng Institute of Technology, Taoyuan, in 1974. After the B.S., he served in the Aeronautical Industry Development Center (AIDC) as an aircraft structural design engineer. In 1983, he was sent by AIDC to the University of Florida to pursue the study of structural mechanics and returned to AIDC after being granted the M.S. degree. He worked on implementing the CAD/CAM system for the design, tooling, and manufacturing of aircraft structures. He also joined the taskforce in composite parts development during the period of 1983 to 1990. He returned to the University of Florida in 1990 and from then until now he has been working on the study of the dynamic responses of composites and sandwich structures embedded with shape memory alloy in the laminates. He is married to Lee Yao Ping and has two children, Lee Mei-Sheng and Lee Mei-Ling.

I certify that I have read this study and that in my opinion it conforms to acceptable standards of scholarly presentation and is fully adequate, in scope and quality, as a dissertation for the degree of Doctor of Philosophy.

C. T. Sun

C. T. Sun, Chairman
Professor of Aerospace,
Mechanics & Engineering Science

I certify that I have read this study and that in my opinion it conforms to acceptable standards of scholarly presentation and is fully adequate, in scope and quality, as a dissertation for the degree of Doctor of Philosophy.

B. Sankar

Bhavani Sankar
Associate Professor of
Aerospace, Mechanics &
Engineering Science

I certify that I have read this study and that in my opinion it conforms to acceptable standards of scholarly presentation and is fully adequate, in scope and quality, as a dissertation for the degree of Doctor of Philosophy.

Lawrence E. Malvern

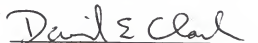
Lawrence E. Malvern
Professor of Aerospace,
Mechanics & Engineering Science

I certify that I have read this study and that in my opinion it conforms to acceptable standards of scholarly presentation and is fully adequate, in scope and quality, as a dissertation for the degree of Doctor of Philosophy.

David Zimmerman

David Zimmerman
Associate Professor of
Aerospace, Mechanics &
Engineering Science

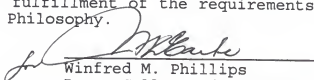
I certify that I have read this study and that in my opinion it conforms to acceptable standards of scholarly presentation and is fully adequate, in scope and quality, as a dissertation for the degree of Doctor of Philosophy.



David E. Clark
Professor of Material
Science and Engineering

This dissertation was submitted to the Graduate Faculty of the College of Engineering and to the Graduate School and was accepted as partial fulfillment of the requirements for the degree of Doctor of Philosophy.

August 1993



Winfred M. Phillips
Dean, College of Engineering

Madelyn M. Lockhart
Dean, Graduate School